



University of
Stavanger

FACULTY OF SCIENCE AND TECHNOLOGY

MASTER'S THESIS

Study programme/specialisation:

Marine and Offshore Technology

Spring semester, 2020

Open

Author: Alexandr Vyrodiv

Student number: 252893

Supervisors:

Professor Ove Tobias Gudmestad (UiS),

Professor Anatoly Borisovich Zolotukhin (Gubkin University)

Title of master's thesis:

Carbon Dioxide Application for Enhanced Oil Recovery in conditions of the Caspian Sea Shelf

Credits: 30 ECTS

Keywords: Offshore Field Development, The North Caspian Sea, Carbonated Water, Carbon dioxide, CO₂-EOR, Oil Recovery Factor, Field "A", Ice ridge, Economic Feasibility, Carbon Dioxide Sequestration

Number of pages: 97

+ supplemental material/other: 19

Stavanger, 12.06.2020
date/year

Abstract

Keywords: CO₂-EOR, Field “A”, carbonated water, The North Caspian region, Oil Recovery Factor, Development Concept, carbon dioxide, economic feasibility.

CO₂ injection into the hydrocarbon-bearing reservoirs is considered as one of the most promising technologies for enhanced oil recovery. This technology has gained significant attention due to its economic benefits as there has been an increasing amount of carbon dioxide sources in various branches of industry. Besides incremental oil recovery extraction, the CO₂ injected remains sequestered in underground formations. Thus, such a technology mitigates carbon dioxide emissions in an economically feasible way, and an additional oil volume production accompanies it. State of the art science displays two primary methods for carbon dioxide application in an enhanced oil recovery process; these are gaseous CO₂ injection and carbonated water injection.

The current study focuses on CO₂-EOR technology for offshore oil Field “A” located on the North Caspian Sea shelf. Each of the two methods mentioned above was analyzed to determine the potential oil recovery factor as a result of carbon dioxide injection. Moreover, possible CO₂ sources and transportation routes were also considered. The preliminary assessment revealed that injection of 5 % carbonated water (CWI) displays the most optimal economic and technological parameters.

The investigation study also includes a field development concept designed for carbonated water injection based on Field “A’s” existing infrastructure. The Arctic-related environmental conditions of the region were considered to develop a robust technological flowsheet. Within the concept development offshore and onshore pipelines were designed, as well as ejector units for carbon dioxide dissolution in seawater; equipment assembly and detailed drawings were completed. Subsea pipeline protection against ice ridges is analyzed.

The primary purpose of the thesis is to formulate a methodology for preparing an estimate for the applicability of carbon dioxide injection in an offshore enhanced oil recovery process.

Acknowledgements

I want to express my sincere thanks to Gubkin State University of Oil and Gas and the University of Stavanger. In an unstable modern world, scientific cooperation can lead humankind to mutual understanding and prosperity. Due to this double-degree Master program, I derived an opportunity to learn the variety of approaches to verity.

I would especially like to outline considerable contribution to the double-degree program of its ideological masterminds: Professor Ove-Tobias Gudmestad and Professor Anatoly B. Zolotukhin, who are also my supervisors. I appreciate their wise advises and lectures, which are the primary basis of this Master thesis. All the knowledge I gained from these gentlemen will stay with me forever, as well as the sincere respect to them. There is no doubt that people like my supervisors forge the future of the oil and gas industry.

I am also very grateful to Professors Yihan Xing and Muk Chen Ong, who encouraged me to dive deeper into the Master thesis's topic, they gave me a strong motivation. Moreover, I appreciate the contribution of the University of Stavanger who supplied me with a workspace and any help I needed.

I would like to pass a sincere thanks to my mentor during the internship in NCOC company - Emanuele Volterra, who shared his experience and knowledge.

Finally, the enormous gratefulness goes to my family and friends. Their faith in me made my study possible.

Contents

Abstract.....	2
Acknowledgements	3
List of Figures	7
List of Tables	9
Introduction.....	11
1. Environmental conditions of the North Caspian Sea shelf.....	13
1.1. Geography and resources of the North Caspian Sea region	13
1.2. Weather conditions	15
1.2.1. Air temperature.....	15
1.2.2. Air humidity	17
1.2.3. Wind conditions.....	18
1.3. Hydrological conditions	20
1.3.1. Wave conditions	22
1.3.2. Currents	24
1.4. Soil conditions at Field “A” location.....	25
1.5. Ice conditions.....	26
1.5.1. Ice ridges	27
2. The development concept for Field “A”.....	29
2.1. Reservoir conditions	31
2.2. Offshore and onshore technological flowsheet.....	32
3. Background and future trends in the sphere of offshore CO ₂ -EOR.....	35
4. CO ₂ -EOR application approaches for Field “A”.....	41
4.1. Pure carbon dioxide injection.....	41
4.2. Carbonated water injection.....	43
5. Comparative analysis of various CO ₂ -EOR applications for the particular conditions of Field “A”	47
5.1. Gaseous CO ₂ injection	47
5.1.1. Oil recovery factor assessment.....	47
5.1.2. Required CO ₂ amount assessment.....	50
5.2. Carbonated water injection.....	51
5.2.1. Oil recovery factor estimation.....	51
5.2.2. Injection of the carbonated water rim.....	59

5.2.3.	Required CO ₂ amount estimation	60
5.3.	CO ₂ sources	61
5.4.	Comparison between 5% and 30% carbonated water injection scenarios	63
5.4.1.	Feasibility assessment of CO ₂ transportation.....	63
5.4.2.	Economic evaluation between 5 % and 30 % carbonated water injection 67	
6.	Field A development concept for carbonated water injection	69
6.1.	General information	69
6.2.	Carbonated water processing.....	69
6.2.1.	Unit for CO ₂ dissolution.....	69
6.2.2.	Seawater transportation for carbonated water processing	71
6.3.	Subsea pipeline design	72
6.3.1.	Diameter selection	73
6.3.2.	Material selection.....	76
6.3.3.	Corrosion aspects.....	76
6.3.4.	Wall thickness selection.....	77
6.3.5.	Von-Mises stress criteria.....	79
6.3.6.	Pipeline burial depth evaluation	80
6.4.	Island D – EPC2 – EPC3 pipeline design.....	84
6.5.	Pumps selection for carbonated water injection into the well	86
6.6.	Concept feasibility study.....	87
6.6.1.	Capital expenditures.....	87
6.6.2.	Economic parameters.....	89
	Conclusions.....	91
	References.....	93
	Appendix 1.....	99
	Appendix 2.....	100
	Appendix 3.....	101
	Appendix 4.....	102
	Appendix 5.....	103
	Appendix 6.....	104
	Appendix 7.....	105
	Appendix 8.....	106

Appendix 9.....	107
Appendix 10.....	108
Appendix 11.....	109
Appendix 12.....	110
Appendix 13.....	111
Appendix 14.....	112
Appendix 15.....	113
Appendix 16.....	115

List of Figures

Figure 1.1. Potential of the Caspian Sea [4].....	13
Figure 1.2. Perspective hydrocarbon fields within the Kazakh sector of the North Caspian Sea [4]	14
Figure 1.3. Offshore Wind Rose for Field A [6]	19
Figure 1.4. Annual mean Caspian Sea Level [7].....	20
Figure 1.5. CSL Forecast according to GCM Model [7]	21
Figure 1.6. Rose plot of H_s and the mean wave direction [8]	23
Figure 1.7. The annual rose plot of all measured currents [8]	25
Figure 1.8. Ice ridges location in the North Caspian Sea [4].....	28
Figure 2.1. Development sketch of Field A	30
Figure 2.2. Offshore technological flowsheet [11].....	33
Figure 2.3. Onshore processing plant flowsheet [14]	34
Figure 3.1. Concept suggested by Aker Solutions, including existing and new infrastructure [3]	37
Figure 3.2. Critical elements of a typical treatment concept for CO ₂ -EOR [15].....	39
Figure 3.3. Combination of subsea production, power generation and CO ₂ -EOR [15]	40
Figure 4.1. Correlation between oil viscosity and CO ₂ oil bubble point [19]	42
Figure 4.2. Minimum miscibility pressure correlation with a molecular weight of C ₅ + components and formation temperature [20]	43
Figure 4.3. Correlation between CO ₂ solubility in water and thermobaric conditions [17]	45
Figure 5.1. The relationship between the molecular weight of hydrocarbons C ₅ + and the reservoir fluid density [24]	48
Figure 5.2. Relative phase permeability curves	54
Figure 5.3. Fractional flow function for waterflooding by seawater and carbonated water (5 % dissolved CO ₂).	56
Figure 5.4. Fractional flow function for waterflooding by seawater and carbonated water (5 % CO ₂) with pole P.	58
Figure 5.5. Fractional flow function for 5 % carbonated water rim injection	60

Figure 5.6. Dependence of capital costs per pipeline unit length on the mass flow of CO ₂ and the length of the pipeline	66
Figure 5.7. Dependence of CO ₂ transportation cost on the mass flow of CO ₂ and the length of the pipeline	66
Figure 6.1. Ejector unit schematic diagram [36]	69
Figure 6.2. Chart diagram of the iterative approach for pipeline diameter selection [41]	74
Figure 6.3. P, T diagram of the binary water-CO ₂ system [43]	74
Figure 6.4. Idealized geometry of a first-year ridge [51].....	81
Figure 6.5. Forces applied to the soil-ice ridge model [52]	81
Figure 6.6. Development concept sketch for carbonated water injection	86
Figure 6.7. Net Present Value plot.....	90

List of Tables

Table 1.1. Kazakhstan shelf deposits of the North Caspian Sea [4]	14
Table 1.2. Extreme minimum dry air temperature in Celsius degree [6]	16
Table 1.3. Extreme maximum dry air temperature in Celsius degree [6]	16
Table 1.4. Extreme ambient temperature [6].....	16
Table 1.5. Monthly Statistics of Operational Air Temperature [6]	17
Table 1.6. Ambient Temperatures for Equipment Design [7]	17
Table 1.7. Monthly Statistics of Relative Humidity (%) [6].....	17
Table 1.8. Extreme Wind Criteria for Field A [6]	18
Table 1.9. Mean wind speed – Ratios for Alternative Averaging Periods (According to ISO 19901-1) [6]	19
Table 1.10. Probabilistic Annual Mean CSL Forecast (m) [7]	21
Table 1.11. Extreme Surge Levels (relative to CSL) [7]	22
Table 1.12. Extreme wave heights and peak periods [8]	23
Table 1.13. Current speed [8]	24
Table 1.14. Seabed data [4], [10], [11]	26
Table 1.15. Minimum and maximum ice periods for the North Caspian Sea [8].....	27
Table 1.16. Extreme level ice thickness [8]	27
Table 1.17. The estimated 100-yr thickness of rafted ice [8]	27
Table 2.1. Field A reservoir conditions [11]	31
Table 2.2. Field A formation fluid characteristics [11], [13].....	31
Table 2.3. Formation fluid material balance [11]	32
Table 4.1. CWI series [22]	44
Table 4.2. Carbonated water injection results [22].....	45
Table 5.1. Estimation results	50
Table 5.2. Field A relative phase permeability [26]	54
Table 5.4. Dimensionless coefficients [28]	55
Table 5.5. ORF estimation for flooding with carbonated water of various concentrations.	59
Table 5.6. Carbon dioxide amount estimation	61
Table 5.7. Summary data of required CO ₂ amount	61

Table 5.8. Annual CO ₂ required amount for considered cases	62
Table 5.9. CO ₂ sources for 30 % carbonated water [34]	62
Table 5.10. CO ₂ source for 5 % carbonated water [34]	62
Table 5.11. Economic assessment of CO ₂ transport along the Volgograd -Astrakhan- Atyrau route	64
Table 5.12. Economic assessment of CO ₂ transport along the Volgograd – Atyrau and Astrakhan-Atyrau routes	65
Table 5.13. Economic assessment of CO ₂ transport in case of 5 %carbonated water scenario	65
Table 5.14. Feasibility evaluation of 5 % and 30 % carbonated water injection.....	67
Table 6.1. Initial data for the ejector unit design.....	70
Table 6.2. Jet unit calculation result	70
Table 6.3. Initial data for pipeline diameter selection	71
Table 6.4. Initial data for pipeline diameter selection	75
Table 6.5. Initial data for pipeline wall thickness calculation [37], [42].....	79
Table 6.6. Wall thickness for the steels of various grades	79
Table 6.7. Parameters for combined loading calculation [50]	80
Table 6.8. Initial data for pipeline burial depth calculations [53], [54], [55], [56], [57]	84
Table 6.9. Pipeline D – EPC2 – EPC3 calculated parameters	85
Table 6.10. CAPEX.....	88
Table 6.11. Economic parameters of the project.....	90

Introduction

With increasing energy consumption on our planet, the amount of carbon dioxide emitted into the atmosphere is also rising, which negatively affects the state of the environment. Attempts to solve such a problem resulted in the Paris Agreement in climate change [1].

Paris Agreement called for maintenance of balance between anthropogenic activity aimed at the industry development and diminution of climate changes. According to such an agreement, the global response to the threat of climate change is undertaken by keeping global temperature increase current century below 2 degrees Celsius above the time preceding the industrial revolution. To deal with this aim, it was decided to diminish anthropogenic CO₂ emissions into the atmosphere [1].

Oil and Gas Climate Initiative reports that the petroleum industry is responsible for at least 1 billion tonnes of direct CO₂ emissions annually. Thus, up-to-date approaches are required to mitigate carbon dioxide emissions in the petroleum industry to diminish its contribution to global climate change and to respect the Agreement in Climate Change [1].

Multiple studies have found that carbon dioxide can serve as an effective displacing agent that enhances oil recovery. Thus, by pumping carbon dioxide into the reservoir to increase oil recovery, along the way, the problems of collecting carbon dioxide and its utilization are solved [2].

A lot of research has been done to demonstrate the effectiveness of carbon dioxide injection onshore, while the experience of using CO₂ injection for offshore fields includes only one large-scale project and no more than six small-scale projects. The main difficulties are the lack of the required carbon dioxide amount near the field and the transportation of CO₂ from the source [3].

The current thesis is dedicated to modelling the CO₂ releases mitigation strategy in an economically feasible way via its injection into the productive formation of the Field “A”, which is situated in the Northern Caspian Sea.

The modelling process in the current thesis is performed according to the following structure:

- Chapter 1: Environmental conditions of the North Caspian Sea shelf. Description of the region hydrocarbon potential, weather and climate conditions, such as wind, waves, currents, ice and air temperature conditions.
- Chapter 2: The development concept for field “A”. This chapter includes a review of existing infrastructure at an ongoing Field “A”, as well as reservoir and formation fluid parameters.
- Chapter 3: Background and future trends in the sphere of offshore CO₂-EOR. The state of the art technologies and concepts in the sphere of offshore CO₂-EOR are analyzed.
- Chapter 4: CO₂-EOR application approached for Field “A”. The section contains theoretical justification and description of two basic CO₂ injection types: (1) gaseous CO₂ injection and (2) water with dissolved carbon dioxide (carbonated water) injection.
- Chapter 5: Comparative analysis of various CO₂-EOR applications for particular conditions of Field “A”. There is an oil recovery factor estimation as a result of gaseous CO₂ and carbonated water injection. Moreover, the required amount of carbon dioxide and potential CO₂ sources are analyzed. Both technologies are considered and compared from the economic frame of reference.
- Chapter 6: Field “A” development concept for carbonated water injection. The chapter includes equipment and infrastructure design and development to implement carbonated water injection. All the environmental aspects from Chapter 1 is considered here. Feasibility study of the designed project is conducted.

1. Environmental conditions of the North Caspian Sea shelf

1.1. Geography and resources of the North Caspian Sea region

Even though the Caspian Sea, located on the territory of Azerbaijan, Iran, Kazakhstan, Russia and Turkmenistan, is the world's oldest oil-producing region, its northern part has been developed only over the past two decades. Currently, this region is of particular interest to global companies due to the vast reserves of oil and gas.

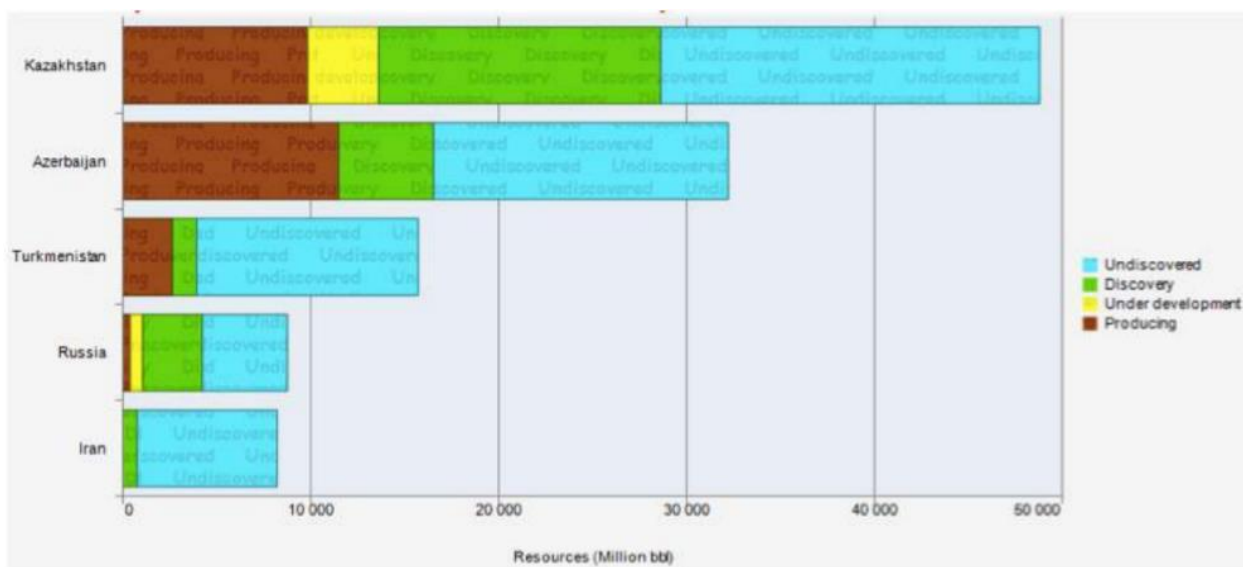


Figure 1.1. Potential of the Caspian Sea [4]

The resource potential of the North Caspian region belonging to the Republic of Kazakhstan is estimated at 50 billion barrels of oil equivalent [5]. The most considerable contribution to the resource base of the northern Caspian is made by the Kashagan field, the largest explored field in the last 40 years, as well as the largest offshore oil field in the world.

Besides Kashagan, about 120 oil fields (Fig. 1.2., Table 1.1) were discovered in the northern part of the Caspian Sea. The greatest prospects for development are possessed by such fields as Kairan, Aktoty and Kalamkas-Sea, which are located nearby Kashagan. The Satpayev and Zhambyl deposits situated in the north-eastern part of the Caspian Sea have significantly fewer reserves than those listed above [4].

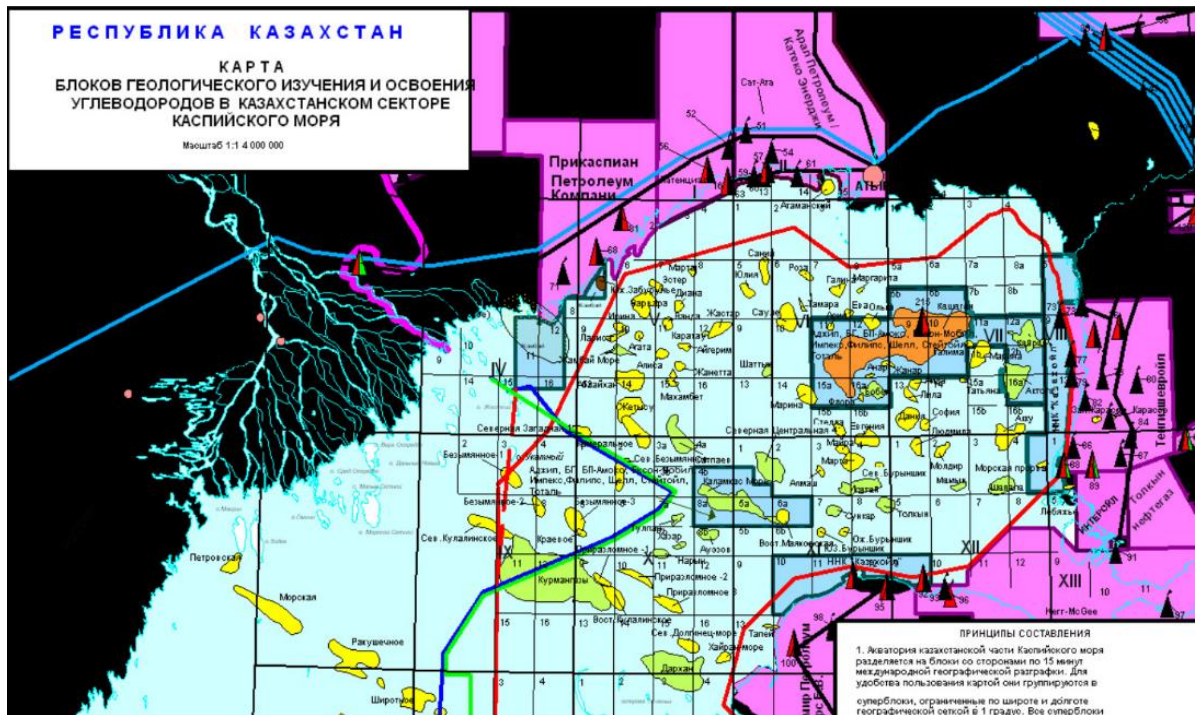


Figure 1.2. Perspective hydrocarbon fields within the Kazakh sector of the North Caspian Sea (Yellow colour – explored fields, green – ready for the further development, brown – have been developed) [4]

Table 1.1. Kazakhstan shelf deposits of the North Caspian Sea [4]

Field name	Year of discovery	Oil resources (mln t)	Gas resources (bm ³)	Year of production start	Owner
Kashagan	2000	1700	1	2013/2016	NCOC
Kairan	2003	36	-	-	NCOC
Aktoty	2003	100	169	-	NCOC
Kalamkas-offshore	2002	67,6	70	2023	NCOC
Zhambay	2002	41	-	-	KazMunaiGaz
Auezov	2007	10	3	-	KazMunaiGaz
Khazar	2007	31	1,4	-	KazMunaiGaz

1.2. Weather conditions

The Northern Caspian is influenced by a continental climate regime, which results in broad ranges of temperature and widely varying seasonal wind regimes. Summers are hot and dry, and the winters are cold with relatively low snowfall. During the winter, the weather is dominated by the Siberian anti-cyclone that creates east to South Easterly winds of cold, clear air over the northern Caspian. During the summer, the climate is influenced by the Azores high-pressure, with the strongest and most persistent winds from between west and north [6].

The area is slightly dry; about 200 mm per year of precipitation falls over the area, most of the year as rainfall and in the winter months as snow. Consequently, snow cover during winter is generally 10-20 cm or less [6].

In the northern Caspian, the strongest winds occur between November and April, with typical annual maxima of around 20 m/s, rising to more than 27 m/s for a 100-year return period storm. The summer months are more benign, with wind speeds only rarely exceeding 15 m/s. The strongest winds tend to be from between Southwest and West, although a more North Easterly component is apparent during the latter part of the year.

Daily mean air temperatures vary significantly seasonally and from year to year, specifically during the winter period, when temperatures can fall to below -30°C in some years, but only to around -20°C in others. In the summer air temperatures often rise to between 35°C and 40°C [6].

1.2.1. Air temperature

Extreme maximum and minimum air temperatures for different averaging periods and return periods of the North Caspian Sea region are given in Tables 1.2 and 1.3 [6].

Table 1.2. Extreme minimum dry air temperature in Celsius degree [6]

Return Period Years	Averaging Period (hours)						
	10 min	0.5	1	3	6	12	24
1	-23.62	-23.52	-23.43	-23.15	-22.73	-21.61	-19.74
5	-27.39	-27.27	-27.17	-26.85	-26.36	-25.06	-22.89
10	-29.04	-28.92	-28.81	-28.47	-27.95	-26.57	-24.27
25	-31.23	-31.10	-30.98	-30.61	-30.05	-28.58	-26.10
50	-32.89	-32.75	-32.63	-32.24	-31.65	-30.10	-27.48
100	-34.56	-34.41	-34.28	-33.88	-33.26	-31.62	-28.88

Table 1.3. Extreme maximum dry air temperature in Celsius degree [6]

Return Period Years	Averaging Period (hours)						
	10 min	0.5	1	3	6	12	24
1	34.85	34.24	33.66	32.42	31.73	30.86	29.70
5	37.14	36.49	35.87	34.55	33.82	32.88	31.65
10	38.13	37.46	36.82	35.48	34.72	33.76	32.49
25	39.44	38.75	38.09	36.69	35.91	34.92	33.61
50	40.43	39.72	39.05	37.62	36.81	35.80	34.45
100	41.41	40.69	39.99	38.53	37.70	36.66	35.29

Thus, designing the development concept, the calculation takes into account the minimum and maximum temperatures over a 100-year period.

Table 1.4. Extreme ambient temperature [6]

Maximum ambient temperature, °C	+42
Minimum ambient temperature, °C	-35

Operational monthly air temperature statistics for the North Caspian Sea area are shown in Table 1.5.

Table 1.5. Monthly Statistics of Operational Air Temperature [6]

	Jan	Feb	Mar	Apr	May	Jun	Jul	Aug	Sep	Oct	Nov	Dec	Year
Min.	-30.2	-26.0	-21.8	-3.7	7.7	13.6	15.9	14.6	7.1	-5.8	-17.9	-22.3	-30.2
Mean	-6.4	-6.1	0.9	10.3	19.5	24.6	26.5	26.2	19.6	11.2	3.3	-3.0	10.2
Max.	5.5	7.9	17.2	25.4	34.2	36.5	38.5	37.6	36.7	26.7	14.2	10.0	38.5

Despite the measured temperature range, based on the limiting values of which the design should be carried out, the design temperatures for different equipment may differ, i.e. not all equipment is designed for the extreme temperatures (Table 1.6).

Table 1.6. Ambient Temperatures for Equipment Design [7]

Minimum Ambient Temperature for Equipment Design, °C	-36
Maximum Ambient Temperature for Design of Critical Equipment, °C	+42
Minimum Ambient Temperature for Equipment Installed in Building or Rooms, °C	+5
Air Temperature for Equipment Process Design (non-critical), °C	+35
Air temperature for Checking of Degraded Process & Operation, °C	+40
Average Maximum Ambient Temperature (for HVAC design), °C	+35
Average Minimum Ambient Temperature (for HVAC design), °C	-23
Solar Radiation Temperature, °C	+75

1.2.2. Air humidity

Monthly statistics on relative humidity over the period November 2002-December 2016 is displayed in Table 1.7.

Table 1.7. Monthly Statistics of Relative Humidity (%) [6]

	Jan	Feb	Mar	Apr	May	Jun	Jul	Aug	Sep	Oct	Nov	Dec	Year
Min.	42.6	44.7	16.3	18	13.1	11.3	11.2	10.8	19.4	27	39	40.2	10.8
Mean	83.7	84.3	82.8	71.3	64.3	57.9	57.2	56.6	59.5	68.4	78.9	83.6	70.4

Table 1.7. Continuation

Max	100	100	100	99	97.3	93.8	91.7	92.2	97.4	98.2	100	100	100
-----	-----	-----	-----	----	------	------	------	------	------	------	-----	-----	-----

1.2.3. Wind conditions

Operating wind conditions are entirely measured over the period from November 2005 to December 2016.

The wind rose illustrates the distribution of 10 min mean wind speed by direction for the all-year condition. Figure 1.3 is a visual representation of the wind data. Note the length of each arm represents the frequency of wind occurrence in that sector, and the width/color of the bar represents the strength of the wind.

The data, presented is in parts per thousand, shows that a maximum wind speed of >14 m/s is expected for all directions except for the region between SSW to SSE where the maximum winds <12 m/s. Figure 1.3 also shows that, as the wind speed increases, the frequency of those events decreases. Winds are infrequent from the sectors SSE through SSW [6].

The data obtained as a result of measurements of wind directions and speeds are also used for extrapolation to derive the extreme values of wind speed during different return periods (Table 1.8).

Extreme wind speeds for averaging periods greater than 1 hour are estimated, as shown in Table 1.9.

Table 1.8. Extreme Wind Criteria for Field A [6]

Return Period	Offshore Extreme Wind Speed at 10 m ASL, m/c		
	10 min. Mean	3 sec. Gust	1 hr. Mean
1 year	21.3	26.8	19.8
5 years	24.2	31.1	22.3
10 years	25.4	32.9	23.3
25 years	26.9	35.4	24.6
50 years	28.1	37.2	25.6

Table 1.8. Continuation

100 years	29.2	39.0	26.5
-----------	------	------	------

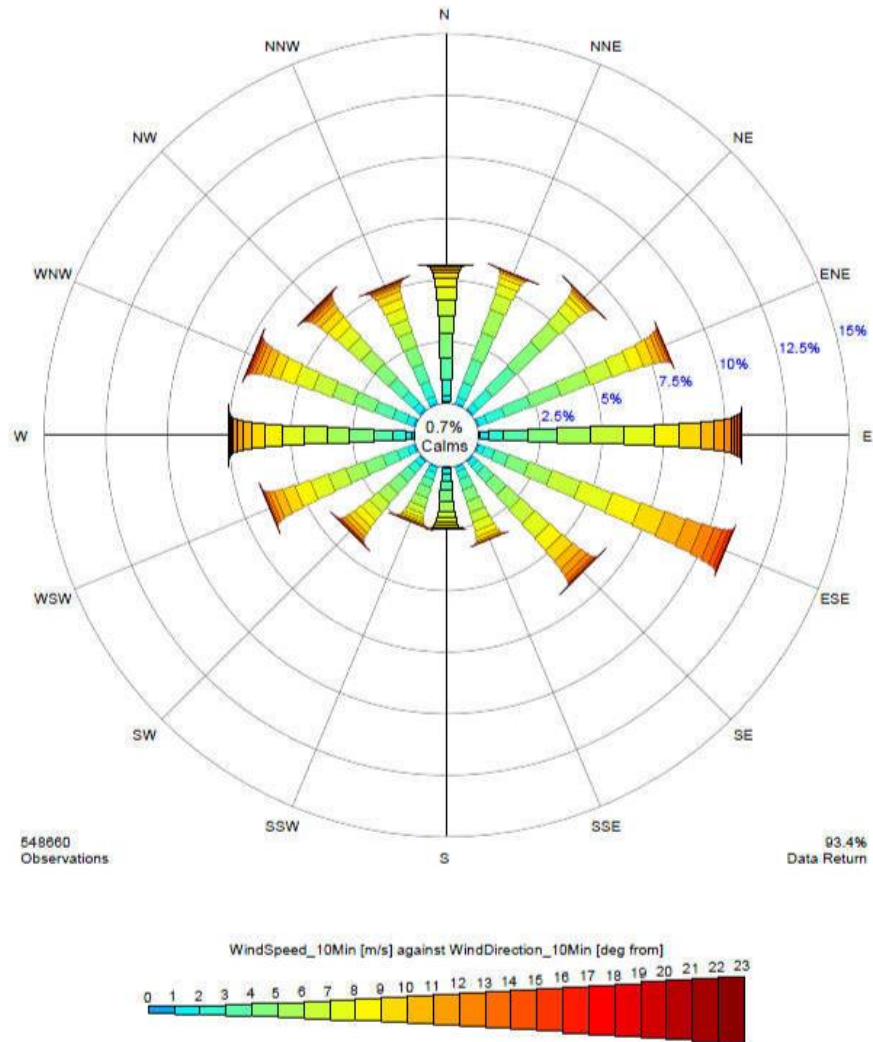


Figure 1.3. Offshore Wind Rose for Field A [6]

Table 1.9. Mean wind speed – Ratios for Alternative Averaging Periods (According to ISO 19901-1) [6]

Averaging Time, hours	Multiplying Factor
1	1.00
3	0.97
6	0.93
12	0.87
24	0.80

A 3-second wind gust will determine the maximum static wind load on individual members; a 5-second wind gust to be applied for maximum total loads on structures whose maximum horizontal dimension is less than 50 m, and a 15-second wind gust for the maximum total static wind load on larger structures [6].

1.3. Hydrological conditions

Based on annual measurements of the water level in the northern basin of the Caspian Sea, it was found that significant sea-level fluctuations can subsequently cause serious problems related to logistics since the general trend of fluctuations was a drop in water level in the Northern region of the Caspian Sea. This trend is shown in Figure 1.4. Accordingly, it was necessary to create mathematical models that would predict sea level during the field A exploitation in the North Caspian region.

A study was carried out by BMT Argoss, using Water Balance Model (WBM), which predicted Caspian Sea Level (CSL) changes by first estimating the volume of water entering and leaving the Caspian each year [7]. Water enters the sea via surface runoff (primarily from the Volga River) as well as through sea-surface precipitation. There is also a small amount of groundwater inflow. Water leaves the sea mostly by sea-surface evaporation, with a small quantity flowing into the Kara-Bogaz-Gol (KBG) [7].

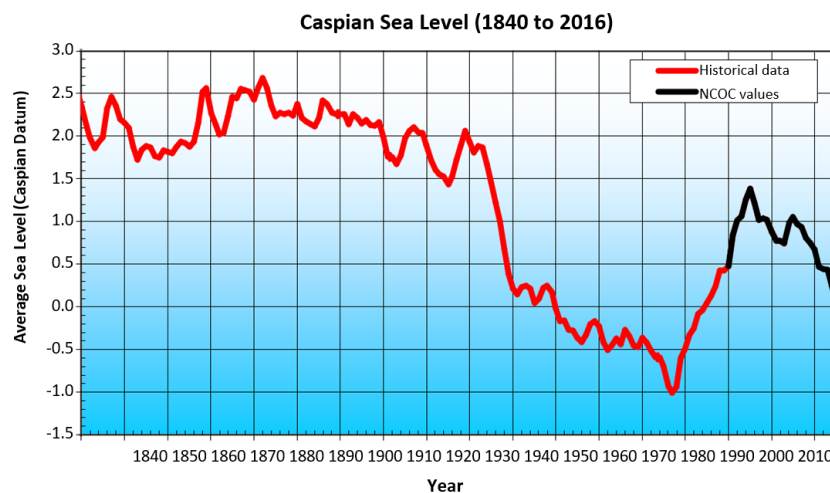


Figure 1.4. Annual mean Caspian Sea Level [7]

Future predictions for the main water balance components are estimated from an ensemble of Global Climate Models (GCMs) [7]. These models predict sea-surface

precipitation and evaporation directly. They also predict precipitation and evaporation over the Caspian drainage basin, but not river runoff. BMT Agross developed a rainfall-runoff model of the Caspian basin to estimate river runoff as a function of precipitation and evaporation. Humans affect the rivers flowing into the Caspian, so predictions of anthropogenic (human) effect are also necessary. GCM predictions of water balance components are bias corrected to match the distribution observed over recent decades yielding a range of future CSL scenarios. Table 1.10 displays changes in mean CSL as a probabilistic model (see also Figure 1.5).

Table 1.10. Probabilistic Annual Mean CSL Forecast (m) [7]

	1%	5%	10%	25%	50%	75%	90%	95%	99%
2020	-0.94	-0.69	-0.56	-0.34	-0.09	0.15	0.37	0.50	0.75
2021	-1.13	-0.84	-0.68	-0.43	-0.14	0.15	0.40	0.56	0.85
2022	-1.31	-0.98	-0.80	-0.51	-0.19	0.14	0.43	0.61	0.93
.....
2055	-7.17	-5.73	-4.97	-3.69	-2.26	-0.84	0.45	1.21	2.65
2060	-8.24	-6.59	-5.72	-4.25	-2.62	-0.99	0.48	1.36	3.01
2065	-9.14	-7.33	-6.36	-4.74	-2.94	-1.15	0.47	1.44	3.26

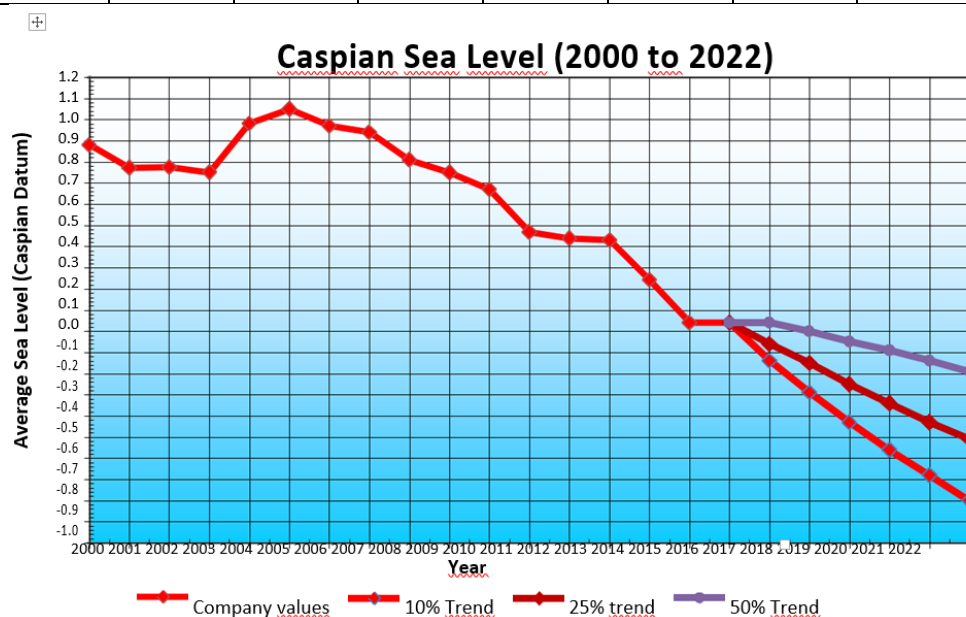


Figure 1.5. CSL Forecast according to GCM Model [7]

Also, the water level of the Caspian Sea, in particular the Northern shelf of the Caspian Sea, can vary seasonally, depending on the directions of waves in a given area

of the sea. Surge is principally induced by the action of wind on the sea surface. Through surface friction, water is blown downwind. Consequently, when the wind is blowing from the SW or W, water is blown into the NE Caspian causing an upsurge, and conversely when the wind blows from the NE or E, water is blown out of the NE Caspian causing a down-surge. Note that moderate winds blowing for sustained periods from the same direction can induce the most significant surges [7].

Table 1.11. Extreme Surge Levels (relative to CSL) [7]

Return period	Field “A” area	
	Positive surge, m	Negative surge, m
1 year	0.94	-1.24
5 years	1.28	-1.80
10 years	1.47	-2.07
25 years	1.77	-2.46
50 years	2.04	-2.77
100 years	2.35	-3.10

1.3.1. Wave conditions

In the northern Caspian, the waves are almost exclusively locally generated as a consequence of the relatively short fetches and the shallow water. Propagation of swell waves from the south is restricted by the shallow water at The Saddle. As a consequence, wave heights are not large, but the short period, steep seas can make working conditions difficult. The extreme wave heights are generally limited both by the fetch and available water depth so that the wave regime can change significantly across the area, with the largest waves typically in the deepest water. Increased water levels during a positive surge will sustain larger waves than would be possible during periods when no surge is present. Although the highest wave from an operational point of view is mainly from the west and northwest, then 10-yr and 100-yr design waves are from the west or southwest (Table 1.12 and Figure 1.6) [8].

Table 1.12. Extreme wave heights and peak periods [8]

Return Period (years)		Sector							
		N	NE	E	SE	S	SW	W	NW
1	H _S	0.85	0.89	0.95	0.93	1.11	1.36	1.35	0.93
	T _P	4.19	4.24	4.32	4.30	4.54	4.83	4.82	4.30
5	H _S	1.07	1.11	1.18	1.16	1.39	1.70	1.69	1.16
	T _P	4.48	4.54	4.63	4.60	4.85	5.16	5.15	4.60
10	H _S	1.17	1.22	1.30	1.27	1.52	1.86	1.85	1.27
	T _P	4.60	4.66	4.75	4.73	4.99	5.31	5.30	4.73
25	H _S	1.24	1.29	1.38	1.35	1.62	1.98	1.97	1.35
	T _P	4.69	4.75	4.85	4.82	5.08	5.41	5.4	4.82
50	H _S	1.28	1.34	1.43	1.40	1.67	2.05	2.04	1.40
	T _P	4.74	4.80	4.90	4.87	5.14	5.47	5.45	4.87
100	H _S	1.32	1.38	1.47	1.44	1.72	2.11	2.10	1.44
	T _P	4.78	4.85	4.94	4.91	5.18	5.51	5.50	4.91

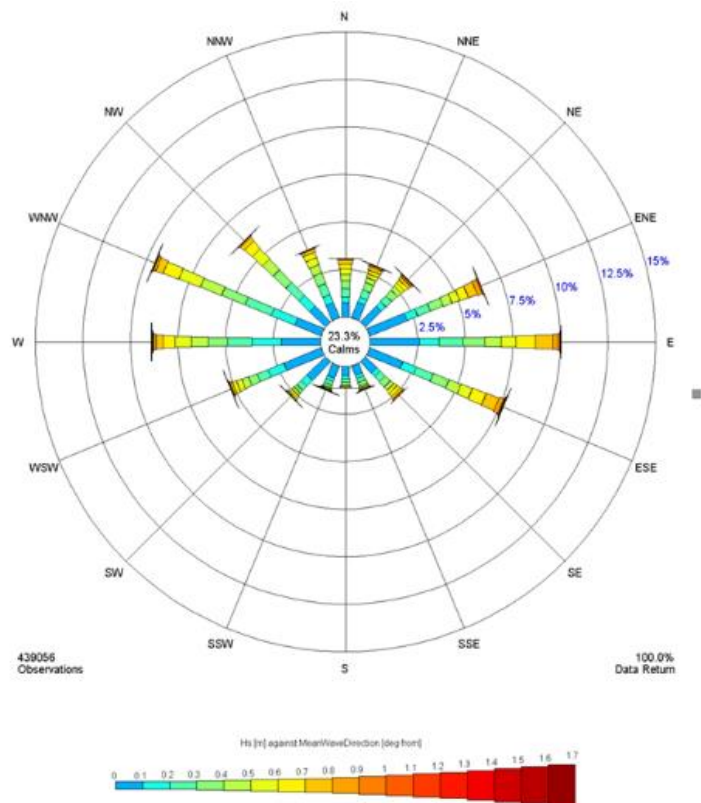


Figure 1.6. Rose plot of H_S and the mean wave direction [8]

1.3.2. Currents

Currents in the Caspian are generally weak and do not show a pronounced periodicity. In the Northern part of the Caspian, currents are more closely related to wind, although there is an underlying clockwise circulation in the eastern region and a general southerly movement across ‘The Saddle’ due to the high freshwater inputs from the Volga, and to a lesser extent the Ural. Currents are dominantly wind-driven; similar to surges and waves, increases in current speed are strictly correlated to an increase in wind speed. As a general rule, the current flows away from the wind blowing direction, although this is often considerably modified due to local topography. Current directions typically change through the passage of a storm, with currents initially flowing in a similar direction to the wind. As the storm progresses, current directions can change and under extreme conditions flow in the opposite direction to which the wind is blowing. The high current speeds included within the criteria will tend to be of short duration [8].

Extreme current speeds have been determined based on 21 months of current data collected nearby Field “A” during several deployments in the period 1997-1998 and 2003-2009. The current profile can be described with a 1/7th power law curve (Table 1.13).

Table 1.13. Current speed [8]

Sea depth, m	100 year current speed, m/s	10 year current speed, m/s	1 year current speed, m/s
3.60	0.80	0.70	0.59
3.20	0.79	0.69	0.58
2.80	0.77	0.68	0.57
2.40	0.75	0.66	0.56
2.00	0.74	0.64	0.54
1.60	0.71	0.62	0.53
1.20	0.68	0.60	0.50
0.80	0.65	0.56	0.48

Table 1.13. Continuation

0.40	0.58	0.51	0.43
0.04	0.42	0.37	0.31

The annual current probability distribution for ice-free water is displayed on rose plot (Figure 1.7).

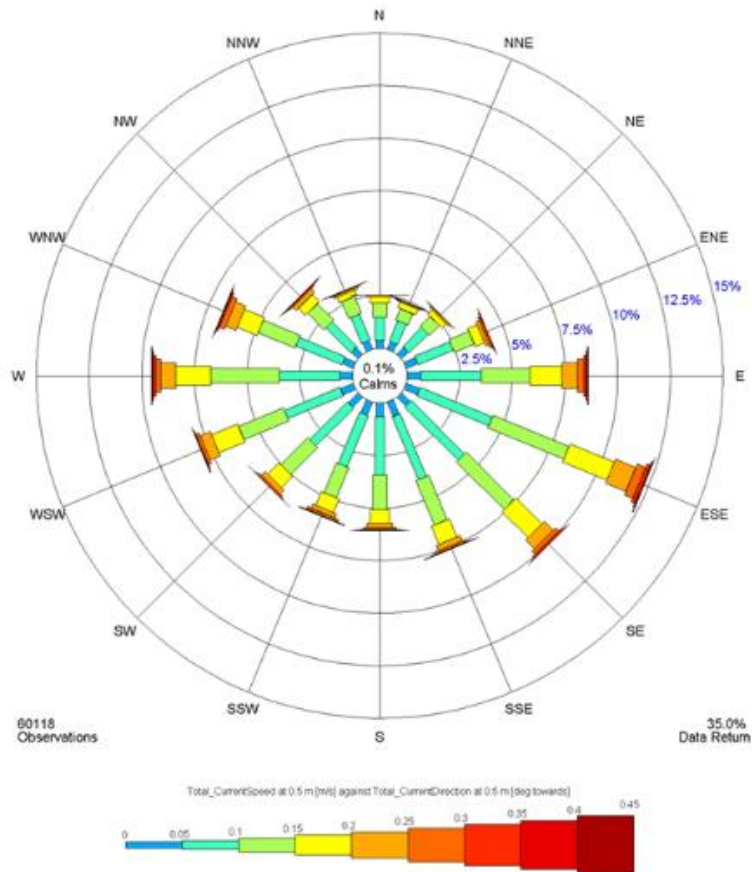


Figure 1.7. The annual rose plot of all measured currents [8]

1.4. Soil conditions at Field “A” location

At the top of the soil profile, a thin layer of soft clay and silt is observed, which extends to a depth between 0.8 m and 1.4 m below the seabed. Towards the south-west of the site, the soft clay largely wedges out and is replaced by loose silica sand. Below the soft clay a very dense, silty silica sand occurs, which may reach a maximum thickness of 4.8 m. Gypsum crystals are commonly observed in the sand. The subsequent layer occurring lower till 10.7 m is an interbedded very silty silica sand (Table 1.14) [9].

The occurrence of gypsum in the sediments is also considered as a stratigraphical marker related to evaporation in very shallow water and mudflat conditions.

Table 1.14. Seabed data [4], [10], [11]

Parameter	Unit	Value
		Silty sand
Wall friction angle, ϕ_w	degrees	18
Internal friction angle, ϕ	degrees	42
Friction coefficient (ice-soil), μ	-	0.4
Soil density, ρ_s	kg/m ³	1750
Seabed slope	radians	0.000059

1.5. Ice conditions

Ice formation in the North-Eastern Caspian Sea usually starts in early December. The level ice thickness gradually increases to typically 50cm during the end of the ice season. First melting of ice is commonly observed in early March; the Caspian area is usually ice-free from the end of March onwards. The wind largely controls the ice movement in the Caspian Sea. For low wind speeds, the ice is mostly stationary. Movement of ice only occurs when the wind speed exceeds a certain threshold, which depends on wind direction, surge levels, as well as the degree of grounded ice in the area. Due to the shallow water conditions, grounded ice rubble is frequently formed against structures and ice barriers, during ice movement events. This ice rubble can be a significant hazard to operations performed from fixed installations in the North-Eastern Caspian. Minimum and maximum ice periods for the North-Eastern Caspian, mean ice thicknesses for various return periods are displayed in Tables 1.15 and 1.16 respectively [8].

Table 1.15. Minimum and maximum ice periods for the North Caspian Sea [8]

	Return Periods (year)					
	1 year	5 years	10 years	25 years	50 years	100 years
Minimum season	105	88	78	63	52	40
Maximum season	105	122	132	147	158	170

Table 1.16. Extreme level ice thickness [8]

	Return Period (year)					
	1 year	5 years	10 years	25 years	50 years	100 years
Thickness, m	0.42	0.57	0.64	0.73	0.79	0.85

In many cases, the ice will be rafted, and ice ridges are formed the design values of rafted ice thickness and the consolidated layer thickness of an ice ridge, which decrease with horizontal dimension (Table 1.17).

Table 1.17. The estimated 100-yr thickness of rafted ice [8]

	Horizontal dimension (m)			
	5	20	50	100
Rafted ice thickness (m)	2.0	1.6	1.2	1.15

1.5.1. Ice ridges

In general, the intensity of the ridges increases from the coast to the outer boundary of the ice sheet, from west to east, and a decrease in its intensity begins from the shear zone. Moreover, ridges are located along the Ural furrow, where the water depth exceeds 8–9 m (Fig. 1.8). The maximum observed ridge height is 6 m, but usually

the height varies in the range of 2-3 m. The keel crest can exceed 12 m, and the average keel depth is up to 3-6 m [4].



Figure 1.8. Ice ridges location in the North Caspian Sea [4]

2. The development concept for Field “A”

Field A is situated in the Caspian Sea offshore Kazakhstan 80 km south of Atyrau. The North Caspian can be characterized by shallow water (3-5 m) and harsh environmental conditions resembling Arctic ones during winter. Field reserves are estimated at 38 billion barrels (P90). Recoverable reserves are estimated at 13 billion barrels of oil [11].

The development of this field embraces a vast number of difficulties, which together create unique conditions for its development (Fig. 2.1), requiring the use of modern technologies. These difficulties are as follows [11]:

- The high concentration of hydrogen sulphide with high associated pressure. Loss of containment of toxic fluids represents a potential risk of death to any personnel exposed, and loss of containment from a high-pressure gas source could potentially extend several kilometres downwind from the source of the release;
- In future, when Gas injection will be in operation, there will be an additional HP source of H₂S gas from a remote location. This will have a considerable impact, owing to the additional number of connections and valves involved;
- The wells are deep, and the high-pressure reservoir has complex geology;
- Harsh environmental conditions, specifically thick moving sea ice, raises Escape, Evacuation and Rescue (EER) Operational and Logistical difficulties for the offshore workforce. Shallow water environment with potential long-term sea-level fluctuations and short-term storm-induced sea level surges and retreats complicates development planning;
- High-pressure pipeline containing sour inventories, including a significant number of multiphase pipelines with associated issues/requirements, such as waxing and hydrate formation requiring storage and transfer of large quantities of wax inhibitor and Methanol;

- Extreme temperature variations between summer and winter. Restrictions of water and waste discharge into the Caspian Sea;

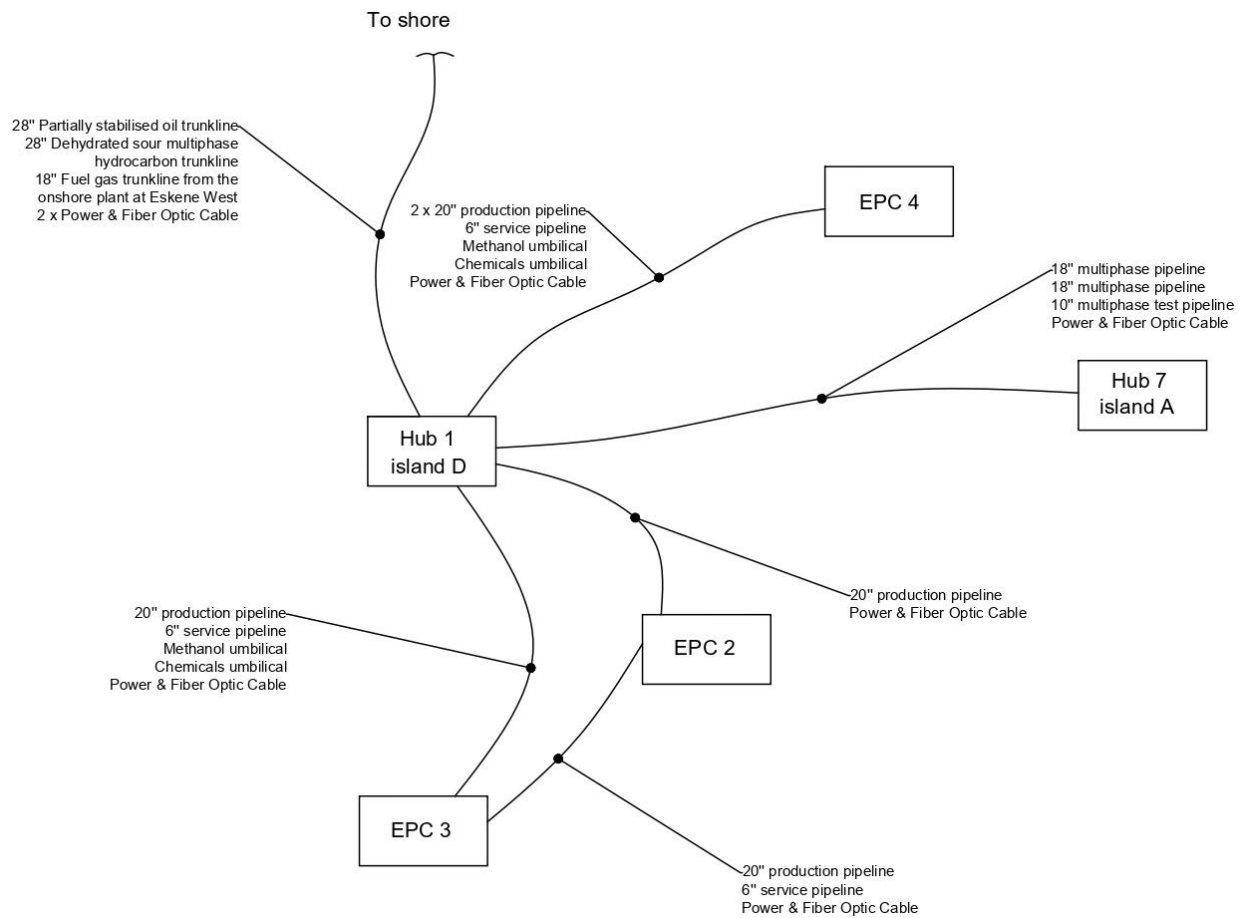


Figure 2.1. Development sketch of Field A

In addition to the main production pipelines, EPC2 is connected to EPC3 and then to HUB 1 by a 6” service line that will be used to depressurize, purge and drain the facilities back to Hub 1. EPC4 is connected directly back to Hub 1 by a 6” service line. The production and service pipelines exit the EPC2, EPC3 and EPC4 islands through catenary risers. Power and communications are provided via a combined power and fiber optic cable. For EPC4, a single combined power and fiber optic cable is provided. The connection is also provided via a fibre-optic cable in the chemical and hydraulic fluid umbilicals. Chemicals and hydraulic fluid are provided by an umbilical running from Hub 1 to EPC3 and EPC2. A second umbilical follows the same path carrying only methanol. Two umbilicals, with the same configuration, provide chemicals from Hub 1 to EPC4 [12].

The primary formation fluid treatment is carried out on island D. The main goal of offshore fluid treatment is to separate the formation fluid into partially stabilized oil and a multiphase fluid consisting of acid gases (H₂S, CO₂, CH₄) and gas condensate. Oil and multiphase flow are transported using two main pipelines 100 km long to onshore hydrocarbon treatment plants for their full process handling [11].

2.1. Reservoir conditions

Table 2.1. Field A reservoir conditions [11]

Reservoir oil-water contact, m	4570
Reservoir top depth, m	3800
Reservoir pressure, MPa	77.7
Reservoir temperature, °C	98
Porosity (average), %	6-8
Permeability, md	0.1-2
Rock type	carbonate
Pore volume, m ³	1.6*10 ⁹

Table 2.2. Field A formation fluid characteristics [11], [13]

Stock tank oil density, kg/m ³	815
Reservoir liquid viscosity, cp	0.19-0.24
Saturation pressure (T=98°C), MPa	28.4
Gas to oil ratio, m ³ /m ³	510
API value	42

Table 2.3. Formation fluid material balance [11]

Component	Fraction, % mol
N ₂	0.934
CO ₂	5.120
H ₂ S	15.161
C ₁	47.302
C ₂	7.361
C ₃	4.113
C ₅	0.902
C ₆	1.348
C ₇	1.536
C ₈	1.702
.....

2.2. Offshore and onshore technological flowsheet

The Offshore Processing Hub (D-Island) consisting of 7 production wells, four injection wells converted from production to injection as of Q2 of 2017. To allow for disposal of the additional gas throughput from the upgraded RGIs (Raw Gas Injection), two existing production wells on D-Island were required to be converted to injection wells; giving a total of six (6) injection wells on D Island.

As a part of production increase project, two production wells on EPC 3 are converted to injectors, two production wells are converted to 1 injector on EPC 2. (EPC 2 - 6 production wells, 2 injection wells; EPC 3 - 4 production wells, 2 injection wells, EPC 4 - 7 production wells) [12].

The extracted reservoir fluid from all producing islands is transported to island D for the initial treatment and separation of the fluid into oil and gas, as shown in Figure 2.1. Products from all islands are collected in a manifold (Fig. 2.2), which, in turn, directs fluid to the two separation lines. Each line consists of high, medium and low pressure separators. Gas separated from the oil in a high-pressure separator passes

through a gas dehydration unit and is sent to compressors for its further injection into the reservoir to maintain reservoir pressure. In the subsequent stages of separation, the released gas is pumped into the main pipeline and transported to land for further handling. Partially stabilized oil with a water content of not more than 2%, respectively, is transported via trunk pipeline onshore [14].

The onshore oil, gas and sulfur treatment plant consists of 2 lines for gas handling with a capacity of 8.6 million standard cubic meters per day, 3 lines for oil treatment with a capacity of 165,000 barrels per day, and 2 production lines for sulphur production with a capacity of 1000 tons per day (Fig. 2.3).

Trains for oil treatment consist of separation units and heat exchangers, oil dehydration unit working on the principle of alternating electric fields application, oil stabilizer unit for oil fractions separation. Meanwhile, simultaneously with the dehydration, stabilization and mercaptan removal processes, there is a two-staged desalination process (Fig. 2.3) [14].

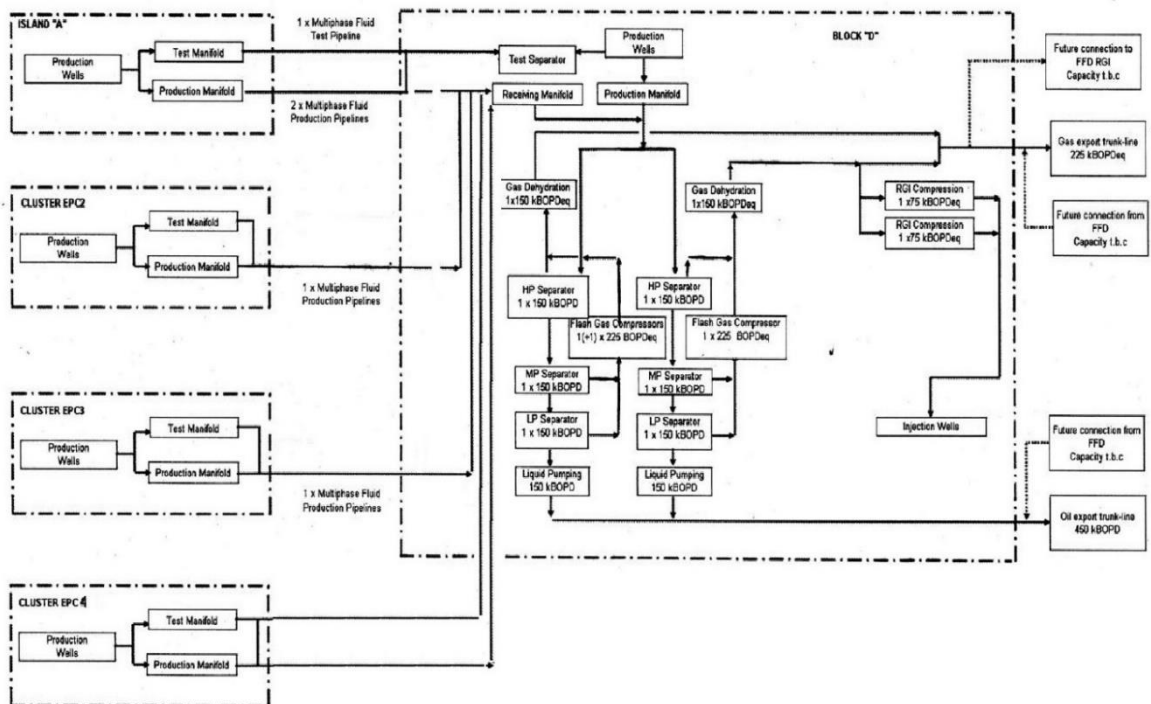


Figure 2.2. Offshore technological flowsheet [11]

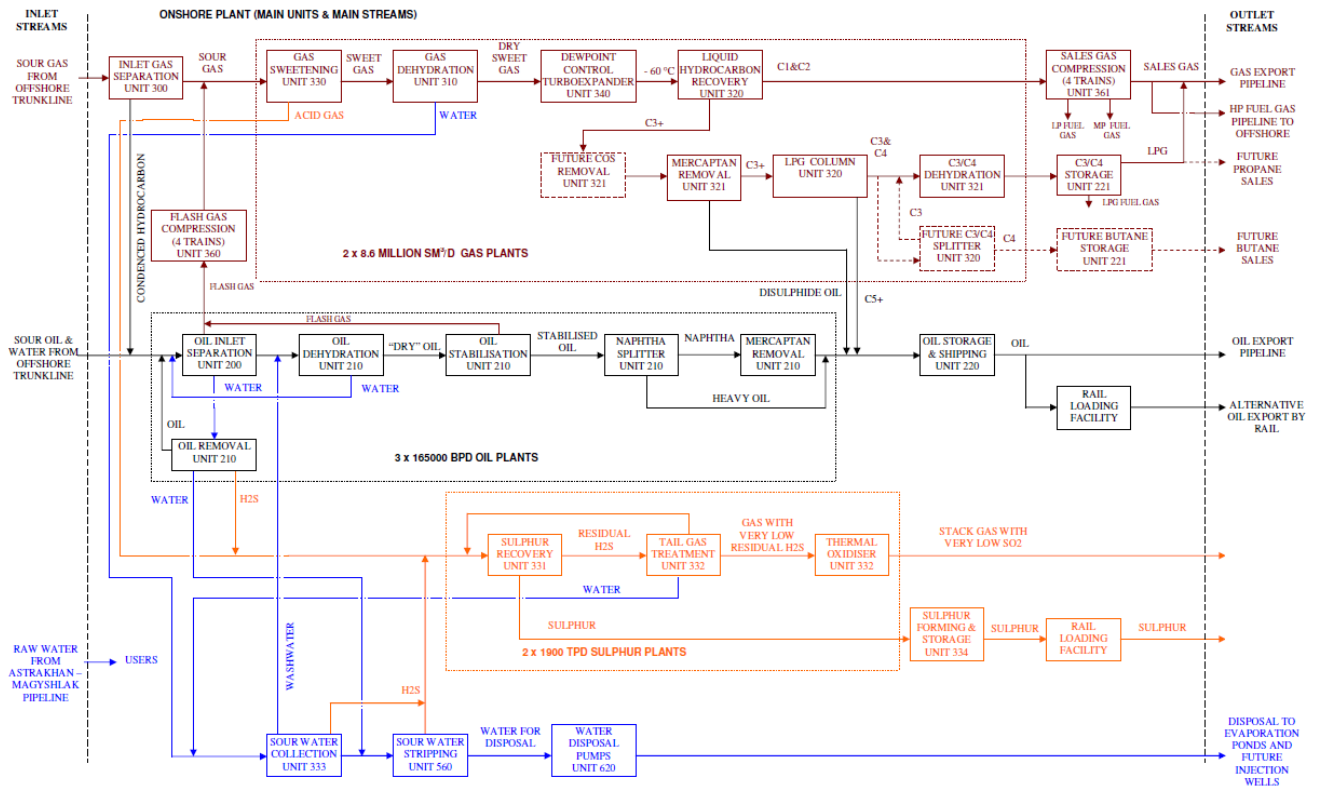


Figure 2.3. Onshore processing plant flowsheet [14]

Before entering the gas-processing lines, the raw gas passes through slug catchers; the gas enters the separator, where, after heating the gas to 52 °C, any droplet liquid is removed. Hydrogen sulfide and carbon dioxide are removed from the gas stream in absorbers, the active agent of which is diethanolamine (DEA). Hydrocarbon gas overheats to a temperature above the dew point. HC gas with water vapour passes through molecular sieves made of a material that adsorbs water vapour. Derived HC gas expands on the turbine blades to achieve cooling effect, C_nH_{2n+2} ($n=3, 4, 5\dots$) condense, furthermore they are headed to the LPG production units [14].

3. Background and future trends in the sphere of offshore CO₂-EOR

The experience of the current project thesis is based on a paper by the Carbon Sequestration Leadership Forum [3], where some barriers to offshore CO₂-EOR worldwide implementation were outlined. Despite all the advantages of such an operation, technological and economic obstacles should be overcome to enable the CO₂-EOR process [15]. The main barriers revealed for projects are [3]:

- high CAPEX necessary for the offshore vessels and other production installations upgrading;
- loss of cash flow during modification;
- shortage of carbon dioxide for significant oil recovery rate increase as a result of the Enhanced Oil Recovery process;
- the CO₂ has to be transported to the offshore site via ship or pipeline, these methods establish a range of technological and economic problems, as carbon dioxide is a highly corrosive substance.

The possibility for a combination of EOR method and carbon dioxide sequestration makes the concept attractive and results in further investigation and development of the pilot projects.

According to the report of the Carbon Sequestration Leadership Forum (CSLF) [3], there is the only one ongoing large-scale offshore CO₂-EOR project, this is in Brazil, however, a number of small-scale pilots has existed; 1 – in Vietnam and 5 – in the Gulf of Mexico. Various approaches were undertaken for each of these projects to avoid the primary problems listed above.

The only successful CO₂-EOR concept was applied in the development of Lula Field located 230 km from the coast of Brazil in 2200 m water depth. Pipeline or ship transportation of carbon dioxide was not required as the field possessed the CO₂ content of around 11% in the associated gas. Carbon dioxide was separated through membranes on the topside of the floating production storage and offloading (FPSO) unit, as it was the only process defined that could withstand a wide range of CO₂ content during the

field production life. As the carbon dioxide amount was not sufficient for full-scale implementation, a decision was adjusted for either an injection of CO₂-rich mixture of gases or water-alternating gas (WAG) injection. Thermobaric reservoir conditions were favorable for a miscible displacement of oil by carbon dioxide. Despite no significant operational challenges have been defined, the applied concept had some drawbacks [15]:

- additional expenditures were required for procurement of high corrosion resistant injection riser to carry out carbon dioxide injection;
- powerful compressors, whose high energy consumption resulted in additional CO₂ emissions were installed to increase the pressure of injected gas above the reservoir pressure.

A small-scale CO₂-EOR test was performed on the Rang Dong Oilfield situated 135 km off the coast of Vietnam. During the project, about 111 tonnes of carbon dioxide were pumped down into a production well to assess the short-term increase in oil recovery. Despite successful results, such as incremental oil production, water-cut diminishing, and oil viscosity reduction, the feasibility study revealed that transportation of CO₂ by pipelines from two nearby sources: a CO₂ impregnated gas field and a fertilizer plant, to be unprofitable for the project. Moreover, modernization of the platform topside equipment for handling and reinjection of CO₂ was an additional cost driver. Thus, hydrocarbon gas injection was considered as possessing better NPV despite the lower amount of swept oil [15].

In the North Sea, several case studies both in the UK and Norwegian sectors were conducted to evaluate the economic and technical feasibility of CO₂-EOR implementation [15]. Shipping and pipeline were considered as the major types of CO₂ transportation. Despite the fact that the analysis recognized a significant oil recovery rate comparative to a conventional waterflooding (above 3000 million barrels of incremental oil production from all the fields on the UK continental shelf and 4.1% of Stock Tank Oil Initial in Place (STOIIP) from Gullfaks Field), both sides concluded that profit from the additional hydrocarbons that would have been produced would not

offset the cost of carbon dioxide purchase/capture and transportation. Therefore, CO₂-EOR can be economically viable only in case of a near-zero delivery price [15].

Aker Solutions have previously done several studies related to CO₂-EOR concept in the North Sea. This concept is based on capturing CO₂ from an onshore power plant and pumping the gas in a pipeline to the offshore facilities. The gas would be further injected into the various injectors from the offshore satellites. The main modifications to the facilities were limited to injection arrangements for the gas pumps and injection manifolds. The removal of CO₂ is planned to take place at an onshore power plant, so no treatment facilities have been included in this scope. The CO₂ being degassed from the various separation stages poses a significant increase in gas load on the equipment. The equipment is said to have sufficient capacity to handle the increased gas rates but will require replacement of steel/cladding to withstand the corrosive nature of the gas. The described concept is illustrated on Figure 3.1 [3].

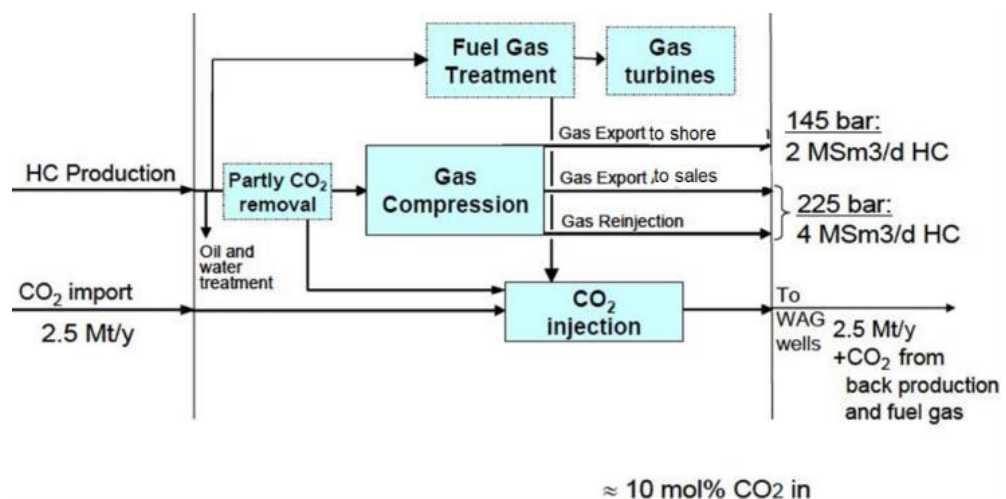


Figure 3.1. Concept suggested by Aker Solutions, including existing and new infrastructure [3]

Two methods of separation are envisaged for the handling and extraction of carbon dioxide: absorption employing amine-containing substances and membrane separation. Absorption is selected as the more preferred carbon dioxide separation process. This choice was made despite the large size and weight of the entire system compared to membrane separation. The reason was a better understanding of the absorption process via amine-containing substances in comparison with membrane separation. Based on this study [3], conclusions were drawn regarding the carbon dioxide separation process:

- For relatively small volumes of carbon dioxide, an absorption-type separation based on amine-containing absorbents is preferred due to the robust process and the higher quality of separation;
- Membrane separation is preferable in conditions of limited footprint, as well as in terms of significant fluctuations in the rate of carbon dioxide.

Several pilot projects in the Gulf of Mexico were operated at the shore near Louisiana's coast. In these projects, CO₂ was transported to the site by vessels where carbon dioxide was at a compressed state. Results of testing were considered successful, showing an increase in oil production [3].

The same results were obtained during CO₂-EOR investigation in the Persian Gulf and in the South China Sea [4], where the reservoir illustrated favorable light oil compositions (high value of API), high porosity and permeability, low water depth [3].

Hence, it can be summarised that successful offshore CO₂-EOR projects were conducted in near-shore regions allowing to diminish the cost for CO₂ transfer. Besides, remote oilfields possessing high carbon dioxide content in the formation fluid was also economically and technically viable for CO₂-EOR.

To provide the opportunity for more offshore projects to overcome the challenges described in the previous background, several options were proposed [15]:

- Subsea treatment of CO₂ for re-injection;
- Combination of subsea production, power generation and CO₂-EOR;
- Supply chain alteration.

The first option was proposed by Aker Solutions (Figure 3.2). According to this concept, the well stream is separated into liquid and gas in a gas/liquid separator, the liquid is carried out to an oil/water separator; afterwards the water is injected into the reservoir for pressure maintenance. Meanwhile, the gas is headed to a separator to separate the carbon dioxide from the hydrocarbon gases before CO₂ compression for injection purposes. The stream of the carbon dioxide is cooled at the compressor discharge to turn the CO₂ into a dense phase. Hydrocarbon gas with some unseparated content of carbon dioxide and oil-remaining water mixture are sent to the treatment

facilities. The root problem in the subsea solution is the technology for hydrocarbon gas and CO₂ handling, no one state of the art process is appropriate for subsea utilization.

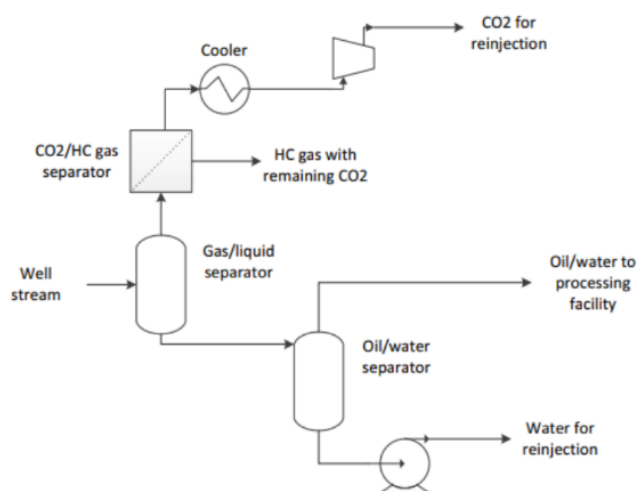


Figure 3.2. Critical elements of a typical treatment concept for CO₂-EOR [15]

An alternative concept being a combination of subsea production, power generation and CO₂-EOR was also suggested by Aker Solution (Figure 3.3). According to this concept, extracted gas is burnt in a chemical reaction with oxygen in a subsea power plant. The product consists of CO₂ and water which are injected simultaneously into the formation as a water-alternating gas process, while generated electricity is utilized as a power source for offshore facilities. Except for economic improvements, the current concept incorporates significant technical advantages [15]:

- Cold seawater provides natural cooling, eliminating the necessary post-combustion facilities for the flue gas;
- Short distances to the wells eliminate high expenditures on large infrastructure construction.

To satisfy the feasibility requirements for remote areas, pipeline CO₂ transportation can be replaced by shipping. Nowadays in Europe, transport of carbon dioxide is carried out by ships and barges in a small amount. Analysis confirms that ship transportation is not an obstacle for large-scale CO₂-EOR projects. However, some technology optimization and adjustment are required in offshore loading and offloading operations. These operations may include offloading from the ship utilizing a buoy and offloading through an intermediate offshore storage facility [15].

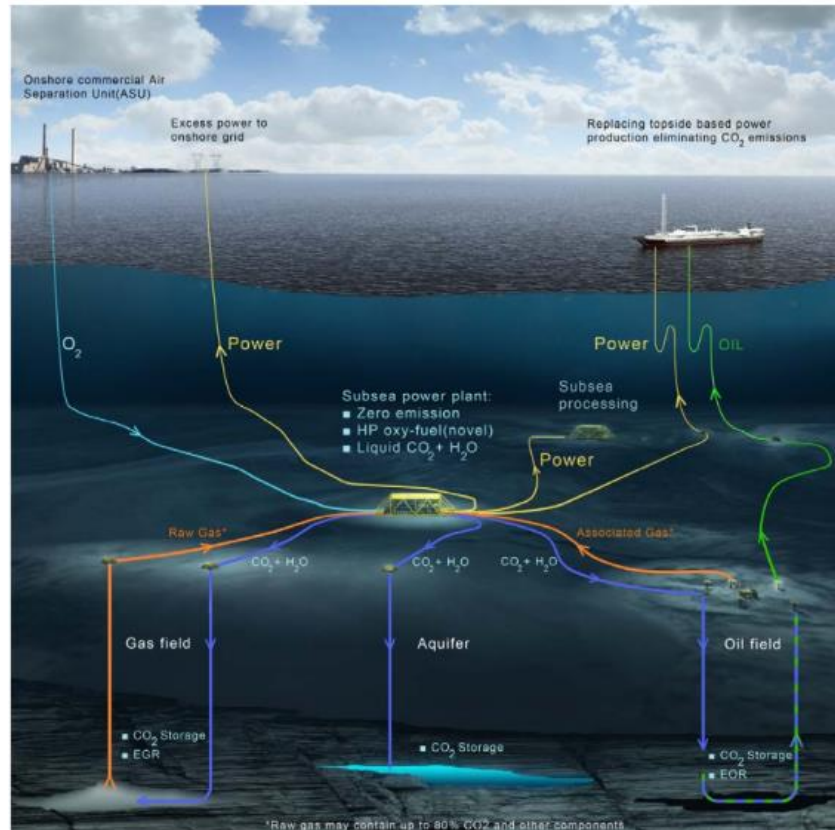


Figure 3.3. Combination of subsea production, power generation and CO₂-EOR [15]

4. CO₂-EOR application approaches for Field “A”

Carbon dioxide injection for enhanced oil recovery purposes (EOR) is a well-known and widespread technology of recovering incremental oil from conventional light, medium and heavy oil reservoirs. Physical phenomena which contribute to an incremental oil recovery are concerned with the reduction of interfacial tension, alteration of wettability of rocks and decrease in oil viscosity, which result in changing of gas/oil mobility ratio. By means of that, CO₂-EOR is able to recover additional 15-25% of Original Oil in Place, to prolong reservoir production life after secondary recovery methods by around 15 years [16]. In terms of EOR CO₂ injection possesses several benefits comparative to hydrocarbon gases usually applied for these purposes in offshore conditions, they are as follows: the minimum miscibility pressure (MMP) compared with the oil pressure is lower than that of other hydrocarbon gases; high density at reservoir conditions; and extracted hydrocarbon gases can be sent to transportation for sales.

The injection of carbon dioxide into the reservoir during the CO₂-EOR process may also have several advantages, depending on the method of applying CO₂ in this process:

- Pure carbon dioxide injection;
- Carbonated water injection.

4.1. Pure carbon dioxide injection

Carbon dioxide is beneficial for increasing oil recovery property; in particular, it possesses the ability to reduce the viscosity of the oil when dissolved in it (Fig. 4.1). Consequently, the interfacial tension between oil and water decreases [17], [18].

The displacing ability of carbon dioxide depends on phase transitions between oil and gas, as well as on the properties of a mixture of carbon dioxide and oil, which, in turn, are largely dependent on reservoir temperature, pressure and oil composition. Two main processes are distinguished: miscible displacement and immiscible displacement [3].

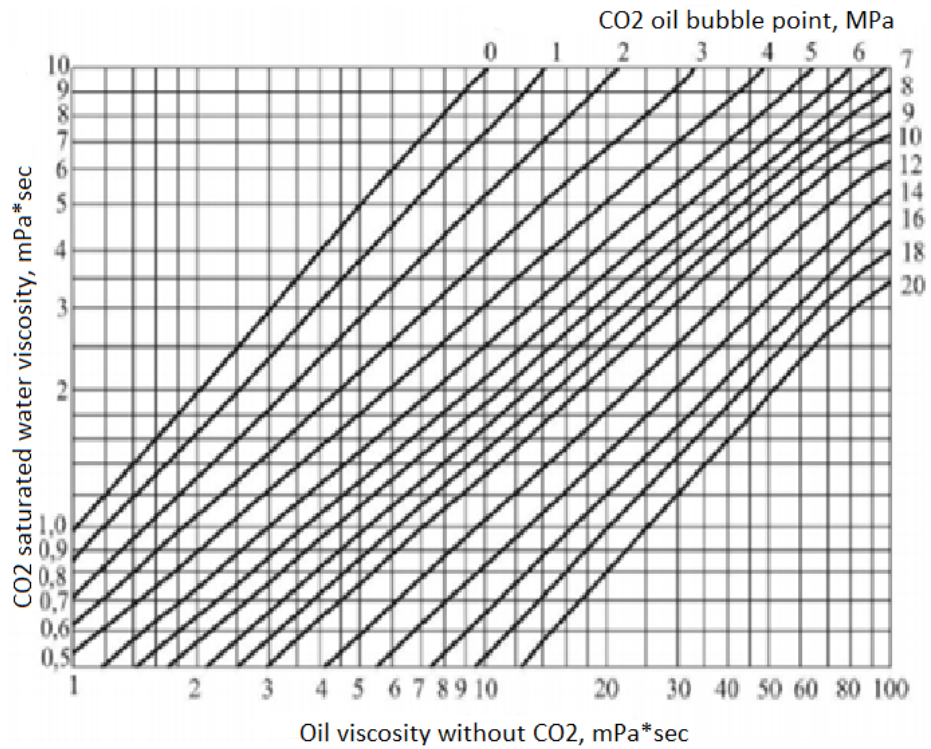


Figure 4.1. Correlation between oil viscosity and CO₂ oil bubble point [19]

Miscible CO₂-EOR is a multiple contact process involving interactions between the injected CO₂ and the reservoir's oil. During this multiple contact process, CO₂ vaporizes the lighter oil fractions into the injected CO₂ phase, and CO₂ condenses into the reservoir's oil phase. This leads to two reservoir fluids that become miscible (mixing in all parts), with favourable properties of low viscosity, enhanced mobility, and low interfacial tension. The primary objective of miscible CO₂-EOR is to remobilize and dramatically reduce the residual oil saturation in the reservoir's pore space after water flooding [3].

Immiscible CO₂-EOR occurs when the insufficient reservoir pressure is available, or the reservoir's oil composition is less favorable (heavier). The main mechanisms involved in immiscible CO₂ flooding are oil phase swelling, as the oil becomes saturated with CO₂; viscosity reduction of the swollen oil and CO₂ mixture; extraction of lighter hydrocarbon into the CO₂ phase; and, fluid displacement. This combination of mechanisms enables a portion of the reservoir's remaining oil to be still mobilized and produced and is commercial in many instances [3].

Pressure determining the type of process described earlier is called minimum miscibility pressure (MMP). The correlation between reservoir temperature, oil composition and MMP is shown on the plot of Mungan, Holm and Josendal (Fig. 4.2).

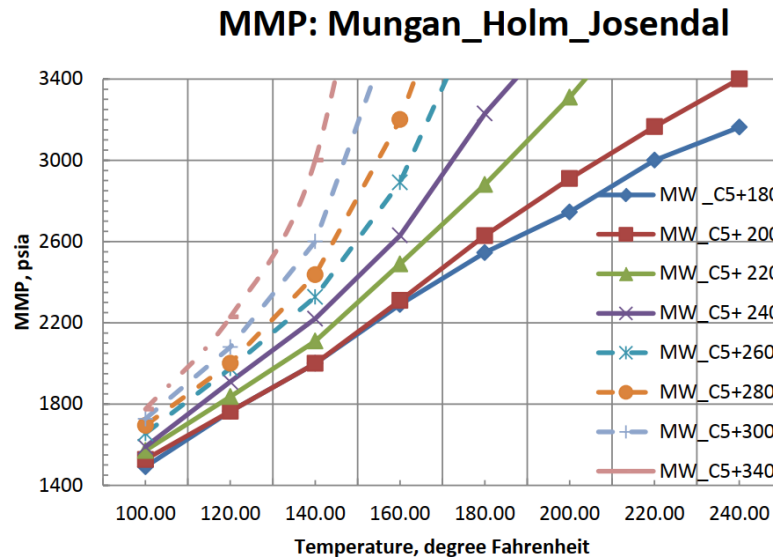


Figure 4.2. Minimum miscibility pressure correlation with a molecular weight of C5+ components and formation temperature [20].

Based on the reservoir data of Field “A” (Table 2.1), as well as on the material balance of the reservoir fluid (Table 2.2), it is highly probable that, when CO₂ is injected into the reservoir of Field A, a mixed displacement process will occur.

4.2. Carbonated water injection

Carbonated Water Injection (CWI) needs less CO₂ concentration comparatively to conventional CO₂ injection for achieving a significant increase in oil recovery. Carbon dioxide required for dissolution in water can be derived from the extracted formation fluid after the separation or from nearby oil and gas fields. High initial pressure makes the capture and processing process cheaper [21].

The possibility of obtaining CO₂ from the formation fluid is of great importance for offshore fields, as it eliminates any transportation systems for CO₂. Furthermore, application of CW allows a CO₂-EOR process for oilfields with a CO₂ content of less than 10% in the formation fluid.

The density of carbonated water is higher than water as a native formation brine. So, CW provides a viable alternative for carbon dioxide storage because of the

buoyancy-driven leakage absence. The density and mobility contrast in CW-Oil system is lower than a CO₂-Oil system and a supercritical CO₂-Oil system; this fact increases sweep efficiency, resulting in more oil extracted and more carbon dioxide sequestered. Displacement efficiency is no more dependent on the minimum miscibility pressure, as the displacement process is controlled by the carbon dioxide mass transfer between CW and oil. The mobility ratio (formula 4.1) decreases as a consequence of oil viscosity diminishing due to the CO₂ mass transfer into the oil [16].

$$M_{w,o} = \frac{\frac{k_{rw}(S_{or})}{\mu_w}}{\frac{k_{ro}(S_{wc})}{\mu_o}}, \quad (4.1)$$

where:

$k_{rw}(S_{or})$ and $k_{ro}(S_{wc})$ – relative water and oil permeabilities, respectively

μ_o and μ_w – dynamic viscosities of oil and water.

The viscosity of water also increases with increasing concentration of carbon dioxide. As pressure increases, carbon dioxide begins to dissolve more actively in water (Fig. 4.3) [2]. According to Figure 4.3, the solubility of carbon dioxide decreases as temperature increases up to 80 °C.

Several studies were conducted in the Malay basin in order to identify how the CO₂ concentration in water affects the oil recovery efficiency [22]. The study was carried out via the following injection series illustrated in Table 4.1 [22].

Table 4.1. CWI series [22]

№	Concentration CO ₂ (vol. %)	Injection Mode	
		Secondary	Tertiary
1	10	CWF	WF+ CWF
2	30	CWF	WF+ CWF
3	40	CWF	WF+ CWF
4	50	CWF	WF+ CWF

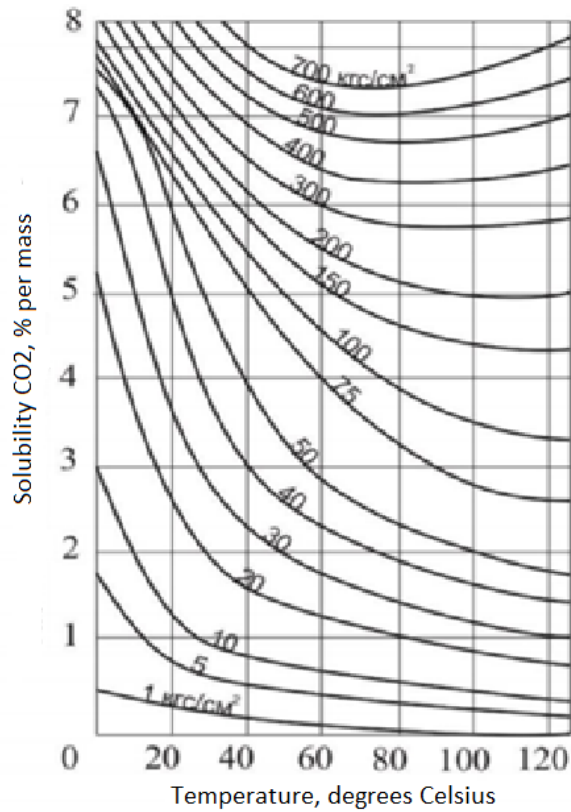


Figure 4.3. Correlation between CO₂ solubility in water and thermobaric conditions [17]

The results of the conducted experiments are illustrated in Table 4.2.

Table 4.2. Carbonated water injection results [22]

	10% CO ₂		30% CO ₂		40% CO ₂		50% CO ₂	
	2 nd	3 rd	2 nd	3 rd	2 nd	3 rd	2 nd	3 rd
Incremental oil recovery, %	5.65	6.61	16.81	10.23	19.52	13.11	28.43	16.23

The conclusions of the experiment are as follows [22]:

- Carbonated water injection increases oil recovery for secondary and tertiary flooding. The higher the CO₂ concentration the greater oil recovery.
- 50% carbon dioxide concentration illustrated the greatest oil recovery improvement; during the secondary mode, it appeared to be 28% while during the tertiary mode, it was 16%.

- Wettability improvements were reached as a result of CO₂ concentration increase (wettability angle diminishing from 62.9° to 58.7° while the carbon dioxide concentration was 0% and 10%, respectively).

At the same time, laboratory experiments conducted by the Ufa Research Institute established that the displacement of oil by carbonized water with a concentration of CO₂ of 5.3% allows an increase in oil recovery by 14% compared to the displacement of distilled water [23].

Thus, this technology requires a relatively small amount of carbon dioxide to significantly increase oil recovery, thereby reducing the cost of procurement and transporting additional volumes of CO₂.

5. Comparative analysis of various CO₂-EOR applications for the particular conditions of Field “A”

5.1. Gaseous CO₂ injection

5.1.1. Oil recovery factor assessment

The critical parameter to evaluate carbon dioxide injection effectiveness is the oil recovery coefficient (ORC). The final ORC value is the sum of the ORC as a result of primary/secondary development methods and the ORC as a result of utilizing carbon dioxide.

$$K = K_1 + K_2, \quad (5.1)$$

where:

K_1 – primary/secondary recovery coefficient,

K_2 – tertiary recovery coefficient.

To assess the applicability of carbon dioxide as a method of increasing oil recovery for field A, two criteria were established in the framework of this model to deal with the initial data uncertainty [24]:

- The API value (density) of the formation fluid should be between 17.5 and 50, as the analysis model is built based on data from fields with an oil density belonging to the specified range;
- Productive reservoir depth should be at least 915 meters. This requirement is justified by the need for sufficient reservoir pressure for miscible displacement. Immiscible displacement is not considered in this model.

The average miscibility pressure (Fig. 4.2) is described by the ratio (5.2) [24].

$$MMP = 15.99 * T * (0.744206 + 0.0011038 * MWC_{5+}), \quad (5.2)$$

where:

MMP – minimum miscibility pressure, psi;

T – formation fluid temperature, °F;

MW C₅₊ - molecular weight of pentanes and heavier oil fractions.

The molecular weight of C5 + can be estimated from the ratio shown in Fig. 5.1 and described by equation (5.3).

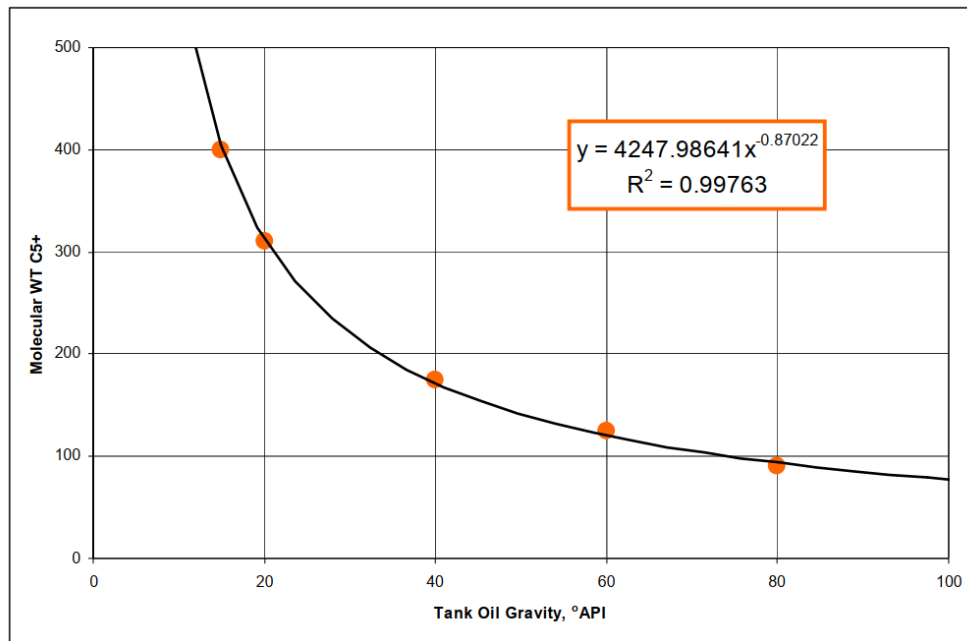


Figure 5.1. The relationship between the molecular weight of hydrocarbons C5+ and the reservoir fluid density [24]

$$MW C_{5+} = 4241.98641 * API^{-0.87022} \quad (5.3)$$

Substituting the API density value shown in Table. 2.2 into (5.3), the molecular weight of Field A hydrocarbons $MW C_{5+}$ is calculated as 164 atomic mass unit.

The minimum miscibility pressure value is calculated using the formula (5.2) through the data in Table. 2.1 and $MW C_{5+}$ values.

$$MMP = \frac{15.99 * 208.4^{\circ}F * (0.744206 + 0.0011038 * 164)}{145} = 21.3 \text{ MPa}$$

Given the magnitude of the reservoir pressure (Table 2.1), it can be concluded that during gaseous CO₂ injection into the reservoir of Field A, a process of miscible oil displacement will occur. Consequently, the reservoir conditions of Field A satisfy this model assumption regarding consideration of miscible displacement.

To determine the relationship between reservoir characteristics and carbon dioxide injection efficiency, data from the 213 fields mentioned above were selected as a proxy model. To estimate the dependence of ORC on reservoir characteristics, a regression analysis was carried out, the primary purpose of which is to assess the influence of independent variables on the dependent. The ORC obtained as a result of

the carbonate formation exposure to gaseous carbon dioxide acts as a dependent variable; independent variables – reservoir depth and oil density, expressed in units of API. Each field included in the proxy model group has parameters favorable for utilizing CO₂ as method of increasing oil recovery [24].

The result of the constructed model is the relationship (5.5). An additional restriction for applying this relationship is the geothermal gradient value, which should not exceed 0.092 °C/m (0.028 °F/ft). This limitation is justified by the estimation error increase in comparison with the experimental data for deposits with a geothermal gradient exceeding the above value [24]. The value of 0.092 °C/m (0.028 °F/ft) is the average geothermal gradient value of the fields included in the proxy model. At values exceeding 0.092 °C/m (0.028 °F/ft), high temperature contributes to a significant decrease in oil viscosity. This phenomenon significantly affects the processes occurring in the reservoir when carbon dioxide is injected into it; such processes were not taken into account in the regression analysis.

The geothermal gradient of field A is calculated based on the data in Table. 2.1 by the formula (5.4) [24].

$$Grad T = \frac{T}{D} = \frac{208.4}{14993} = 0.014^{\circ}F/ft, \quad (5.4)$$

where:

T – reservoir temperature, °F;

D – productive reservoir depth, ft.

$$K_2 = 0.14 + 1.5 * 10^{-3} * API + 4.0 * 10^{-6} * D \quad (5.5)$$

Thus, the increase in oil recovery factor K_2 as a result of carbon dioxide injection into the reservoir of Field A is estimated at 26.3%.

The final ORC value K is estimated at 61.3%.

Taking into account the reserves of Field “A” (see Chapter 2), the recoverable reserves amount in total to 23.29 billion barrels, 9.99 billion barrels are extracted as a result of CO₂ injection.

5.1.2. Required CO₂ amount assessment

The estimate of the amount of carbon dioxide needed to increase the oil recovery in Field “A” by the calculated amount is based on the assumption that the required amount of carbon dioxide will ultimately be “sequestered” in the reservoir after the CO₂ injection operation. Thus, the model is based on the calculation of the reservoir potential for the “sequestration” of carbon dioxide [24].

To assess the reservoir potential mentioned above a regression relation is used, obtained by approximating the empirical values of 213 fields. The resulting relationship establishes the relationship between the characteristics of the carbonate reservoir and its potential for “sequestration” of carbon dioxide (5.6) [24].

$$N_{CO_2} = 0.27 + (2.82 * 10^{-5} * API) + (5.24 * 10^{-6} * D), \quad (5.6)$$

where:

N_{CO_2} – required carbon dioxide amount, ton/barrel;

API – oil density;

D – productive reservoir depth, ft.

The estimated amount of carbon dioxide needed to extract 1 barrel of oil, calculated using formula 5.6, is 0.35 tons.

Consequently, the recovery of 9.99 billion barrels from exposure to gaseous carbon dioxide will require 3.5 Gt of CO₂ throughout the injection process.

The data obtained based on the current model are presented in Table. 5.1.

Table 5.1. Estimation results

Field	Reserves, bbl	ORF, %	Rec. reserves, bbl	Rec. Reserves using CO ₂ , bbl	ORF using CO ₂ , %	CO ₂ /oil ratio, ton/b	CO ₂ , Gt
A	38	35	13	9.99	26.3	0.35	3.5

Based on the fluid material balance in the offshore manifold (Fig. 2.2) (see Appendix 1), the flow of carbon dioxide in the reservoir fluid can be recalculated using formula 5.7 [24].

$$N'_{CO_2} = Q_{mol} * 0.05 * M * 10^{-3}, \quad (5.7)$$

where:

Q_{mol} – multiphase fluid molar flow through the offshore manifold, kg mole/h;

M – carbon dioxide molar weight, gr/mole;

N'_{CO_2} - CO₂ flow rate, ton/h.

According to the field development plan, it is planned to carry out measures to increase oil recovery from 2026 to 2054 [11]. Therefore, for the same period, it can be extracted and reused only 0.025 Gt of carbon dioxide to inject into the reservoir. While the annual carbon dioxide mass required for injection into the reservoir is 125 Mt (Table 5.1).

5.2. Carbonated water injection

5.2.1. Oil recovery factor estimation

To assess the oil recovery of waterflooding with carbonated water as in paragraph 5.1.1. the oil recovery factor (ORF) is used. To evaluate the ORF, the Buckley-Leverett theory is applied, adjusted for alteration in the viscosities of water and oil when carbon dioxide is dissolved in them. As part of this assessment, the one-dimensional flow of displacing fluid and oil is considered [25].

The Buckley-Leverett theory is based on the fundamental equation of continuum mechanics - the continuity equation (5.8).

$$\frac{\partial(\phi\rho)}{\partial t} + \frac{\partial(u\rho)}{\partial x} = 0, \quad (5.8)$$

where:

u – flow front velocity in porous media, m/s;

ϕ – rock porosity;

ρ – fluid density, kg/m³.

The front velocity is expressed using Darcy's law, taking into account the existing viscous and gravitational forces [25].

$$u = -\frac{k}{\mu} \left(\frac{\partial p}{\partial x} + g\rho \sin\alpha \right), \quad (5.9)$$

where:

α – productive formation slope with respect to horizon;

k – reservoir permeability, md;

μ – fluid dynamic viscosity, mPa*s;

g – gravity constant, m/s².

If the pore medium saturation with the phase i is denoted as S_i , then the fraction of the pore medium occupied by the i -th phase is expressed by equation (5.10).

$$\phi_i = \phi * S_i \quad (5.10)$$

Using equation (5.10), we can write the continuity equation for the water and oil phases [25].

$$\frac{\partial(\phi S_i \rho_i)}{\partial t} + \frac{\partial(u_i \rho_i)}{\partial x} = 0, \quad (5.11)$$

where:

i – water or oil phase.

Using the generalized form of Darcy's law (5.9), we can write expressions for the filtration rates of the i -th phases [25].

$$u_i = -k \frac{k_{ri}}{\mu_i} \left(\frac{\partial p_i}{\partial x} + g\rho_i \sin\alpha \right), \quad (5.12)$$

where:

k_{ri} – relative phase permeability for i -th phase.

Using the definition of capillary pressure (5.13) and assuming that the fluids and the porous medium are incompressible, the continuity equation takes the form (5.14) [25].

$$P_c = \frac{\sigma_{ow} * \cos\theta_c}{\sqrt{k/\phi}} * J(S_w), \quad (5.13)$$

where:

σ_{ow} – the interfacial tension between oil and water;

θ_c – wettability angle.

$$\phi \frac{\partial S_w}{\partial t} + u \frac{\partial F(S_w)}{\partial x} + \frac{\partial}{\partial x} \left(\frac{k * k_{ro}}{\mu_o} F(S_w) * \left[\frac{\partial P_c}{\partial x} - g\Delta\rho \sin\alpha \right] \right) = 0, \quad (5.14)$$

where:

$F(S_w)$ – fractional flow function determining water volume fraction in two-phase flow.

$$F(S_w) = \frac{\frac{k_{rw}(S_w)/\mu_w}{\frac{k_{rw}(S_w)}{\mu_w} + \frac{k_{ro}(S_w)}{\mu_o}}}{\mu_w} \quad (5.15)$$

$$F(S_w) = \frac{\lambda_w(S_w)}{\lambda_w(S_w) + \lambda_o(S_o)}, \quad (5.16)$$

where:

$$\lambda_i(S_w) = \frac{k_{ri}(S_w)}{\mu_i} \text{ – relative mobility of the } i\text{-th phase.}$$

Based on the water and oil relative phase permeability of Field A (Table 5.2), the plot of the relative phase permeability and water saturation relationship is constructed (Fig. 5.2).

Table 5.2. Field A relative phase permeability [26]

S_w	K_{rw}	K_{ro}
0,207	0	1
0,287	0,037	0,364
0,328	0,059	0,289
0,407	0,2	0,16
0,447	0,306	0,108
0,544	0,477	0,028
0,575	0,541	0,015
0,61	0,6	0,005
0,775	0,962	0

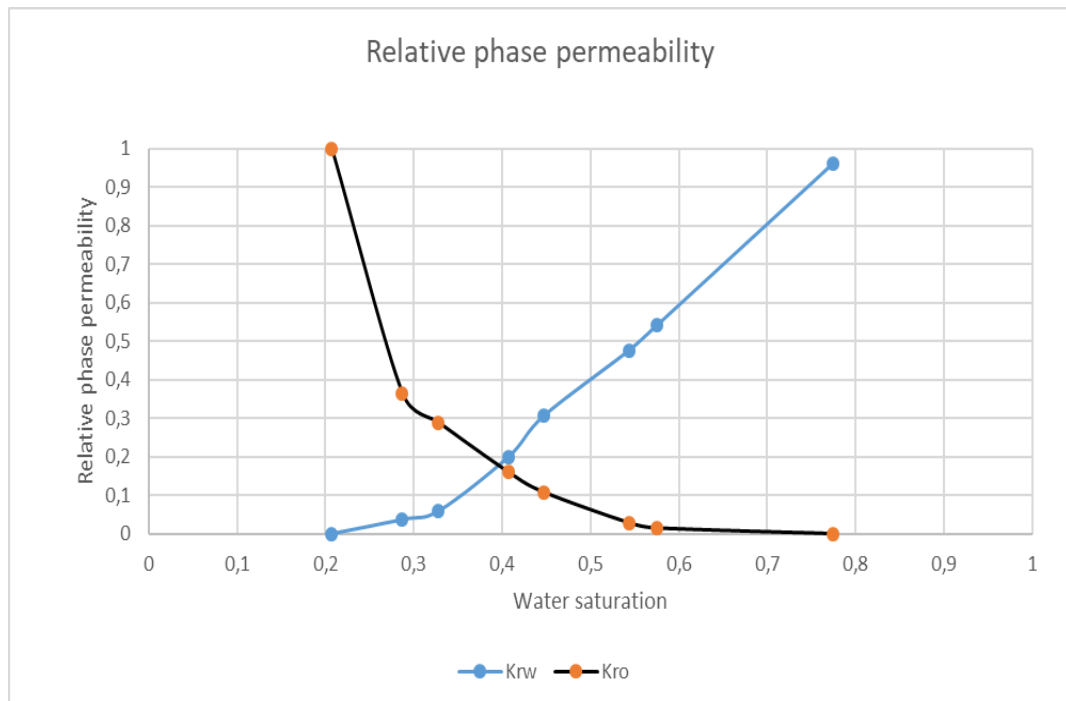


Figure 5.2. Relative phase permeability curves

To calculate the viscosity of water under conditions of high temperature and high pressure (Table 2.1) the Vogel – Fulcher – Tamman dependence (5.17) is used [27].

$$\ln[\eta] = a + b \left(\frac{p}{p_0} \right) + \frac{c + d \frac{p}{p_0}}{\left(\frac{T}{T_0} - 1 \right)} + e_1 \exp \left[-e_2 \left(\frac{T}{T_0} - 1 \right) \right] x, \quad (5.17)$$

where:

$$p_0 = 1 \text{ MPa};$$

$a, b, c, d, e_1, e_2, T_0$ – parameters of equation (5.17) (Table 5.3);

x – mole fraction of carbon dioxide;

η – carbonated water viscosity, mPa*s.

Table 5.3. Vogel – Fulcher – Tamman equation parameters [27]

a	c	b	d	e ₁	e ₂	T ₀
-3.705013	3.98950	0.002893	-0.00326	65.55968	2.46811	141.5

The viscosity of oil depending on the temperature and solubility of carbon dioxide is expressed by the dependence (5.18) [28].

$$\frac{\mu_{CO_2}}{\mu_{oil}} = 1 + (0.01113 * T - 1.78210)Sol, \quad (5.18)$$

where:

Sol – carbon dioxide solubility in oil, expressed by equation (5.19) [28].

$$Sol = (a + b * T) * \ln(p) + (c + d * T), \quad (5.19)$$

where:

a, b, c, d – dimensionless coefficients (Table 5.4);

p – pressure, MPa;

T – temperature, °C.

Table 5.4. Dimensionless coefficients [28]

a	b	c	d
0.36913	-0.00106	0.01280	-0.00160

The fractional flow function (Fig. 5.3) is constructed using formula (5.15) for two cases: flooding with seawater and flooding with carbonated water (5% CO₂).

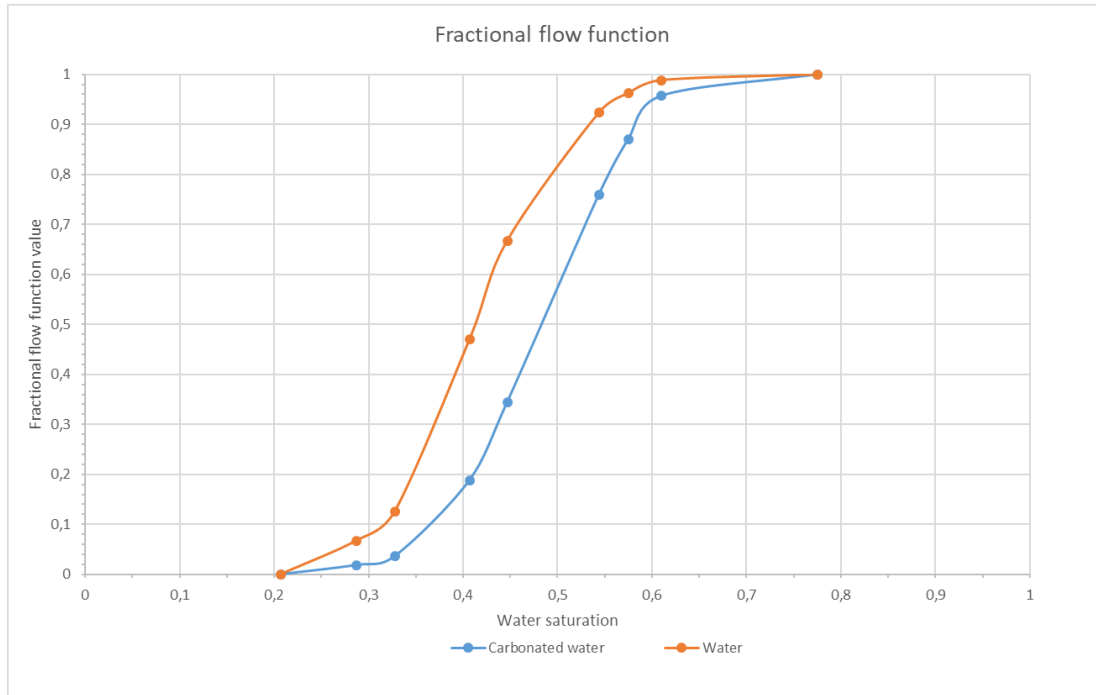


Figure 5.3. Fractional flow function for waterflooding by seawater and carbonated water (5 % dissolved CO₂).

To estimate the coefficient of oil displacement by carbonated water according to the methodology [25] it is necessary to find the coordinates of the pole P, through which the tangent to the fractional flow function passes during flooding with carbonated water.

Pole coordinates P { S_P ; Φ_P } are defined by equations (5.20) and (5.21) [25].

$$\Phi_P = \frac{K_e}{K_e - 1} \quad (5.20)$$

$$S_P = \frac{K_e}{K_e - 1} + \frac{1 - \phi}{\phi} * \frac{\Gamma}{K_e - 1}, \quad (5.21)$$

where:

K_e – the equilibrium constant (the ratio of carbon dioxide mass dissolved in the aqueous phase to carbon dioxide mass dissolved in the oil phase);

ϕ – reservoir porosity (Table 2.1);

Γ – adsorption isotherm constant.

The value of the equilibrium constant for the water-carbon dioxide-oil system is calculated by the formula (5.22) [29].

$$\frac{1}{K_e} = -0.0105P + 3.5155 \quad (5.22)$$

The following assumptions are introduced to describe the process of isothermal adsorption [30]:

- The carbonate reservoir surface is assumed to be uniform;
- Single-layer adsorption.

Langmuir isothermal adsorption theory satisfies these assumptions (5.23) [30].

$$q = \frac{Q_1 \Gamma p}{1 + \Gamma p}, \quad (5.23)$$

where:

Q_1 - mass of gas adsorbed per unit mass of rock, mg/gr;

p – pressure, bar;

Γ – Isothermal adsorption constant (Langmuir constant).

The constant of isothermal adsorption is determined from the literature [30] and is equal to $\Gamma = 0.012$.

Thus, the coordinates of the pole P are equal to {0.80; 0.59}. The tangent to the curve of the fractional flow function passing through the P pole determines the water saturation at the front (B), the average water saturation in the reservoir (C) (Fig. 5.4).

Displacement coefficient η_1 is assessed employing the following relationship [31]:

$$\frac{AC}{AD} = \eta_1, \quad (5.24)$$

where AC and AD are segments determined through Fig. 5.8.

The oil displacement coefficient for the one-dimensional case of considering the Buckley-Leverett theory is estimated using formula (5.25) [25].

$$\eta_1 = \frac{1}{1-A} (PC * [1 - WC] + B - A) \quad (5.25)$$

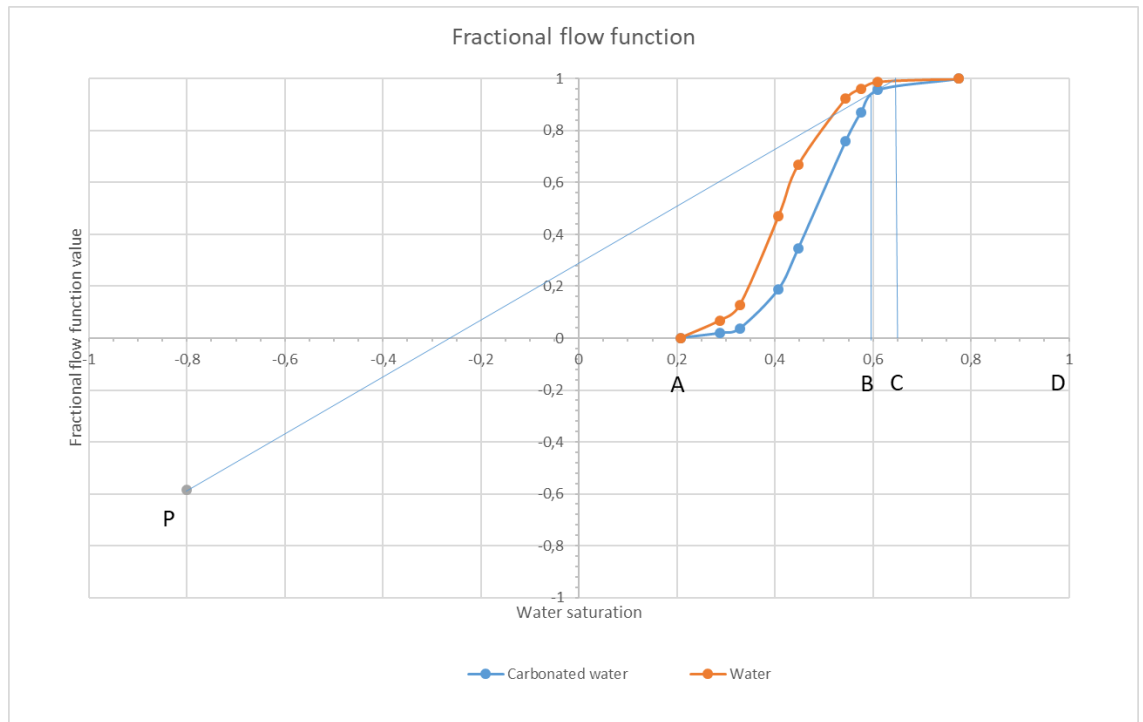


Figure 5.4. Fractional flow function for waterflooding by seawater and carbonated water (5 % CO₂) with pole P.

According to (5.25), the displacement of oil during flooding with 5 % carbonated water equals 0.6 [25].

The oil recovery factor can be calculated based on the Krylov formula (5.26).

$$\eta = \eta_1 * \eta_2, \quad (5.26)$$

where:

η_2 – is the sweep efficiency factor, assuming to be 0.65 as an average value for carbonate reservoir [24].

According to experimental data (chapter 4.2), the higher the carbon dioxide concentration in carbonated water, the higher the value of the oil recovery factor. Using the above-proposed methodology, the calculation of the oil recovery factor for flooding with 30 % and 50 % (mole CO₂ concentration) carbonated water was carried out. In further calculations, it is assumed that the number of injected pore volumes of carbonated water is 0.2. The calculation results are presented in Table 5.5.

Table 5.5. ORF estimation for flooding with carbonated water of various concentrations.

5 % CO ₂		30 % CO ₂		50 % CO ₂	
Pore volumes injected, n	ORF, %	Pore volumes injected, n	ORF, %	Pore volumes injected, n	ORF, %
0.2	40	0.2	43	0.2	44

5.2.2. Injection of the carbonated water rim

In the previous chapters, carbonated water injection efficiency is analyzed. During that analysis, carbonated water is assumed to be the principal displacing agent. However, it is most advisable to inject carbonated water as a rim and use seawater as a buffer. Similarly to those assumptions mentioned above in this chapter, the assumption is made that carbonated water will be injected in the amount of 0.2 pore volume. The amount of sea and carbonated water pore volumes injected is calculated using the graph analytical method [31] (Fig. 5.5).

Point C1 is defined from the equation (5.27).

$$\frac{AC_1}{AD} = 0.6 \quad (5.27)$$

TC1 – the amount of sea and carbonated water pore volumes injected, TC1=2.75 (Fig. 5.5.).

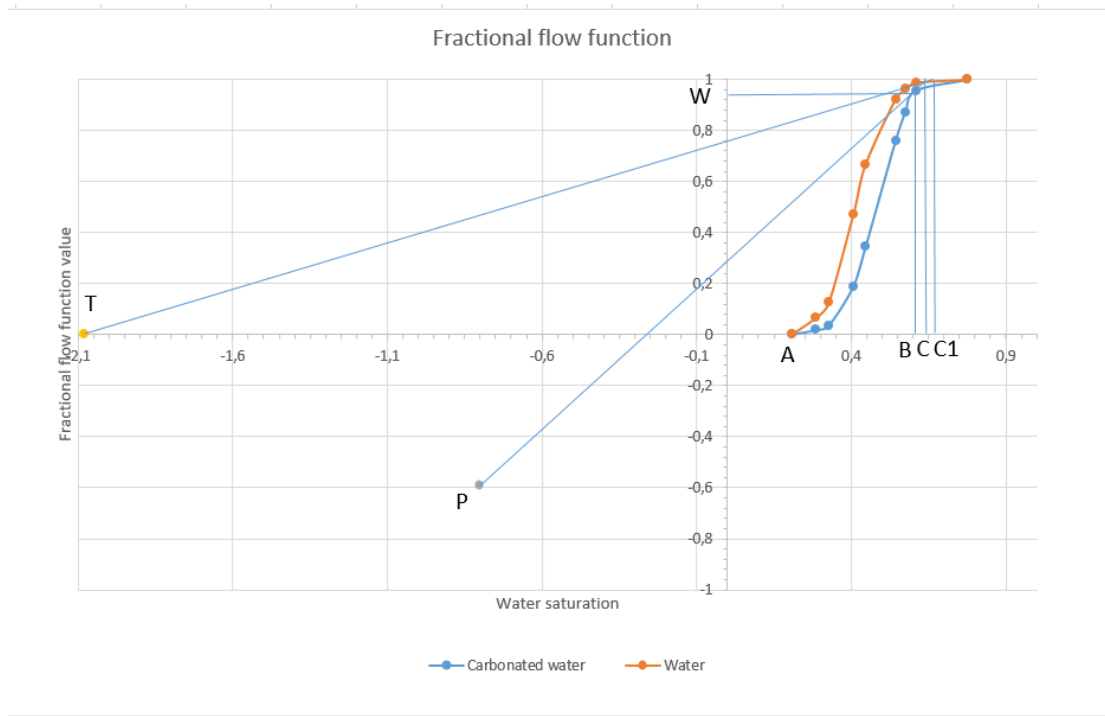


Figure 5.5. Fractional flow function for 5 % carbonated water rim injection

5.2.3. Required CO₂ amount estimation

The required carbon dioxide amount for carbonated water of different molar concentrations is calculated based on the number of injected pore volumes, which are assumed to be 0.2.

The volume of carbonated water required for injection into the reservoir is calculated employing the relation (5.28) [32] and the pore volume of the reservoir V (Table 2.1).

$$V_{inj} = V * n \quad (5.28)$$

The carbonated water amount (mole) is recalculated utilizing formula (5.29) [32].

$$v_{H_2O+CO_2} = \frac{V_{inj} * \rho}{M_{H_2O+CO_2}}, \quad (5.29)$$

where ρ – density carbonated water, kg/m³.

The carbon dioxide amount v_{CO_2} required to prepare a solution with a particular concentration r is determined as follows:

$$v_{CO_2} = v_{H_2O+CO_2} * r \quad (5.30)$$

Thus, the calculations result of the carbon dioxide amount required for each of the three cases (Table. 5.5) are shown in Table 5.6.

Table 5.6. Carbon dioxide amount estimation

5 % CO ₂		30 % CO ₂		50 % CO ₂	
Amount of carbon dioxide, ν_{CO_2} , mole	CO ₂ mass, m_{CO_2} , Gt	Amount of carbon dioxide, ν_{CO_2} , mole	CO ₂ mass, m_{CO_2} , Gt	Amount of carbon dioxide, ν_{CO_2} , mole	CO ₂ mass, m_{CO_2} , Gt
$2.7 \cdot 10^{11}$	0.012	$1.9 \cdot 10^{12}$	0.083	$3.5 \cdot 10^{12}$	0.153

5.3. CO₂ sources

In previous chapters, the required carbon dioxide amount was estimated for each of the CO₂ concentration scenarios. Summary data of the assessments are shown in Table. 5.7.

Due to the shortage of data on carbon dioxide emissions from industrial facilities in Russia, thermal power plants (TPP) operating on natural gas are taken as carbon dioxide sources.

Table 5.7. Summary data of required CO₂ amount

CO ₂ mass for 5 % carbonated water concentration, m_{CO_2} , Gt	CO ₂ mass for 30 % carbonated water concentration, m_{CO_2} , Gt	CO ₂ mass for 50 % carbonated water concentration, m_{CO_2} , Gt	CO ₂ mass for conventional CO ₂ flooding, m_{CO_2} , Gt
0.012	0.083	0.153	3.5

The annual carbon dioxide consumption for each of the above scenarios is summarized in Table. 5.8.

Table 5.8. Annual CO₂ required amount for considered cases

Annual CO ₂ mass for 5 % carbonated water concentration, mCO ₂ /year, mln. t	Annual CO ₂ mass for 30 % carbonated water concentration, mCO ₂ /year, mln. t	Annual CO ₂ mass for 50 % carbonated water concentration, mCO ₂ /year, mln. t	Annual CO ₂ mass for conventional CO ₂ flooding, mCO ₂ /year, mln. t
0.8	5.5	10.2	116.7

Carbon dioxide emissions are related to the amount of energy produced by natural gas-fired power plants as 1.4 kg CO₂ per 1 kWh [33]. Thus, for the scenarios of carbonated water injection with 30% and 5% dissolved carbon dioxide, thermal power plants located in the Astrakhan and Volgograd regions were considered (Table 5.9 and Table 5.10).

Table 5.9. CO₂ sources for 30 % carbonated water [34]

	Annual electricity generation, mln. kWh	Annual CO ₂ emissions, mln. tons	Distance to Atyrau, km
Astrakhan TPP-2	2098.11	2.94	310
Volzhskaya TPP-2	928.68	1.30	557
Volgograd TPP-3	1008.13	1.41	560

Table 5.10. CO₂ source for 5 % carbonated water [34]

	Annual electricity generation, mln. kWh	Annual CO ₂ emissions, mln. tons	Distance to Atyrau, km
Astrakhan TPP-2	2098.11	0.8	310

For the remaining two scenarios of carbon dioxide application, the required amount of CO₂ can be achieved only with the involvement of more than 20 TPPs

located in a radius of more than 1000 km, which significantly complicates the transportation infrastructure, as well as the cost of its construction and maintenance.

5.4. Comparison between 5% and 30% carbonated water injection scenarios

5.4.1. Feasibility assessment of CO₂ transportation

The methodology for calculating the economic indicators of land pipelines is presented in [35].

The following equation is used to calculate capital costs per unit length of the pipeline:

$$C_{cap} = 9970 * m^{0.35} * L^{0.13}. \quad (5.31)$$

The total cost of the pipeline is calculated employing equation (5.32).

$$C_{total} = F_L * F_T * L * C_{cap}, \quad (5.32)$$

where:

C_{cap} – pipeline capital cost, \$/km;

m – CO₂ mass flow rate in the pipeline, tons/day;

L – pipeline length, km;

C_{total} – total pipeline capital cost, \$;

F_L – location factor (assumed to be 1 for near Caspian area);

F_T – terrain factor (assumed to be 1.3 due to Caucasian mountains);

Capital expenditures for the construction of the pipeline can be expressed on an annualized basis using the profitability ratio (5.33).

$$C_{annual} = C_{total} * CRF, \quad (5.33)$$

where C_{annual} – annualized pipeline capital cost, \$/year;

CRF – capital recovery factor, 1/year.

The annual maintenance costs of the pipeline are taken as 2.5% of capital costs [35].

$$O\&M_{annual} = C_{total} * O\&M_{factor}, \quad (5.34)$$

where $O\&M_{factor}$ – O&M cost factor, 1/year.

Total annual costs represent the sum of both capital and maintenance costs [35].

$$C_{annual\ total} = C_{annual} + O\&M_{annual} \quad (5.35)$$

Thus, the cost of transporting CO₂ is expressed in equation (5.36).

$$C_{transport} = \frac{C_{annual\ total}}{m_{year}}, \quad (5.36)$$

where $C_{transport}$ – CO₂ transportation cost, \$/tons CO₂;

m_{year} - CO₂ mass flow delivered to injection site per year, tons/year.

For the 30 % carbonated water scenario, two routes for transporting carbon dioxide are considered: Volgograd-Astrakhan-Atyrau (650 km), as well as two separate pipelines Volgograd-Atyrau (550 km) and Astrakhan-Atyrau (290 km). The results of the calculations by the above methodology are displayed in Tables 5.11 and 5.12.

Table 5.11. Economic assessment of CO₂ transport along the Volgograd - Astrakhan-Atyrau route

Parameters	Designations	Volgograd-Astrakhan	Astrakhan - Atyrau	Total pipelines cost
Capital costs per unit length of the pipeline, mln \$/km	C_{cap}	0.48	0.61	1.10
Total cost of the pipeline, billion \$	C_{total}	0.50	0.61	1.12
annualized pipeline capital cost, mln \$/year	C_{annual}	75.40	91.87	167.27
O&M cost, mln \$/year	$O\&M_{annual}$	12.57	15.31	27.88
Total annual cost, mln \$/year	$C_{annual\ total}$	87.97	107.19	195.15
CO ₂ amount to be transported, mln tons/year	m_{year}	2.71	5.65	8.36
CO ₂ transportation cost, \$/ton	$C_{transport}$	32.44	18.98	51.42

Table 5.12. Economic assessment of CO₂ transport along the Volgograd – Atyrau and Astrakhan-Atyrau routes

Parameters	Designations	Volgograd-Atyrau	Astrakhan-Atyrau	Total pipelines cost
Capital costs per unit length of the pipeline, mln \$/km	C _{cap}	0.51	0.49	1
Total cost of the pipeline, billion \$	C _{total}	0.53	0.49	1.02
annualized pipeline capital cost, mln \$/year	C _{annual}	79.96	72.76	152.72
O&M cost, mln \$/year	O&M _{annual}	13.33	12.13	25.45
Total annual cost, mln \$/year	C _{annual total}	93.29	84.88	178.17
CO ₂ amount to be transported, mln tons/year	m _{year}	2.71	2.94	5.65
CO ₂ transportation cost, \$/ton	C _{transport}	34.41	28.90	63.30

For the use of a 5% solution of carbonated water scenario, only one route for pipe laying - Astrakhan-Atyrau is considered (Table 5.13).

Table 5.13. Economic assessment of CO₂ transport in case of 5 % carbonated water scenario

Parameters	Designations	Astrakhan-Atyrau
Capital costs per unit length of the pipeline, mln \$/km	C _{cap}	0.31
Total cost of the pipeline, billion \$	C _{total}	0.31
annualized pipeline capital cost, mln \$/year	C _{annual}	46.36
O&M cost, mln \$/year	O&M _{annual}	7.73
Total annual cost, mln \$/year	C _{annual total}	54.08
CO ₂ amount to be transported, mln tons/year	m _{year}	0.8
CO ₂ transportation cost, \$/ton	C _{transport}	67,60

The relation between capital costs per pipeline unit length, the CO₂ mass flow and the pipeline length; as well as the CO₂ transportation cost, the CO₂ mass flow and the length of the pipeline are shown in Fig. 5.6 and 5.7, respectively.

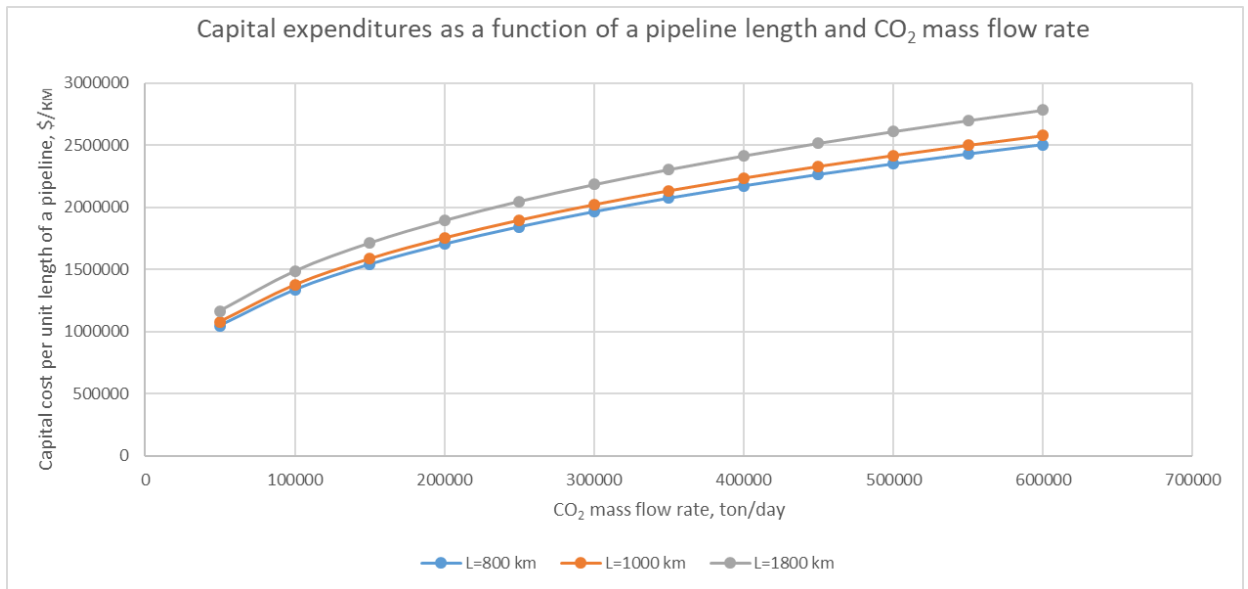


Figure 5.6. Dependence of capital costs per pipeline unit length on the mass flow of CO₂ and the length of the pipeline

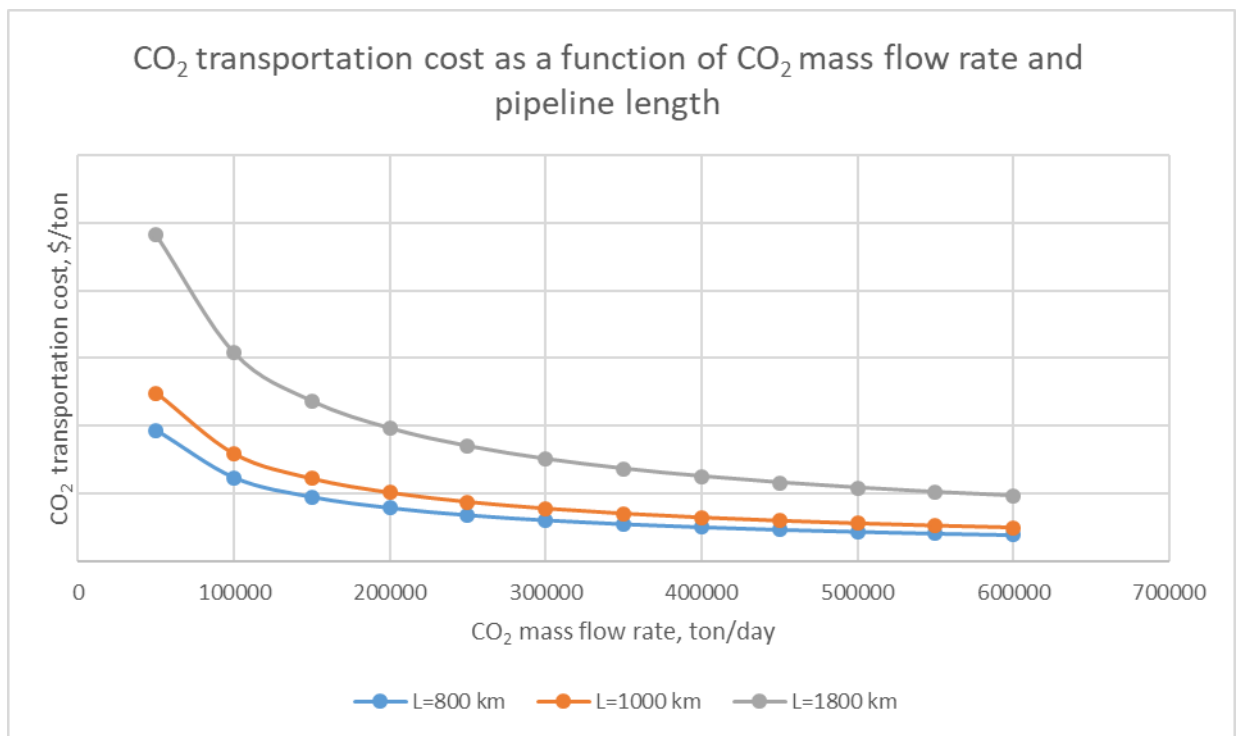


Figure 5.7. Dependence of CO₂ transportation cost on the mass flow of CO₂ and the length of the pipeline

Based on the calculations, it is evident that for a 30% solution, the cost of transporting per a ton of carbon dioxide is less if the Volgograd-Astrakhan-Atyrau pipeline is laid.

5.4.2. Economic evaluation between 5 % and 30 % carbonated water injection

This model does not take into account the cost of construction and maintenance of compressor stations along the pipelines. Additional modernization of the technological scheme does not require significant capital expenditures (Fig. 2.2 and 2.3). The cost of carbon dioxide is the sum of the purchase cost and transportation cost. Extracted oil profit due to CO₂ impact on the reservoir is calculated as the difference between the values of the extracted oil and the injected carbon dioxide. The CO₂ purchase price is accepted in the range of 15\$/ton - 30\$/ton [63].

The calculation results of the economic model for different cases of carbon dioxide cost and price for oil are presented in Table. 5.14.

Table 5.14. Feasibility evaluation of 5 % and 30 % carbonated water injection

An economic evaluation of EOR method							
CO ₂ price	Profit from oil produced during the injection of a 5% solution, billion \$			CO ₂ price	Profit from oil produced during the injection of a 30% solution, billion \$		
	\$/ton	\$30	\$70		\$100	\$/ton	\$30
83	56,0	132,0	189,0	66	85,7	207,3	298,5
85	56,0	132,0	189,0	68	85,6	207,2	298,4
88	55,9	131,9	188,9	71	85,3	206,9	298,1
91	55,9	131,9	188,9	74	85,1	206,7	297,9
95	55,9	131,9	188,9	78	84,7	206,3	297,5
98	55,8	131,8	188,8	81	84,5	206,1	297,3

According to the results of an economic assessment, the most preferred scenario is the injection of a 30% solution of carbonated water and carbon dioxide. However, according to Figure 4.3, to achieve such a concentration of carbon dioxide in carbonated water, it is necessary to provide a dissolution pressure much higher than 70

MPa, which is technologically unrealizable. Thus, the injection of a 5% solution of carbonated water seems to be a more optimal concept.

6. Field A development concept for carbonated water injection

6.1. General information

Field A is located 98 kilometres from the onshore oil and gas processing plant. As shown in Figure 2.1, partially stabilized oil and gas are transported to land via pipelines; the offshore and coastal parts of the pipelines are 68.3 km and 29.7 km, respectively. Injection wells are located on islands D, EPC2 and EPC3 6, 2 and 2 injection wells, respectively. The distance between the islands of EPC2 and D is 2.6 km, EPC3 and D is 4.6 km, EPC2 and EPC3 is 2.1 km. The depth of the sea at the location of the islands is 4 m [11].

6.2. Carbonated water processing

6.2.1. Unit for CO₂ dissolution

The dissolution of carbon dioxide in water is carried out onshore in the jet unit. The ejector unit design is carried out under the methodology described in the manual of Y. A. Sazonov [36]. Key unit parameters are shown in the sketch (Fig. 6.1).

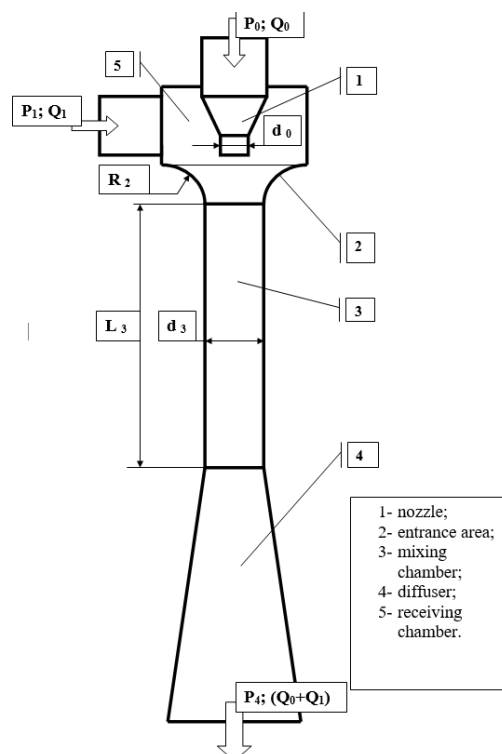


Figure 6.1. Ejector unit schematic diagram [36]

To achieve the required carbon dioxide concentration in water, it is necessary to install six ejector units designed according to the methodology mentioned above. The

initial data for calculating the geometric parameters of the ejector units are summarized in Table. 6.1, the calculation results are displayed in Table. 6.2.

Table 6.1. Initial data for the ejector unit design

No	Parameter	Designations	Unit	Value
1	The gas flow rate at the inlet of the jet unit (normal conditions)	Q1n	m ³ /s	2
2	The gas pressure at the inlet of the jet unit	P1	MPa	1
3	Outlet pressure	P4	MPa	4.5
4	Inlet gas temperature	T1	°C	40
5	Hydraulic fluid temperature	T0	°C	30

Table 6.2. Jet unit calculation result

Calculation results	
Hydraulic fluid flow rate (Q0), m ³ /h	396
Hydraulic fluid pressure at the nozzle inlet (P0), MPa	13.7
Ejector outlet pressure (P4), MPa	4.5
Ejector unit efficiency	0.313
Gas flow rate at the ejector inlet (Q1), m ³ /s	2
Nozzle outlet hole diameter (d0), m	0.0301
Mixing chamber diameter (d3), m	0.0602
Mixing chamber length (L3), m	1.355
Diffuser cone angle (γ4), degree	7
Diffuser outlet hole diameter (d4), m	0.181

The mass flow rate of carbon dioxide in one ejector unit is 14400 kg/h, and the water flow rate is 399960 kg/h. A mixture of CO₂ and water in such proportions provides a carbonated solution with a 3.52% carbon dioxide mass concentration. The total volume of the solution produced by one ejector unit is 400 m³/h. The capacity of

6 ejector units is 2400 m³/h, which corresponds to the flow rate of carbonated water in the offshore trunk pipeline (Table 6.4).

Thus, the jet unit outlet pressure satisfies the condition for the solubility of carbon dioxide in water at a concentration of 3.6% by mass (5% molar concentration of CO₂) at the maximum possible ambient temperature (Table 1.3).

6.2.2. Seawater transportation for carbonated water processing

The pipeline diameter is selected to minimize pressure loss during transportation of seawater at a distance of 29.7 km [11]. It is known from the previous chapter that the ejector unit inlet pressure must satisfy the requirement of 13.7 MPa (Table. 6.2).

The methodology for selecting the pipeline diameter is described in chapter 6.3.1, here only the pipeline diameter selection results are introduced.

Table 6.3. Initial data for pipeline diameter selection

Initial data		
Seawater density, ρ	kg/m ³	1010
Seawater viscosity, ν	Pa*s	0.001
Pump discharge pressure, P_1	MPa	14.4
Pipeline outlet pressure, P_2	MPa	13.7
Pipeline length, L	M	29700
Flow rate, Q	m ³ /s	0.66

Diameter, wall thickness and pipeline material are selected according to API standard [37]. The minimum allowable value of the wall thickness of the pipeline is calculated using the formula of hoop stress [38]:

$$t \geq \frac{(P_1 - P_{\text{atm}}) * D_o}{2(f_1 * \sigma_y + P_1)}, \quad (6.1)$$

where:

P_{atm} – atmosphere pressure, Pa;

D_o – pipeline outlet diameter (according to API [37]), m;

f_1 – design or usage factor, considered to be 0.72 [38];

σ_y – material yield stress, Pa [37].

The calculation result is a pipeline with a diameter of 813 mm, a wall thickness of 19.1 mm, and steel grade X60.

For seawater transportation, the oil electric pump “HM 1250-400” was selected [39]. To ensure the necessary flow rate and discharge pressure, the characteristics of this pump are recalculated to higher shaft rotation value employing relations (6.2) and (6.3) [40].

$$\frac{Q_2}{Q_1} = \frac{n_2}{n_1}, \quad (6.2)$$

$$\frac{H_2}{H_1} = \left(\frac{n_2}{n_1}\right)^2, \quad (6.3)$$

where Q_2 and H_2 – flow rate (m³/h) and pressure (m) corresponding to shaft rotation velocity n_2 , (rotation/minute);

Q_1 and H_1 – flow rate and pressure corresponding to shaft rotation velocity n_1 .

Based on the above ratios, at a pump shaft speed of $n_2 = 5700$ rpm, the flow and pressure are 2375 m³/h and 1444 meters of water head (14.4 MPa), respectively.

6.3. Subsea pipeline design

The engineering design of the subsea pipeline includes various stages, and each one is carried out in strict accordance with international and industry standards. Key design stages are as follows [41]:

- Route selection and optimization;
- Hydraulic and thermal analysis is performed to select pipeline diameter and to prevent gas hydrates formation, waxes and paraffin precipitation;
- Wall thickness and pipeline material selection;
- Verification of the strength, vibration and other pipeline characteristics for compliance with the requirements of the standards;
- Pipeline drawings development;

- Corrosion prevention measures design.

Since this work is conceptual, the design process is simplified to the following basic calculations:

- Material selection;
- Corrosion aspects evaluation;
- Pipeline diameter selection;
- Wall thickness determination;
- Pump selection.

6.3.1. Diameter selection

The pipeline conceptual design begins with the pipeline diameter selection. The existing approaches in the literature are based on an iterative approach to choosing the external pipeline diameter at a constant required flow rate (Fig. 6.2) [38]. The internal diameter is determined based on the necessary wall thickness of the pipeline, which, in turn, is determined from the strength characteristics material. Subsequent calculations are based on the DNV [42] and API [37] standards' recommendations, as well as the basic principles of hydraulics. Therefore, the calculation of the inner diameter is based on the following aspects: fluid properties (density and viscosity), fluid flow rate, allowable pressure drop.

For diameter calculations, a single-phase theory of fluid motion in a pipeline is employed. The condition for the applicability of this theory is to maintain the pressure in the pipeline above the minimum miscibility pressure of carbon dioxide and water (Fig. 4.3); moreover, the minimum pressure in the pipeline is also restricted by the hydrate formation pressure in the operating temperature range (+3 to +40) (Fig. 6.3).

Thus, the condition for the applicability of the single-phase theory of fluid motion is to maintain the pressure in the pipeline at least at 4.5 MPa. The equipment for pumping carbonated water is selected following the required flow rate and pressure in the catalogue of Promresurs LLC [44]. The selected pump is converted to a rotation frequency of 4300 rpm using the relations (6.2) and (6.3). Therefore, the selected pump "HM 1700-300" has a flow rate of 2440 m³/h and a pressure of 6.2 MPa.

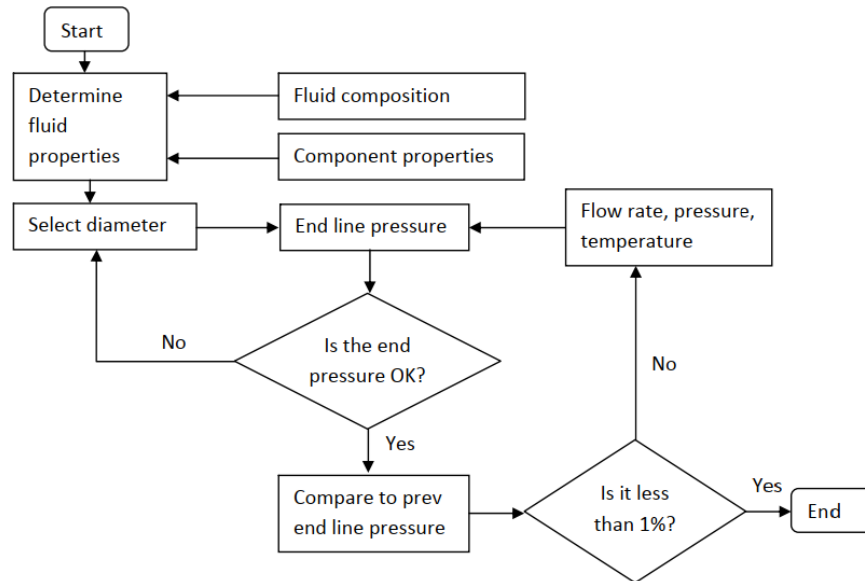


Figure 6.2. Chart diagram of the iterative approach for pipeline diameter selection

[41]

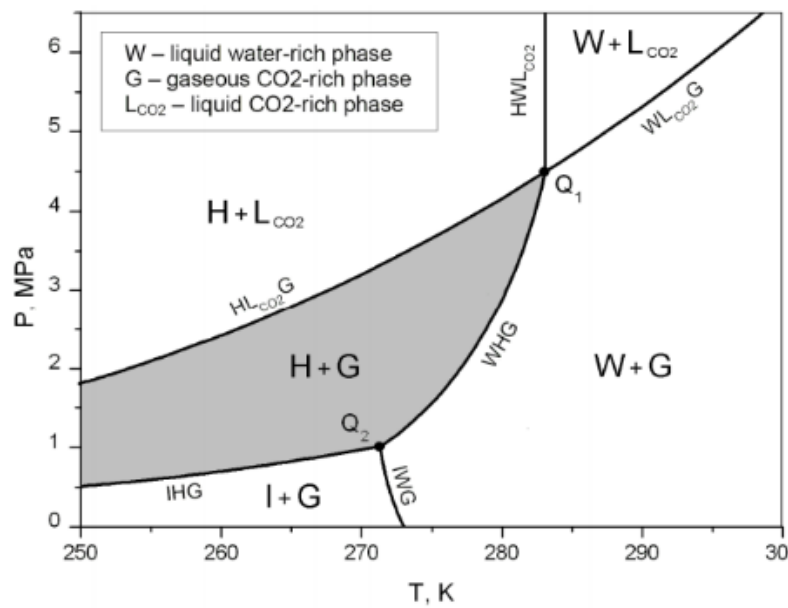


Figure 6.3. P-T diagram of the binary water-CO₂ system [43]

The carbonated water viscosity is determined by the relation (5.17). According to this ratio, the viscosity of carbonated water in the range of operating temperatures varies from 0.002 to 0.001. In the single-phase model, pressure losses are calculated for each of the boundary viscosity values.

Table 6.4. Initial data for pipeline diameter selection

Initial data		
Carbonated water density, ρ_{cw}	kg/m ³	1036
Carbonated water viscosity, ν_{cw}	Pa*s	0.001-0.002
Pump discharge pressure, P'_1	MPa	6.2
Pipeline end pressure, P'_2	MPa	4.5
Pipeline length, L	m	98000
Level difference, z	m	4
Flow rate, Q	m ³ /s	0.68

The optimal diameter for the pipeline can be previously estimated by the relation (6.4) [38].

$$D = 840 * \sqrt{Q} \quad (6.4)$$

The pipeline external diameter is selected according to the API standard [37] as the closest value to found by employing formula (6.4): the outer diameter is 813 mm, the wall thickness is 10.3 mm.

The fluid velocity inside the pipeline is determined by formula (6.5) [38].

$$U = \frac{4 * Q}{\pi * d^2}, \quad (6.5)$$

where d – inner pipeline diameter, m.

The erosional velocity is calculated based on (6.6) [38].

$$Re = \frac{\rho_{cw} * U * d}{\nu} \quad (6.7)$$

The fanning friction coefficient between the fluid and the pipeline wall is found from the analytical relationship derived by Coe (6.8) [45].

$$f = 0.0014 + \frac{0.125}{Re^{0.32}} \quad (6.8)$$

The pressure drop in the selected pipeline at the above-mentioned flow parameters is determined through the friction losses and the height difference (6.9) [38].

$$\Delta P = \frac{2 * L * f * \rho * U^2}{d} - \rho * g * z \quad (6.9)$$

The selected pipeline satisfies the required pressure drop, as well as the erosion velocity of the pipeline material.

6.3.2. Material selection

Traditionally, carbon steel is used to manufacture pipelines. The base steel grades considered in this work are Steel X52, Steel X56, Steel X60 [37].

From the economic frame of reference, steel production costs increase with an increase in the steel grade; nevertheless, high-grade steels have better strength characteristics, which makes it possible to reduce the thickness of the pipeline wall, thereby reducing the metal consumption of the structure.

Higher steel grades have lower weldability compared to higher carbon content steels. At the same time, the lower metal consumption of the structure can significantly reduce the tension of the pipeline during its installation. All of the above factors should be taken into account when choosing a pipeline material.

6.3.3. Corrosion aspects

The carbonated water transported has high corrosion activity, while the selected carbon steels have low corrosion resistance. The existing methods for assessing corrosion are based on the calculation of the partial pressure of CO₂ in the mixture of the transported fluid. These methods are not applicable in the corrosion assessment from exposure to carbonated water, because carbon dioxide is dissolved in water and has no partial pressure. The corrosion rate of carbon steel when interacting with carbonated water also depends on the acidity of the medium, which can only be estimated experimentally under thermobaric transportation conditions.

It was experimentally proved that one of the most effective and cost-effective methods of protection against carbon dioxide corrosion is the use of amino-containing corrosion inhibitors. For example, in the Ormen Lange gas field, amino-containing corrosion inhibitors were used to protect the pipeline from carbonic acid [46]. The acceptable level of corrosion is assumed to be 0.1 mm/year. A similar criterion for the allowable corrosion rate is also prescribed in GOST R 55990-2014 [47], which states that a corrosion inhibitor should be used at an experimentally measured corrosion rate exceeding 0.1 mm/year. According to GOST 9.502-82 [48], an environment with a corrosion rate exceeding 0.1 mm/year refers to systems with increased corrosion activity.

Within the framework of this master's thesis, it is assumed that the corrosion rate as a result of the action of amino-containing inhibitors is 0.1 mm/year. Recommended carbon dioxide inhibitors are morpholine, cyclohexylamine, and nitrogen-containing heterocyclic compounds [49]. The consumption and effectiveness of carbon dioxide inhibitors are established empirically.

6.3.4. Wall thickness selection

The pipeline wall thickness is determined by the external and internal pressure on the pipeline. Since the designed pipeline lies in the shallow water zone, the critical factor determining the wall thickness is the internal fluid pressure. The wall thickness calculation is carried out according to the “limit states” method described in DNV [42].

DNV uses the following criteria for the internal pressure of the pipeline (6.10):

$$p_i - p_e \leq \frac{p_b(t_1)}{\gamma_m * \gamma_{sc}}, \quad (6.10)$$

where p_i and p_e – external and internal pressure applied to the pipeline, Pa;

γ_m and γ_{sc} – material resistance factor and safety class resistance factor (Table 6.5);

$p_b(t_1)$ – pressure containment resistance, Pa.

$$p_b(t_1) = \frac{2 * t_1}{D - t_1} * f_{cb} * \frac{2}{\sqrt{3}}, \quad (6.11)$$

where

$$f_{cb} = \text{Min} \left[f_y; \frac{f_u}{1.15} \right] \quad (6.12)$$

In equation (6.12), f_y and f_u are the characteristic yield strength and tensile strength of the material.

$$f_y = (SMYS - f_{y,temp}) * \alpha_U, \quad (6.13)$$

$$f_u = (SMTS - f_{u,temp}) * \alpha_U, \quad (6.14)$$

where $SMYS$ and $SMTS$ – specified minimum yield strength and specified minimum tensile strength determined by the API standard [37] (Table 6.5), Pa;

$f_{y,temp}$ and $f_{u,temp}$ – de-rating values of the yield strength and the tensile strength respectively due to temperature (equals to 0 in the current thesis), Pa;

α_U – material strength factor (Table 6.5).

Thus, the formula for calculating the minimum allowable wall thickness of the pipeline is as follows:

$$t_1 = \frac{\sqrt{3} * \gamma_m * \gamma_{sc} * D * (p_i - p_e)}{4 * f_{cb} + \sqrt{3} * \gamma_m * \gamma_{sc} * (p_i - p_e)} \quad (6.15)$$

The initial data for calculating the minimum allowable wall thickness of the pipeline are shown in table 6.5.

For the long-term pipeline maintenance, it is necessary to take into account the corrosion tolerance t_{corr} , the fabrication tolerance t_{fab} [42].

$$t'_1 = t_{stan} - t_{corr} - t_{fab}, \quad (6.16)$$

where t_{stan} – wall thickness per the API standard [37], mm.

The condition for the wall thickness selection is (6.17).

$$t_1 \leq t'_1 \quad (6.17)$$

Table 6.5. Initial data for pipeline wall thickness calculation [37], [42]

Initial data		
Internal pressure, p_i	MPa	6.2
External pressure, p_e	MPa	0.04
Material resistance factor, γ_m	-	1.15
Safety class resistance factor (low safety class), γ_{sc}	-	1.046
Material strength factor, α_U	-	0.96
SMYS and SMTS for Steel X52	MPa	359; 455
SMYS and SMTS for Steel X56	MPa	386; 490
SMYS and SMTS for Steel X60	MPa	414; 517
Corrosion allowance, t_{corr}	mm	1.5
Fabrication tolerance, t_{fab}	mm	0.7

The wall thickness calculation results for steels of the above grades are summarized in Table. 6.6.

Table 6.6. Wall thickness for the steels of various grades

Steel X52	Steel X56	Steel X60
10.3 MM	9.5 MM	9.5 MM

To maintain a balance between the cost of the steel and the metal consumption X56 steel is chosen.

6.3.5. Von-Mises stress criteria

Checking the combined load of the pipeline is carried out according to the Von-Mises formula (6.18) [38].

$$\sigma_{eq} = (\sigma_h^2 - \sigma_h\sigma_l + \sigma_l^2)^{1/2} < f_1 * SMYS \quad (6.18)$$

Hoop σ_h and longitudinal σ_l stresses are determined via formulas (6.19) and (6.20) [38].

$$\sigma_h = \frac{p_i R}{t} \quad (6.19)$$

$$\sigma_l = \frac{\mu * p_i * R}{t} - E\alpha\theta \quad (6.20)$$

The parameters in equations (6.19) and (6.20) are summarized in Table 6.7.

Table 6.7. Parameters for combined loading calculation [50]

Young modulus, E	Pa	201*10 ⁹
Poisson coefficient, μ	-	0.3
Thermal expansion coefficient, α	1/°C	12*10 ⁻⁶
Temperature gradient, θ	°C	17
Design or usage factor, f_1	-	0.72

The pipeline meets the strength requirements.

6.3.6. Pipeline burial depth evaluation

Sea ice can be compacted into an ice ridge under pressure or shear, caused by the driving force of ice migration. Ice ridges can form at the boundary between fast ice and drifting ice cover, where the ice cover is compressed. The underwater volume of the destroyed and crushed ice under the ridge, submerged under the pressure of the overlying layers of ice, is called the ice keel. Ice ridges can be divided into year-old and perennial. ISO 19906 shows a standard cross-section of an ice ridge (Figure 6.4). [51].

According to [52], the relationships between the identified geometric parameters are:

$$h_k = (4 \div 5)h_s \quad (6.21)$$

$$h_c = (1.2 \div 2.1)h \quad (6.22)$$

$$w_k = 3.9h_k \quad (6.23)$$

$$w_b = w_k - 2h_k \text{ctg} \alpha_k \quad (6.24)$$

The indicated ratios have a significant effect on the loads that the ice ridge will exert on the seabed or the pipeline.

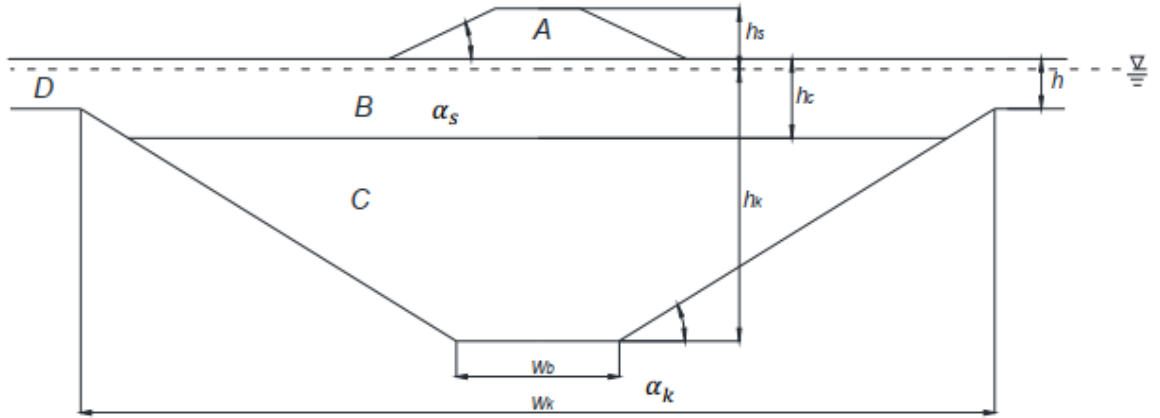


Figure 6.4. Idealized geometry of a first-year ridge; h_c – is the thickness of the consolidated layer, h_s – sail height, h – level ice thickness, h_k – keel height (from the sea level to its bottom), w_k , w_b – keel width at the sea level and the bottom respectively, α_s – sail angle, α_k – angle of the keel shape [51]

One of the most important physical parameters of any type of ice ridge is the macro-porosity, which characterizes the strength of an ice keel. Based on the assumption that the entire volume of brine is small and that all pores are occupied by water or air, the porous keel part density of the ice ridge can be described as [52]:

$$\rho_{iw} = \eta \rho_w + (1 - \eta) \rho_i \quad (6.25)$$

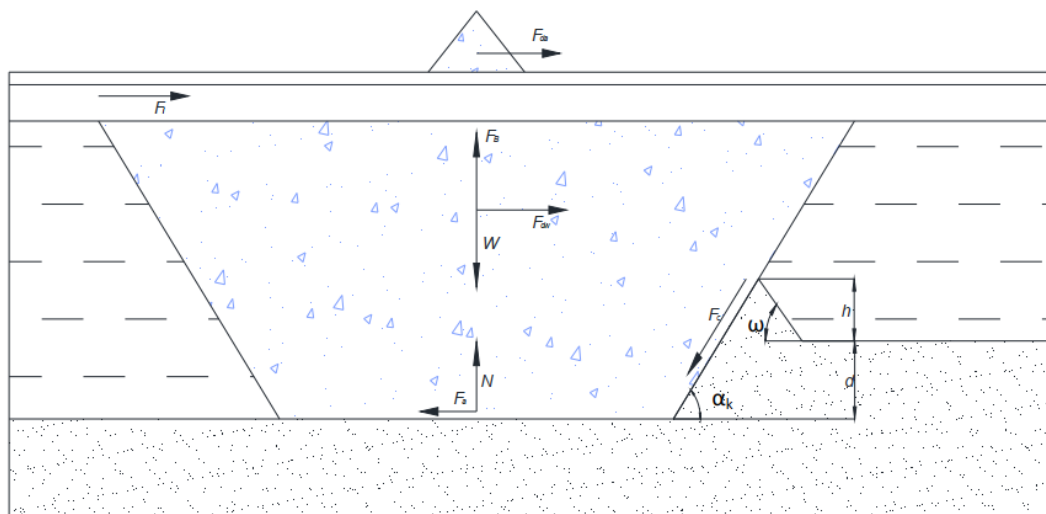


Figure 6.5. Forces applied to the soil-ice ridge model [52]

In the sketch $F_{da}, F_{dw}, F_b, W, N, F_a, F_c, F_i, \omega, \alpha_k, h', d$ – are drag forces from the air, drag forces from water, buoyancy force, the weight of the ridge, the reaction from the seabed, friction force on the bottom of the ridge, Coulomb's passive friction force, the driving force from surrounding floe, angle of the front surcharged soil slope, keel angle, the height of the frontal mound, scour depth, respectively.

The force equilibrium equation is expressed in the horizontal and vertical directions, respectively as [52]:

$$F_{da} + F_{dw} + F_i - F_a - F_c \cos \alpha_k = 0 \quad (6.26)$$

$$F_b - W - F_c \sin \alpha_k + N = 0 \quad (6.27)$$

Air drag force is expressed by equation (6.28) [52].

$$F_{da} = \frac{1}{2} \rho_a C_{da} A_{a1} u_a^2 + C_{sa} \rho_a A_{a2} u_a^2, \quad (6.28)$$

where $C_{da}, C_{sa}, u_a, \rho_a$ - are drag coefficient, skin friction coefficient, wind velocity, air density, respectively.

The projected areas of the wind impact are expressed as follows [52]:

$$A_{a1} = \left(h_s - \frac{\rho_w - \rho_i}{\rho_w} h_i \right) B \quad (6.29)$$

$$A_{a2} = \omega_k B \quad (6.30)$$

Current drag force can be expressed as [52]:

$$F_{dw} = \frac{1}{2} C_{dw} \rho_w A_w u_c^2, \quad (6.31)$$

where C_{dw}, ρ_w, A_w, u_c – are drag coefficient for current, water density, underwater projection area, current velocity respectively.

The ice ridge weight is defined as the weight of each geometric part [52]:

$$W = \rho_{iw} B g * \left[\frac{\rho_{ia}}{\rho_{iw}} \left(h_s - \frac{\rho_w - \rho_i}{\rho_w} h \right)^2 \operatorname{ctg} \alpha_s + \frac{\rho_i}{\rho_{iw}} h w_k + \frac{1}{2} (w_k + w_b) \left(h_k - \frac{\rho_i}{\rho_w} h \right) \right] \quad (6.32)$$

The empirical expression for calculating the strength of ice exposure is [52]:

$$F_i = 0.43 * 4.059 * B^{0.622} * h_i^{0.628} \quad (6.33)$$

The passive friction force, which describes the interactions of the ice ridge frontal part and the soil, is expressed by equation (6.34) [52]:

$$F_c = \mu P \cos \theta_w, \quad (6.34)$$

where P, θ_w, μ are the earth pressure, wall friction angle and friction coefficient between ice and soil, respectively.

The pressure of the frontal soil part is expressed as [52]:

$$P_f = \frac{1}{2} K_p \rho_s g (h' + d)^2 B + 2c \sqrt{K_p}, \quad (6.35)$$

where c, K_p, ρ_s, h' – the soil cohesion, the passive earth pressure coefficient, soil density, height of frontal mound, respectively.

$$K_p = \frac{\cos \varphi^2}{\cos \theta_w \left[1 - \sqrt{\frac{\sin(\varphi + \theta_w) * \sin(\varphi + \beta)}{\cos \theta_w \cos \beta}} \right]^2}, \quad (6.36)$$

where φ is internal friction angle of soil.

$$h' = \sqrt{\frac{d^2 \operatorname{ctg} \varphi}{\operatorname{ctg} \varphi + \frac{d}{3B} \operatorname{ctg} \varphi * \operatorname{ctg} \beta}} \quad (6.37)$$

For side resistance, the evaluation is as follows (6.38) [52]:

$$P_s = \frac{1}{6} K_p \rho_s g d^2 w_b (w_b + d * \operatorname{ctg} \alpha_k) \quad (6.38)$$

It follows from the equilibrium condition that the ice ridge weight and the buoyancy force are equal; thus, the reaction force of the soil is similar to the vertical projection of the Coulomb force. Then the projection of all effects on the horizontal axis has the form:

$$F_{da} + F_{dw} + F_i - \mu F_{cy} - F_{cx} = 0 \quad (6.39)$$

Solving the equation with one variable (6.39), we obtain the ice ridge penetration depth into the soil.

The initial data for the calculation are displayed in Table 1.14, 6.8.

Calculations using the above method show that the minimum burial depth of the pipeline to protect it from the effects of ice ridges in the Northern Caspian region is 2 meters.

Table 6.8. Initial data for pipeline burial depth calculations [53], [54], [55], [56], [57]

Parameter	Unit	Value
Maximum level ice thickness (100-year value), h_i	m	0,85
Ice velocity (100-year value), v_i	m/s	0,2
Ridge sail height, h_s	m	2
Consolidated layer thickness, h	m	0,7
Keel angle, α_k	degree	30
Sail angle, α_s	degree	18
Single-keel breadth, B	m	20
Ice density, ρ_i	kg/m ³	900
Ridge average block size, T_b	m	0,3
Sail porosity, η_s	-	0,18
Air density, ρ_a	kg/m ³	1,3
Water density, ρ_w	kg/m ³	1010
Current speed, u_c	m/s	0.8
Current drag coefficient, C_{dw}	-	0.7
Wind speed, u_a	m/s	26,5
Wind drag coefficient, C_{da}	-	0.7

6.4. Island D – EPC2 – EPC3 pipeline design

The pressure of carbonated water inside the pipeline is determined for the same reasons as the pressure inside the trunk line (see chapter 6.3.1). Carbonated water transportation along with the route D - EPC2 - EPC3 is performed by a single pipeline using a pump installed on island D (Fig. 6.6). A certain amount of carbonated water is drawn from a pipeline on the island EPC2 using a specially designed side outlet. In the framework of this work, the design of the lateral branch is not performed.

The pipeline diameter and wall thickness selection are carried out according to the methodologies described in chapters 6.3.1, 6.3.4 and 6.3.5. This chapter provides only the results of the calculations (Table. 6.9).

Table 6.9. Pipeline D – EPC2 – EPC3 calculated parameters

Parameter	Unit	Value
Inside pressure, p_i	MPa	5.2
External pressure, p_e	MPa	0.04
End line pressure, p_{en}	MPa	4.94
Outer diameter, D	mm	406.4
Corrosion allowance, t_{cor}	mm	1.5
Fabrication tolerance, t_{fab}	mm	0.7
Wall thickness (Steel X52), t_1	mm	5.6
Wall thickness (Steel X56), t_1	mm	5.2
Wall thickness (Steel X60), t_1	mm	5.2
Burial depth, d	m	2
Von-Misses stress, σ_{eq}	MPa	189.5

According to the Table. 6.9 the most optimal material is X56 steel grade [37] (for justification see chapter 6.3.2). For this steel, the wall thickness is 5.2 mm; the combined load condition is fulfilled. The corrosion protection method is similar to that proposed in chapter 6.3.3. The driving pump “HM 710-280” [39] was selected with the recalculated flow and pressure characteristics (formulas (6.2) and (6.3)) at a shaft rotation frequency of 4100 rpm.

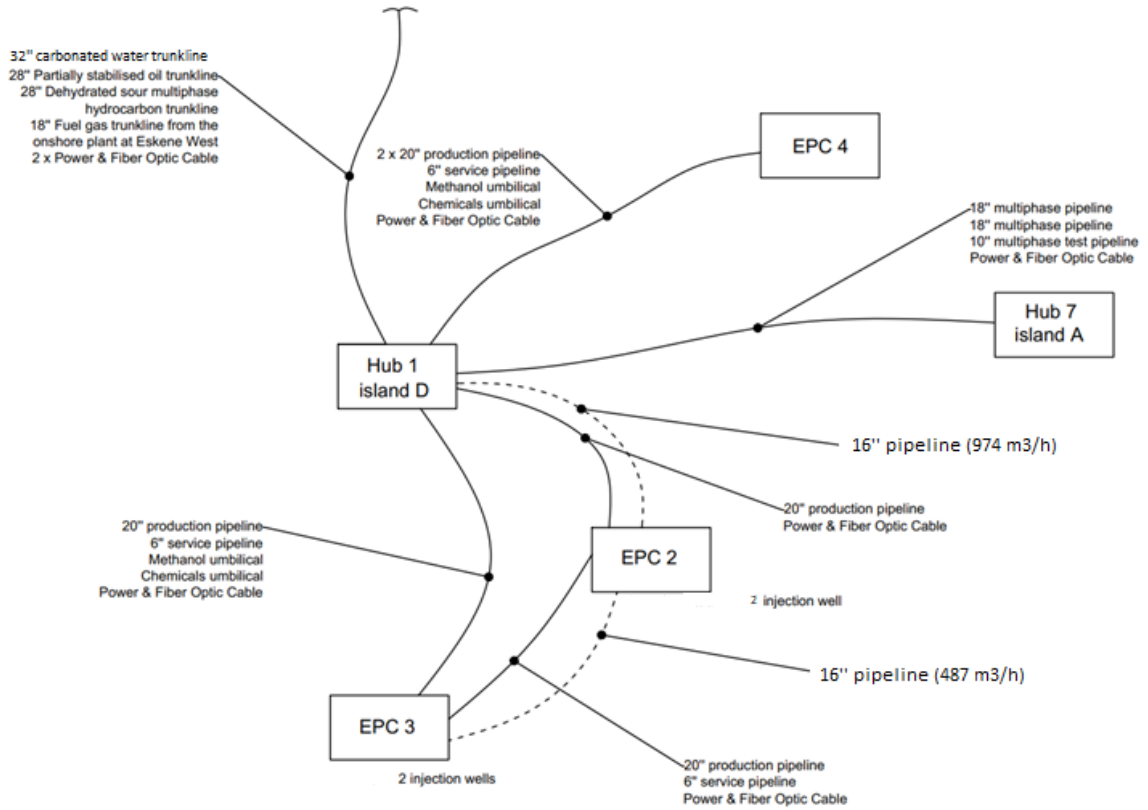


Figure 6.6. Development concept sketch for carbonated water injection

6.5. Pumps selection for carbonated water injection into the well

The required pump discharge pressure is determined by the difference in reservoir pressure and the pressure of the liquid column. The discharge pressure of the pump is determined by the formula (6.40).

$$p_{inj} = p_{res} - \rho gh, \quad (6.40)$$

where p_{res} – reservoir pressure, MPa;

ρ – carbonated water density, kg/m³;

g – gravity constant, m²/s;

h - well depth, m.

Thus, utilizing Field A data (Table 2.1) and taking the density of carbonated water constant, we obtain $p_{inj} = 31.2$ MPa. The carbonated water injection rate into a well is $q = 240$ m³/h.

According to the catalogue of the company Drillmec [58], we select a pump with the required characteristics: 14T2200.

6.6. Concept feasibility study

6.6.1. Capital expenditures

For the economic assessment of the proposed carbonated water injection concept, it is necessary to evaluate the capital costs for the installation of the following facilities:

- Pipelines for transporting carbon dioxide from a source;
- Pipelines for transporting seawater to ejector units;
- Subsea trunkline for transporting carbonated water to island D;
- Subsea pipeline for transporting carbonated water to the islands EPC2 and EPC3;
- Pumping equipment procurement;
- CO₂ procurement.

The current economic assessment is based on several assumptions:

- Price for oil is considered 60 \$/barrel;
- Price for CO₂ is considered 29 \$/ton;
- Capital expenditures for the modernization of the coastal processing plant are not taken into account.

Cost assessment of the subsea trunk line for the carbonated water transportation is performed by the formula [59]:

$$C = f_s * C_o * L, \quad (6.41)$$

where f_s – size factor with respect to 10-in pipeline manufactured from X60 steel grade [59];

C_o – basic cost per unit length, \$/m;

L – pipeline length, m.

The cost of pipe-laying is calculated from the cost of the shallow water vessel's daily rent and the average speed of laying the offshore pipeline [59]. These parameters are respectively equal to 400 thousand \$/day and 1.7 km/day.

The burial of the pipeline to a depth of 2 meters is calculated from the ratio of 104 \$/m [60].

The cost of engineering work is generally accepted as 8% of the pipeline capital costs [59].

The carbon dioxide pipeline cost is evaluated in Table 5.13.

The pipeline transporting seawater to the ejector units is assessed following the methodology presented in chapter 5.4.1.

The cost of the subsea pipeline connecting islands D, EPC2 and EPC3, its laying, burial and engineering are calculated similarly to the methodology used for the subsea trunkline connecting coast and island D.

The pumps used for carbonated water pumping into the reservoir, as well as for pumping fluids through pipelines, are estimated by the power of the electric drive from the ratio of \$ 8000 for each 3.6 kW of energy [61].

The total capital costs of infrastructure are summarized in Table. 6.10.

Table 6.10. CAPEX

Element	Capital expenditures
Subsea trunkline coast - island D, mln \$	92.3
Pipeline CO ₂ source - ejector, mln \$	310
Seawater pipeline, mln \$	28
Subsea pipeline connecting islands D – EPC2 – EPC3, mln \$	3.7
Pumps, mln \$	18.4
Price for CO ₂ , mln \$	240
Total, mln \$	692.4

6.6.2. Economic parameters

The primary economic indicator is the net present value (NPV), which is estimated at US millions of dollars. NPV is calculated by the formula [62]:

$$NPV = \sum_{i=0}^T \frac{Cashinflow_i - Cashout flow_i}{(1 + d)^i}, \quad (6.42)$$

where:

$$Cashinflow_i = Revenue_i - Depreciation_i;$$

$$Cashoutflow_i = CAPEX + Taxes + OPEX;$$

i – calculation year;

d – discount rate assumed to be 12% for oil and gas projects.

The internal rate of return (IRR) - is a criterion that shows the profitability of the project. The project is profitable only if $IRR > d$. This indicator is calculated by the formula [62]:

$$NPV = \sum_{i=0}^T \frac{Cashinflow_i - Cashout flow_i}{(1 + IRR)^i} = 0 \quad (6.43)$$

The discounted payback period (PB) - is an indicator showing the payback period of an investment.

The profitability Index (PI) - is a criterion showing the relationship between net present value (NPV) and capital expenditure (CAPEX). This indicator should be greater than 1 [62].

$$PI = 1 + \frac{NPV}{CAPEX} \quad (6.44)$$

The above indicators can assess the profitability of the proposed project and the development concept. Depreciation and income tax are taken as respectively 20% and 25% [62]. The calculation results of the economic model is presented in Table. 6.11.

Table 6.11. Economic parameters of the project

NPV, billion \$	10.4	>0
IRR, %	216	>d
PB, year	1	
PI	16.09	>1

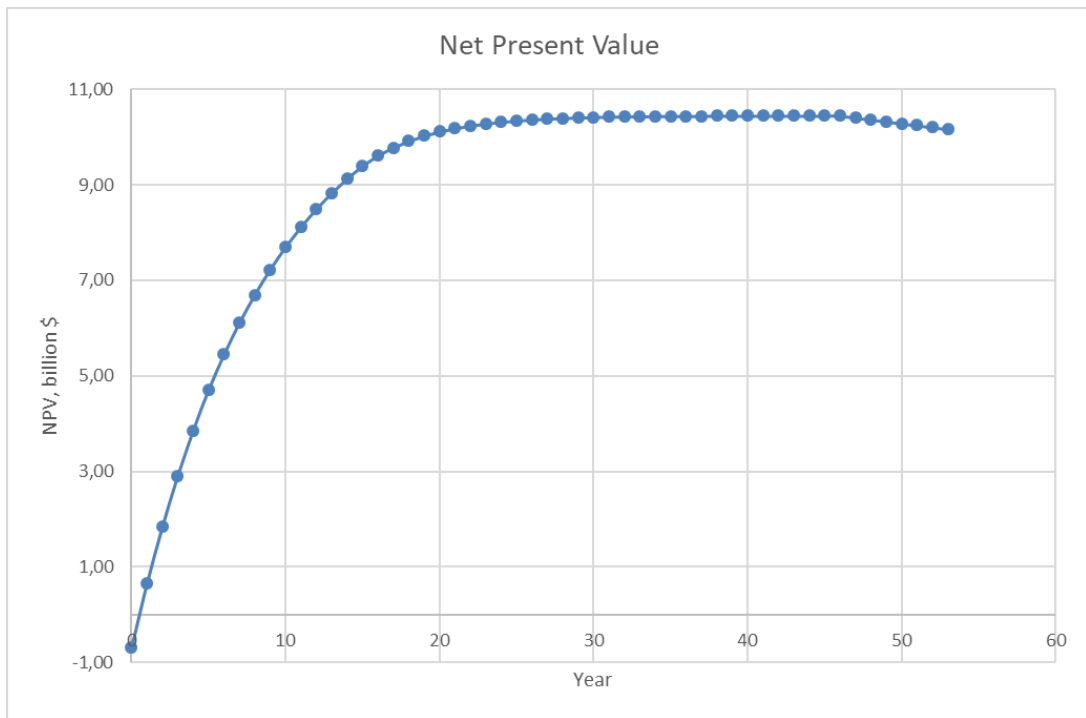


Figure 6.7. Net Present Value plot

From the NPV plot (Fig. 6.7), it can be concluded that after 46 years of the technology application, the net present value starts to decrease. The development period and, consequently, the injection of fluid into the reservoir is limited to this year.

Thus, the period of seawater injection as a buffer for the carbonated water rim is 31 years. During this period, 0.6 pore volumes of seawater will be pumped into the reservoir.

With the increase in CAPEX, which may be associated with the necessary technological lines modernization for the processing of an increased amount of oil, the period of the technology application will decrease due to an earlier fall in NPV.

Conclusions

The Northern region of the Caspian Sea has significant prospects for hydrocarbon deposits development. The development of deposits in this sector leads to the regions' and countries' economic stability. Field "A", which is the oil and gas locomotive of this region, is considered in this paper.

The purpose of this master's thesis is to consider the technological and economic feasibility of carbon dioxide application as a method of increasing oil recovery for the field mentioned above. To characterize the unique environmental conditions, the climatic conditions of the region, hydrological conditions of the sea, soil characteristics of the seabed and ice conditions were considered. Parameters that complicate field development such as abnormally high reservoir pressure, high hydrogen sulfide content in the reservoir fluid and deep formation reservoir are also recognized; moreover, production lines designed to deal with these complicated oil production conditions have been described.

The current work reviews the existing world experience in the use of carbon dioxide as an EOR method in marine conditions; the analysis of the most relevant concepts that are potentially able to make the carbon dioxide application to increase oil recovery on the shelf economically attractive.

Within this study, two basic scenarios for carbon dioxide utilization were considered: CO₂ injection in gaseous form and in dissolved form in carbonated water with various concentrations of carbon dioxide. An assessment of these technologies applicability for Field A was carried out in three stages.

At the first stage, the oil recovery factor was estimated for each of the two mentioned technologies, the amount of carbon dioxide required was determined, as well as possible CO₂ sources and its transportation routes.

The second stage includes an economic assessment of each of the CO₂ application cases and a technical assessment of the scenarios.

The third stage includes the field development concept designed for the enhanced oil recovery method application selected in the second stage, as well as an economic

analysis of the project. The concept is designed taking into account the harsh operating conditions, which are considered for the following project aspects: subsea pipelines diameter and material selection, pipelines' wall thickness selection, and pipelines' burial depth calculation to protect them against ice ridge impact. Economic analysis reveals the cost-effective period of the project.

The primary purpose of this work is to develop a methodology for a preliminary assessment of the carbon dioxide applicability to increase oil recovery in offshore fields. The result of several techniques applied in this paper is suitable of further more detailed modelling of each stage listed above.

References

1. National centers for environmental information NOAA, National centers for environmental information NOAA, 2019. Available: <https://www.ncdc.noaa.gov/global-warming/temperature-change>. (requested: 01.11.2019).
2. Khromykh L.N., Litvin A.T., Nikitin A.V. (2018). Application of carbon dioxide in enhanced oil recovery. The Eurasian Scientific Journal, [online] 5(10). Available at: <https://esj.today/PDF/06NZVN518.pdf> (in Russian).
3. Task force on offshore CO₂-EOR: Enabling large-scale CCS using offshore CO₂ utilization and storage infrastructure development // Carbon Sequestration Leadership Forum (CSLF) Technical Group, 2017. URL: <https://www.cslforum.org/cslf/sites/default/files/documents/OffshoreEORTaskForce-FinalReport.pdf> (requested: 02.10.2019).
4. Sultanbaev A. E. Development Concepts for the Northern Caspian Sea, Master thesis, Department of Marine and Offshore Technologies, University of Stavanger. Stavanger, 2015.
5. Shell company confidential document, “Geotechnical report”.
6. Shell company confidential document, “Site and Engineering Data for Field “A” Offshore Facilities”.
7. Shell company confidential document, “Site and Engineering Data for Field “A”, Part 2.
8. Shell company confidential document, “Ice and Metocean Design Criteria for New Compression Facilities”.
9. Duzceer R., Gokalp A., Yoruk R. Artificial Island Construction in North Caspian Sea, Kazakhstan // International Conf. on Case Histories in Geotechnical Engineering, New York, April, 2004.
10. Lengkeek H. J., Croasdale K. R., Metge M. Design of Ice Protection Barrier in Caspian Sea // International Conf. on Offshore Mechanics and Arctic Engineering, Cancun, June, 2003.
11. Shell company confidential document, “Basis of Design”.
12. Shell company confidential document, “Design Basis of Bundle 1”.

13. Bealesio A. B., Alonso N. A., Mendes N. J., Sande A. V. A review of enhanced oil recovery (EOR) methods applied in Kazakhstan // Texas A&M University, US.
14. Shell company confidential document, “Onshore Processing Facilities”.
15. Enabling Large-Scale Carbon Capture, Utilization, and Storage (CCUS) Using Offshore Carbon Dioxide (CO₂) Infrastructure Developments / Eide L. I. [и др.]. Energies. – Vol. 12, 2019.
16. Chauhan J. S. Transport of CO₂ in porous media – a visualization study, Master thesis, Department of Energy Resources, University of Stavanger, Stavanger, 2018.
17. Gimatudinov S.K. Physics of oil and gas reservoir. – Ripol Classic, 1982. (in Russian)
18. Gas-cyclic injection of carbon dioxide into production wells to intensify the production of high-viscosity oil / Volkov V. A. // Oil. Gas. Innovation, № 4. 2017. (in Russian)
19. Proselkov E. B., Proselkov Y. M. Reservoir physics / Kuban State Technological University. – Krasnodar, 2011. – 188 p.
20. Verma M. K. Fundamentals of carbon dioxide-enhanced oil recovery (CO₂-EOR) – a supporting document of the assessment methodology for hydrocarbon recovery using CO₂-EOR associated with carbon sequestration // Geological Survey Open-File Report. – V. 24, 2015. URL: <http://dx.doi.org/10.3133/ofr20151071> (requested: 10.12.2019).
21. Bisweswar G., Al-Hamairi A., Jin S. Carbonated water injection: an efficient EOR approach. A review of fundamentals and prospects // Journal of petroleum exploration and production technology. – V. 13, 2019. URL: <https://doi.org/10.1007/s13202-019-0738-2> (requested: 10.01.2020).
22. Junin R. Carbonated water injection for recovery of oil and wettability analysis // Applied Mechanics and Material. – V. 6, 2015. URL: [10.4028/http://www.scientific.net/AMM.695.499](http://www.scientific.net/AMM.695.499) (requested: 15.12.2019).
23. Trukhina O. S., Sinsov I. A. The experience of using carbon dioxide to enhance oil recovery // The successes of modern science, № 3, 2016.

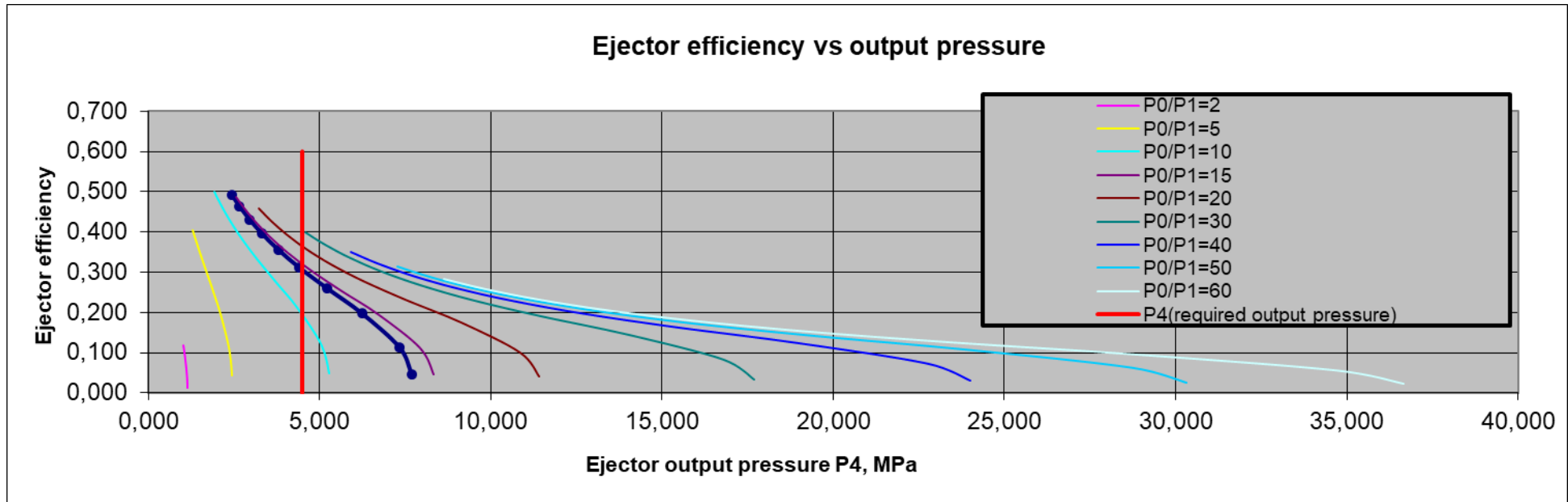
24. CO₂ storage in depleted oilfields: global application criteria for carbon dioxide enhanced oil recovery // IEA Environmental Projects Technical Report, 2009.
25. Zolotukin A. B., Ursin J. Fundamentals of petroleum reservoir engineering. Norway: Norwegian Academic Press, 2000. 407 p.
26. Shell company confidential document, “Rock properties”.
27. McBride-Wright M., Maitland G. C., Martin Trusler J. P. Viscosity and Density of Aqueous Solutions of Carbon Dioxide at Temperatures from 273 to 449 K and at Pressures up to 100 MPa // Journal of chemical & engineering data. – V. 60, 2015. URL: [dx.doi.org/10.1021/je5009125](https://doi.org/10.1021/je5009125) (requested: 15.03.2020).
28. Barclay T. H., Mishra S. New correlations for CO₂-Oil solubility and viscosity reduction for light oils // Journal of Petroleum Exploration & Production Technology. – V. 6, 2016. URL: doi: 10.1007/s13202-016-0233-y (requested: 17.03.2020).
29. Mass Transfer of CO₂ in a Carbonated Water-Oil System at High Pressures / Shu G. [и др.]. // Journal of Industrial & Engineering Chemistry Research, № 56. 2016. URL: <https://doi.org/10.1021/acs.iecr.6b03729> (requested: 30.03.2020).
30. Impact of Surfactant on the Retention of CO₂ and Methane in Carbonate Reservoirs / Eliebid M. [и др.]. // Energy & Fuels, № 32. 2018. URL: <https://doi.org/10.1021/acs.energyfuels.8b00213> (requested: 02.04.2020).
31. Zolotukhin A. B. Flow of fluids in porous media, FFF and its applications, unpublished.
32. Engineering handbook: [site]. URL: <https://dpva.ru/Guide/GuideChemistry/Concentration/ConcentrationMeasurement/>.
33. Belousov V.N., Smorodin S.N., Lakomkin V.Yu. Energy saving and Greenhouse Gas (CO₂): tutorial, 2014. – 52 с.
34. Energy base: [site]. URL: <https://energybase.ru/map>.

35. McCollum D. L., Ogden J. M. Techno-Economic Models for Carbon Dioxide Compression, Transport, and Storage & Correlations for Estimating Carbon Dioxide Density and Viscosity // University of California, 2006.
36. Sazonov Y. A. Jet pumps and compressors calculations. Tutorial. // Gubkin State University of Oil and Gas , 2005.
37. API Specification 5L. *Specification for Line Pipeline*. 42d edition, Washington D. C., USA, 2004. 166 p.
38. Karunakaran D. Pipelines and Risers lecture notes. UIS, Stavanger, 2019.
39. GOST 12124-87. Centrifugal oil pumps for pipe-lines. Types and basic parameters. 1989. 6 p.
40. Kasyanov V. M. Hydraulic machines and compressors: Tutorial for universities // Nedra, 1981. — 295 p.
41. Duplenskiy S. V., Protection of Subsea Pipelines against Ice Ridge Gouging in Conditions of Substantial Surface Ice. Master thesis, Department of Marine and Offshore Technologies, University of Stavanger, Stavanger, 2012.
42. DNV-OS-F101. Submarine pipeline systems. Det Norske Veritas, Høvik, 2013. 372 p.
43. Properties of equilibrium carbon dioxide hydrate in porous medium / Voronov V. P. [и др.]. // Chemical Physics, 2016. URL: <http://dx.doi.org/10.1016/j.chemphys.2016.05.031> (requested: 15.04.2020).
44. LTD «Промресурс» pumps and compressors: [site]. URL: <http://promresurs61.ru/nm>.
45. Wikipedia: [site]. URL: https://en.wikipedia.org/wiki/Fanning_friction_factor.
46. Zapevalov D. N., Vagapov R. K., Melsitdinova R. A. Assessing corrosion environment and internal corrosion remedies for offshore objects // Oil science news, № 4, 2018.
47. GOST R 55990-2014. Oil and gas-oil fields. Field pipelines. Design codes. 2014. 94 с.
48. GOST 9.502-82. Unified system of corrosion and ageing protection. Inhibitors of metals corrosion for aqueous systems. Methods of corrosion tests // Standards, 1993. 25 p.

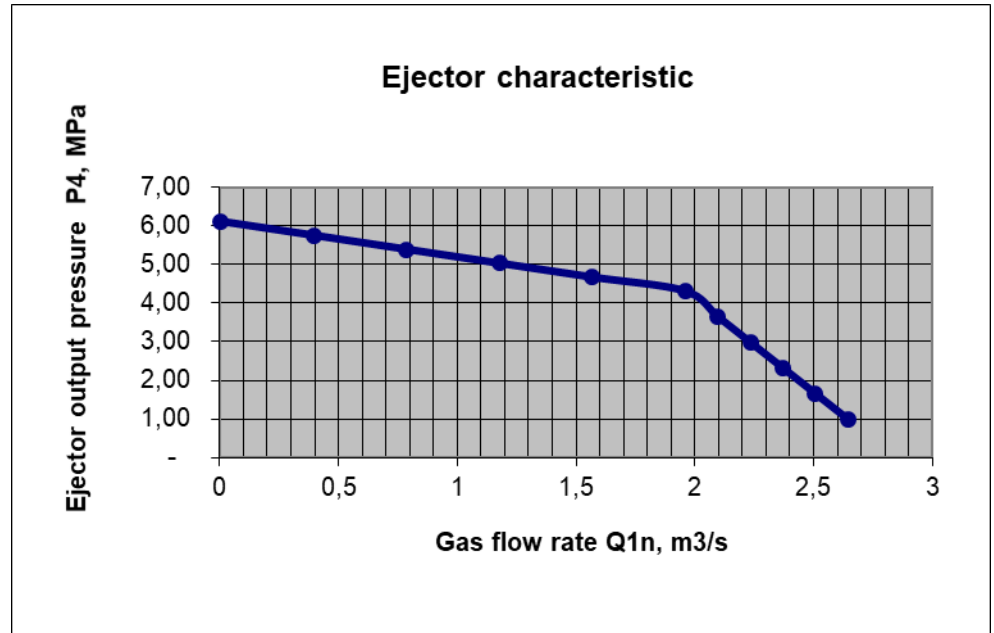
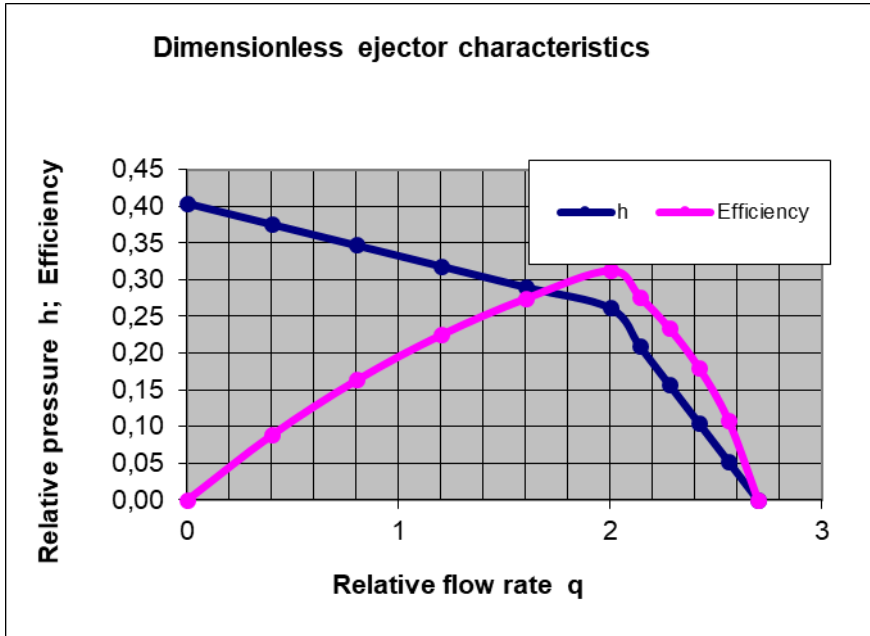
49. Moiseeva L. S., Rashevskaya N. S. Providing protection against carbonic acid corrosion for equipment in the oil and gas and chemical industries // Chemical and Petroleum Engineering. – V. 37, 2001.
50. ASME Boiler and Pressure Vessel Code, II Materials Part D. New York, US, 2013. 1038 p.
51. ISO/FDIS 19906. Petroleum and natural gas industries – Arctic offshore structures. International standard, International Standardization Organization, Geneva, 2010.
52. Duplenskiy S., Gudmestad O. T. Protection of Subsea Pipelines against Ice Ridge Gouging in Conditions of Substantial Surface Ice // 32nd International Conf. on Ocean, Offshore and Arctic Engineering, Nantes, France, June, 2013.
53. Mironov Y. U., Porubayev V. S. Structural peculiarities of ice features on the offshore of the Caspian Sea, the Sea of Okhotsk and the Pechora Sea // 18th Int. Conf. on Port and Ocean Eng. Under Arctic Conditions. – V. 2, 2005.
54. Mironov E. U., Porubaev V. S. Morphometric parameters of ice ridges and stamukhas according to expeditionary studies in the northwestern part of the Caspian Sea // Meteorology and hydrology, № 5, 2011.
55. Ice phenomenas in the Caspian sea: [сайт]. URL: http://caspi.ru/HTML/05/Caspy-mon/Glava_8.pdf
56. DNV-RP-C205. Environmental conditions and environmental loads. Det Norske Veritas, Høvik, 2010. 124 p.
57. Gudmestad O. T. Marine Technology and Operations Theory & Practice. England: WIT Press, 2015. 393 p.
58. Каталог Drillmec: [сайт]. URL: <http://www.drillmec.com/ru/p/mud-pumps-offshore/> (requested: 10.05.2020).
59. Subsea Cost Estimation: [сайт]. URL: http://ocw.snu.ac.kr/sites/default/files/NOTE/FfOP_Lecture%20%286%29.pdf (requested: 13.05.2020).
60. Kaiser M. J. Offshore pipeline construction cost in the U.S. Gulf of Mexico // Marine Policy. – V. 82, 2017.

61. Well drilling and pumping costs: [сайт]. URL: http://lobby.la.psu.edu/066_Nuclear_Repository/Agency_Activities/EPA/EPA_Yucca_Appendix_IV.pdf (requested: 15.05.2020).
62. Zelenovskaya E. V. Oil and gas projects effectiveness. Gubkin University, Moscow, 2018.
63. Sazonov Y. A., Sazonova R. V. Jet pumps calculations. Tutorial. 1997. – 52 p.
64. Anuryev V. I. Handbook of a mechanical engineer: T. 1. // Mashinostroenie, 2001. – 920 p.
65. GOST 28919-91. Flange connections of wellhead equipment. Types, basic parameters and dimensions // Standards, 2005. 15 p.

Stream Description		Manifold
Overall Properties		
Vapour Fraction		0,567
Temperature	°C	75,0
Pressure	barg	97,0
Composition		
Nitrogen	mol%	0,83
CO2	mol%	3,78
H2S	mol%	13,81
H2O	mol%	5,59
Methane	mol%	44,53
Ethane	mol%	6,90
Propane	mol%	4,15
IC4_1*	mol%	0,85
NC4_1*	mol%	2,00
IC5_1*	mol%	0,96
NC5_1*	mol%	0,99
C6_1*	mol%	1,65
Benzene	mol%	0,05
C7_1*	mol%	1,75
Toluene	mol%	0,18
C8_1*	mol%	1,67
p-Xylene	mol%	0,33
E-Benzene	mol%	0,06
C9_1*	mol%	1,20
C10_1*	mol%	1,23
C11_1*	mol%	1,05
C12_1*	mol%	0,90
C13_1*	mol%	0,77
C14_1*	mol%	0,66
CN1_2*	mol%	2,15
CN2_2*	mol%	1,58
CN3_1*	mol%	0,28
M-Mercaptan	ppm mol	116
E-Mercaptan	ppm mol	149
nPMercaptan	ppm mol	157
nBMercaptan	ppm mol	185
CS2	ppm mol	9
COS	ppm mol	24
Total Stream Properties		
Molar Flow	kgmole/h	46 805,8
Mass Flow	kg/h	2237100
Molecular Weight		47,80
Mass Enthalpy	kJ/kg	-2 844
Heat Flow	MJ/h	-6 363 014



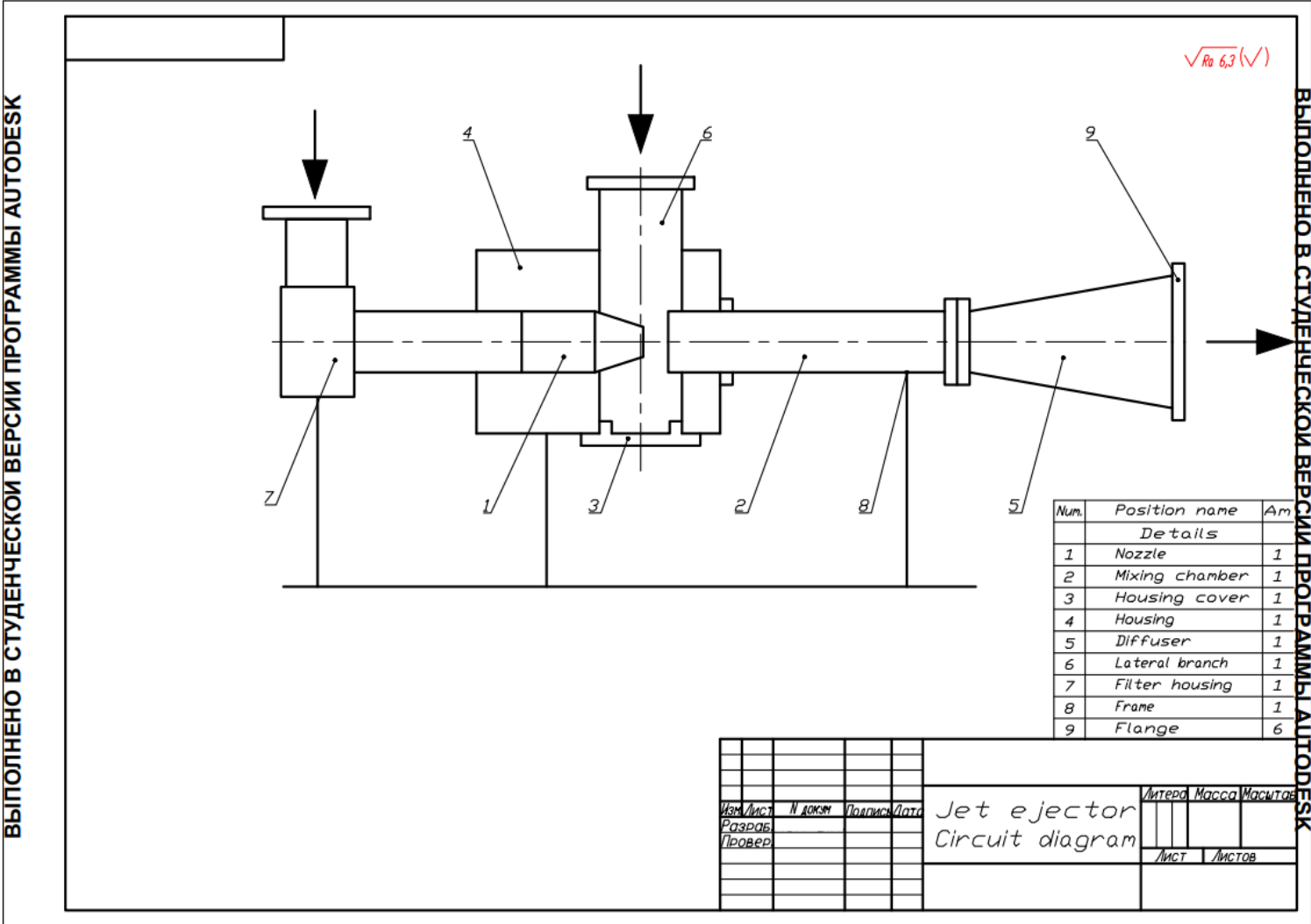
Appendix 3

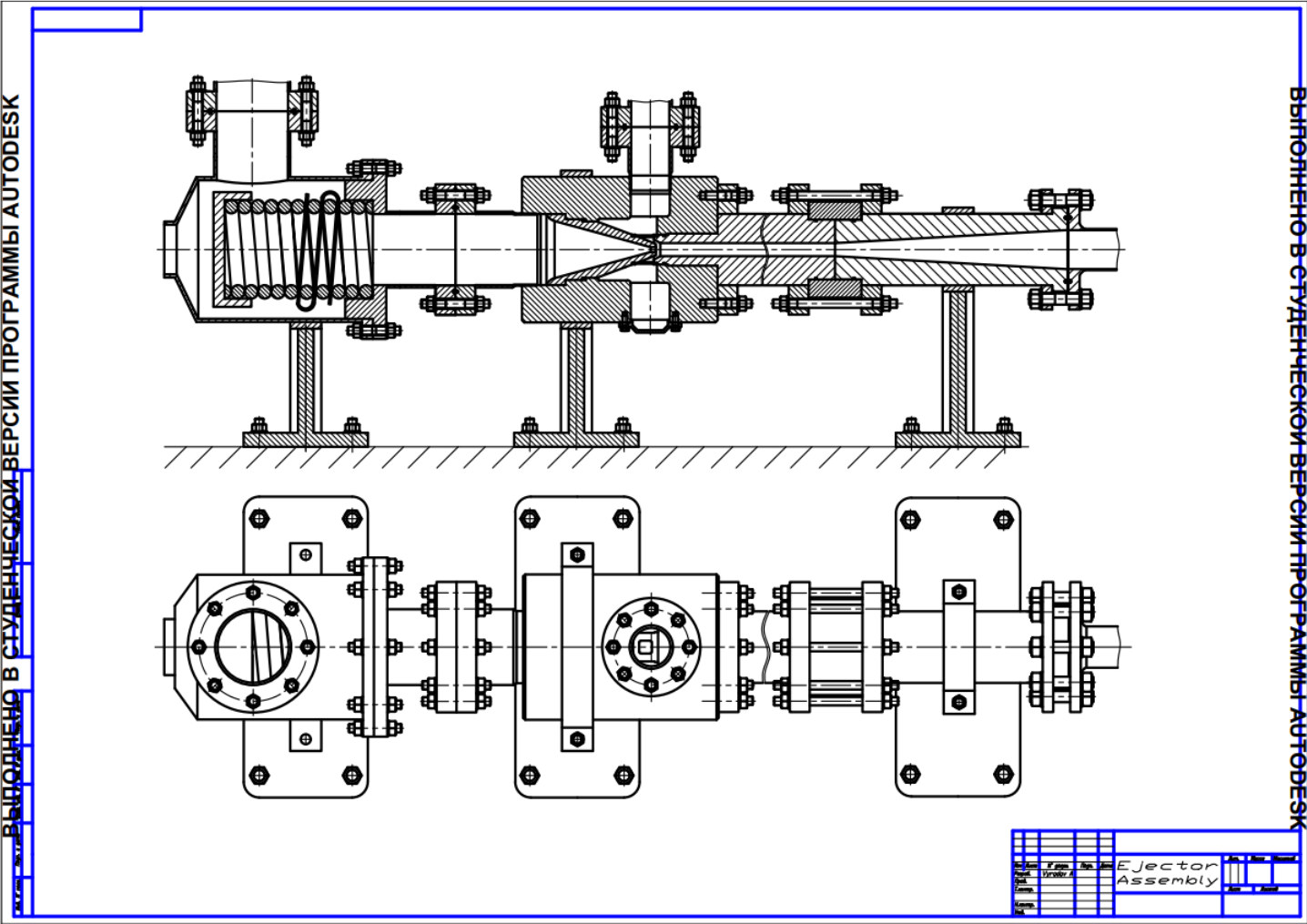


Calculation output	
Seawater flow rate (Q0), m ³ /h	396
Pressure ratio (P0/P1)	13,7
Geometrical parameter (a)	4,00
Max relative pressure (h0)	0,405
Optimal relative flow rate (q)	2,002
Optimal relative pressure (h)	0,262
Optimal relative pressure (h); verification	0,262
Seawater input pressure at the nozzle (P0), Pa	13 671 275,03
Ejector output pressure, Optimal (P4), Pa	4 317 614,50
Ejector efficiency	0,313
Mixing chamber length (L3), m	1,355
Relative mixing chamber length (L3/d0)	22,5
Gas input flow rate at the ejector (Q1), m ³ /s	0,2275
Gas input flow rate at the ejector, normal conditions (Q1n), m ³ /s	1,9583
Max relative flow rate (q_max)	2,700
Max gas input flow rate at the ejector (Q1_max), m ³ /s	0,3068
Max gas input flow rate at the ejector, normal conditions (Q1n_max), m ³ /s	2,6411
Max ejector output pressure (P4_max), Pa	6 128 849,41
Power pump pressure (PN), MPa	13,67
Pump power (NN), kW	1 503,84

Calculation output				
No	Parameter	Designation	Unit	Value
1	Nozzle outlet hole diameter	d0	m	0,0301
2	Mixing chamber diameter	d3	m	0,0602
3	Mixing chamber length	L3	m	1,355
4	Inlet radius	R2	m	0,060
5	Diffuser cone angle	γ_4	degree	7
6	Diffuser outlet hole diameter	d4	m	0,181
7	Seawater flow rate	Q0	m ³ /s	0,11000

Appendix 6



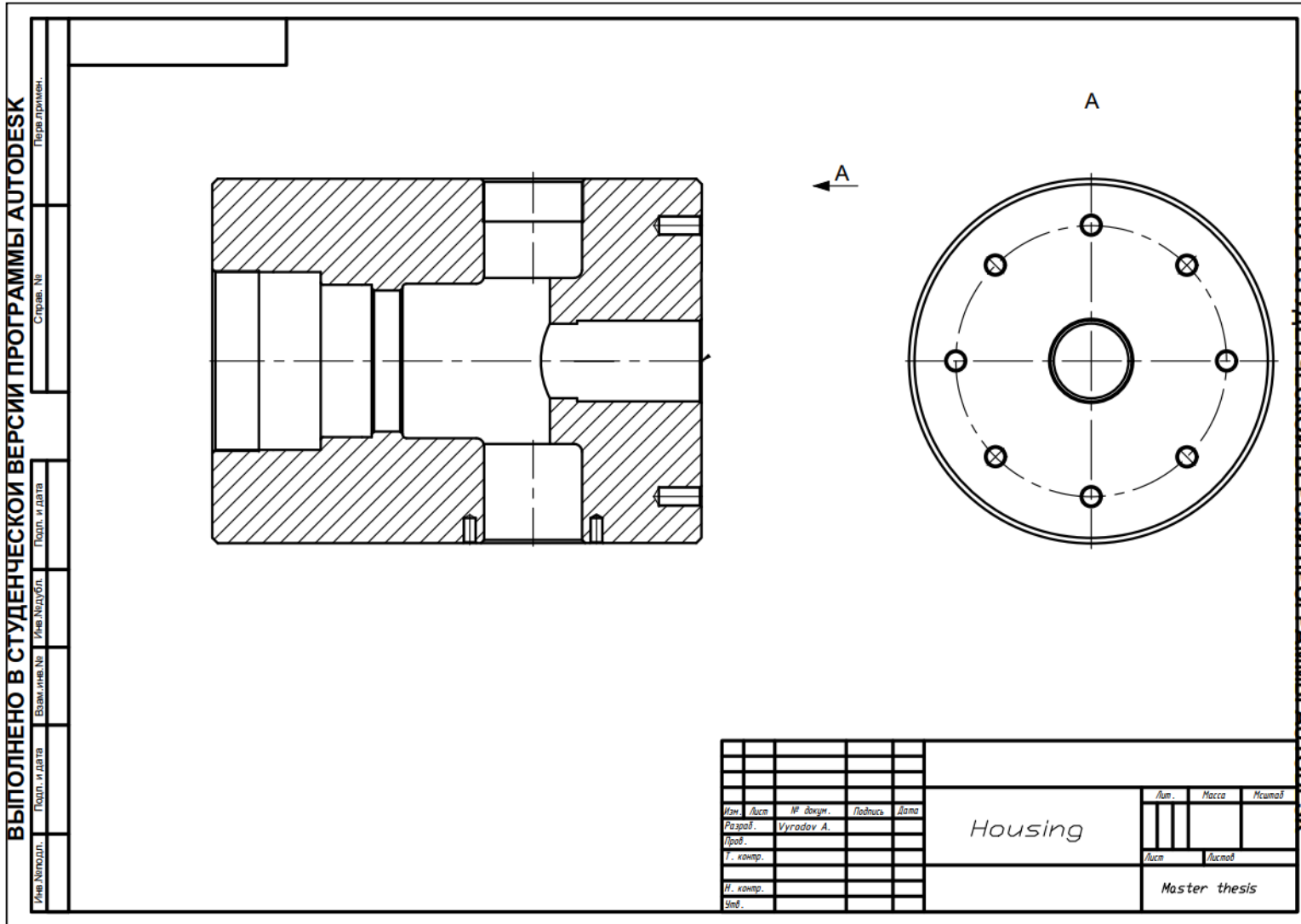


ВЫПОЛНЕНО В СТУДЕНЧЕСКОЙ ВЕРСИИ ПРОГРАММЫ AUTODESK

ВЫПОЛНЕНО В СТУДЕНЧЕСКОЙ ВЕРСИИ ПРОГРАММЫ AUTODESK

Имя, Инициалы	Подп. и дата	Имя, Инициалы	Подп. и дата	Справ. №	Перев. примен.

Изм.	Лист	№ докум.	Подпись	Дата	Diffuser	Лист	Масса	Исчисл.
И. комп.						Лист		
Н. комп.						Лист		
Сод.						Master thesis		



ВЫПОЛНЕНО В СТУДЕНЧЕСКОЙ ВЕРСИИ ПРОГРАММЫ AUTODESK

Перепримен.

Подп. и дата

Имя.Идубл.

Подп. и дата

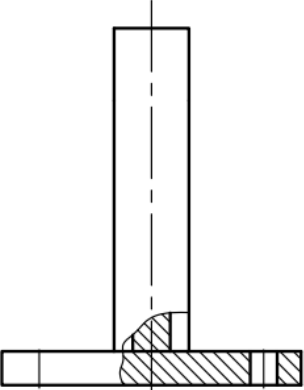
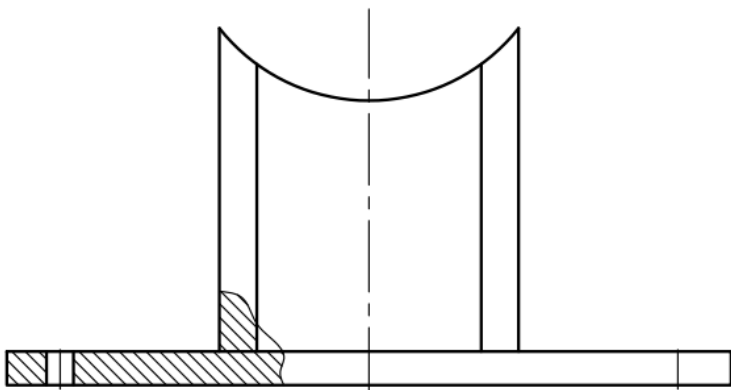
Имя.Идубл.

Подп. и дата

Имя.Идубл.

Подп. и дата

Имя.Идубл.

Изн.	Лист	№ докум.	Подпись	Дата
Разраб.		Vygodov A.		
Проб.				
Г. контр.				
Н. контр.				
Стд.				

Frame

Лист	Масса	Метабд
Лист	Лист	

Имя.Идубл.

Подп. и дата

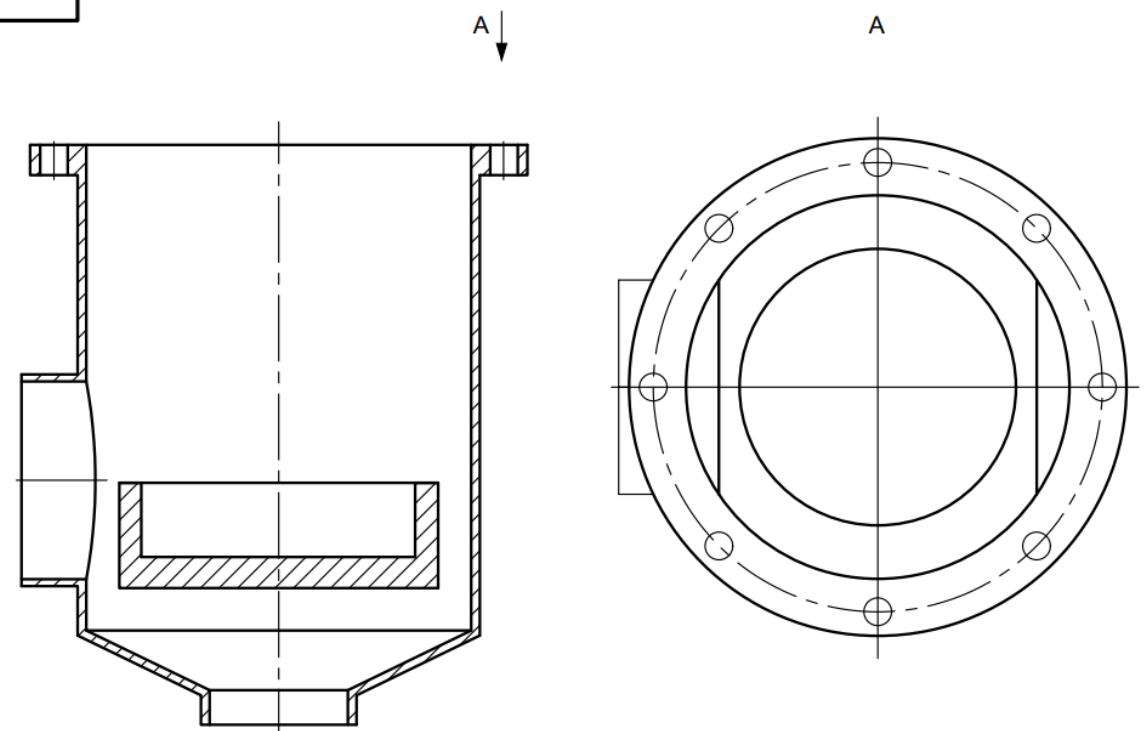
Имя.Идубл.

Подп. и дата

ВЫПОЛНЕНО В СТУДЕНЧЕСКОЙ ВЕРСИИ ПРОГРАММЫ AUTODESK

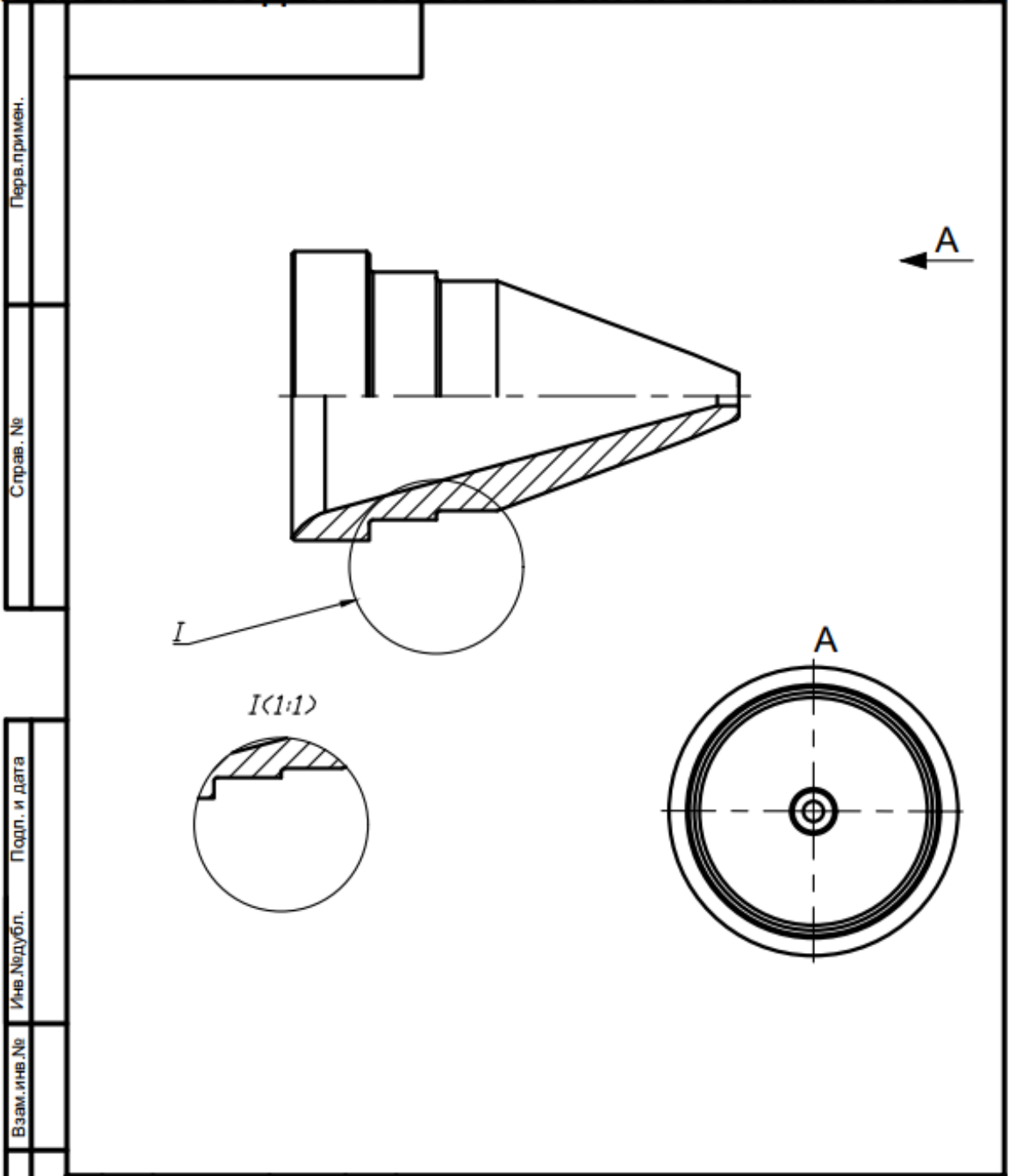
ВЫПОЛНЕНО В СТУДЕНЧЕСКОЙ ВЕРСИИ ПРОГРАММЫ AUTODESK

ВЫПОЛНЕНО В СТУДЕНЧЕСКОЙ ВЕРСИИ ПРОГРАММЫ AUTODESK



Имя	Лист	№ докум.	Подпись	Дата	Filter housing			
Разработ.		Угладов А.						
Проб.								
Г. контр.								
И. контр.								
Вид.								

ЫПОЛНЕНО В СТУДЕНЧЕСКОЙ ВЕРСИИ ПРОГРАММЫ AUTODES



Изм.	Лист	№ докум.	Подпись	Дата	<i>Nozzle</i>	Лит.	Масса	Масштаб
Разраб.		Vygodov A.				Лист	Листов	
Проб.						<i>Master thesis</i>		
Т. контр.								
И. контр.								
Ств.								

ЫПОЛНЕНО В СТУДЕНЧЕСКОЙ ВЕРСИИ ПРОГРАММЫ AUTODES

Subsea pipeline diameter selection

Carbonated water density, kg/m ³	$\rho := 1036$
Carbonated water viscosity, Pa*s	$\nu := 0.00128$
Power pump discharge pressure, MPa	$P_1 := 6.2$
Pipeline end line pressure, MPa	$P_2 := 4.5$
Pipeline length, m	$L := 98000$
Height difference, m	$z := 4$
Flow rate, m ³ /s	$Q := 0.68$

Calculations $g := 9.81$

$$D := \sqrt{Q} \cdot 840$$

$$D = 692.682 \quad \text{mm}$$

$$d := 0.7968 \quad \text{m} \quad \text{API 32 inches}$$

$$U := \frac{4Q}{\pi \cdot d^2}$$

$$U = 1.364 \quad \frac{\text{m}}{\text{s}}$$

$$U_{er} := \frac{122}{\sqrt{\rho}}$$

$$U_{er} = 3.79 \quad \frac{\text{m}}{\text{s}} \quad \text{Erosional velocity}$$

$$Re := \rho \cdot U \cdot \frac{d}{\nu} \quad \text{Reynolds number}$$

$$Re = 8.795 \times 10^5$$

$$f := 0.0014 + \frac{0.125}{Re^{0.32}}$$

$$f = 2.966 \times 10^{-3}$$

$$\Delta P := \frac{L}{d} \cdot 2 \cdot f \cdot \rho \cdot U^2 + \rho \cdot g \cdot z$$

$$\Delta P = 1.365 \times 10^6 \quad \text{Pressure losses are acceptable}$$

Subsea pipeline wall thickness selection

Steel X 52

Outer diameter, m	$D := 0.813$
Internal pressure, Pa	$P_i := 6200000$
External pressure, Pa	$P_e := 39240$
Safety class resistance factor	$\gamma_{sc} := 1.046$
Material resistance factor	$\gamma_m := 1.15$
Specified minimum yield strength, Pa	$SMYS := 359000000$
Specified minimum tensile strength, Pa	$SMTS := 455000000$
Material strength factor	$\alpha_u := 0.96$

$$f_{ytemp} := 0$$

$$f_{utemp} := 0$$

$$f_y := (SMYS - f_{ytemp}) \cdot \alpha_u$$

$$f_u := (SMTS - f_{utemp}) \cdot \alpha_u$$

$$f_{cb} := \min(f_y, f_u)$$

$$t_1 := \frac{\sqrt{3} \cdot \gamma_m \cdot \gamma_{sc} \cdot D \cdot (P_i - P_e)}{4 \cdot f_{cb} + \sqrt{3} \cdot \gamma_m \cdot \gamma_{sc} \cdot (P_i - P_e)}$$

Standard wall thickness is 10,3 mm

$$t_1 = 7.5 \times 10^{-3} \text{ m}$$

Appendix 15

Steel X 56

Specified minimum yield strength, Pa

SMYS1 := 386000000

Specified minimum tensile strength, Pa

SMTS1 := 490000000

$$f_{y\text{adj}} := (SMYS1 - f_{y\text{temp}}) \cdot \alpha_u$$

$$f_{u\text{adj}} := (SMTS1 - f_{u\text{temp}}) \cdot \alpha_u$$

$$f_{\text{adj}} := \min(f_y, f_u)$$

$$t_{\text{adj}} := \frac{\sqrt{3} \cdot \gamma_m \cdot \gamma_{sc} \cdot D \cdot (P_i - P_e)}{4 \cdot f_{cb} + \sqrt{3} \cdot \gamma_m \cdot \gamma_{sc} \cdot (P_i - P_e)}$$

Standard wall thickness for Steel X 56 and X 60 is 9,5 mm

$$t_1 = 6.98 \times 10^{-3} \text{ m}$$

Сталь X 60

Specified minimum yield strength, Pa

SMYS2 := 414000000

Specified minimum tensile strength, Pa

SMTS2 := 517000000

$$f_{y\text{adj}} := (SMYS2 - f_{y\text{temp}}) \cdot \alpha_u$$

$$f_{u\text{adj}} := (SMTS2 - f_{u\text{temp}}) \cdot \alpha_u$$

$$f_{\text{adj}} := \min(f_y, f_u)$$

$$t_{\text{adj}} := \frac{\sqrt{3} \cdot \gamma_m \cdot \gamma_{sc} \cdot D \cdot (P_i - P_e)}{4 \cdot f_{cb} + \sqrt{3} \cdot \gamma_m \cdot \gamma_{sc} \cdot (P_i - P_e)}$$

$$t_1 = 6.512 \times 10^{-3} \text{ m}$$

Pipeline burial depth calculations
Ice data

Consolidated layer thickness, m	$h := 0.7$
Ridge sail height, m	$h_s := 2$
Level ice thickness, m	$h_l := 0.85$
Keel breadth, m	$B := 20$
Ridge block size, m	$T_b := 0.3$
Keel angle, rad	$\alpha_k := 0.524$
Sail angle, rad	$\alpha_s := 0.314$
Ice speed, m/s	$v_i := 0.2$
Ice density, kg/m ³	$\rho_i := 900$
Ridge sail porosity	$\eta_s := 0.18$

Soil data

	$g := 9.8$
Wall friction angle, rad	$\phi_w := 0.314$
Friction between ice and soil	$\mu := 0.4$
Internal friction angle, rad	$\phi := 0.733$
Seabed slope, rad	$\beta := 0.000059$
Soil density, kg/m ³	$\rho_s := 1750$

Environmental data

Air density, kg/m ³	$\rho_a := 1.3$
Water density, kg/m ³	$\rho_w := 1010$
Current speed, m/s	$u_c := 0.8$
Current drag coefficient	$C_{dw} := 0.7$
Wind speed, m/s	$u_a := 26.5$
Wind drag coefficient	$C_{da} := 0.7$
Wind skin friction coefficient	$C_{sa} := 0$

Formulas and Calculations of ice parameters

$$h_k := 3.95 \cdot h_s$$

$$h_k = 7.9$$

$$w_k := 3.91 \cdot h_k$$

$$w_k = 30.889$$

$$w_b := w_k - 2 \cdot h_k \cdot \cot(\alpha_k)$$

$$w_b = 3.548$$

$$\eta := 0.11 \cdot \ln(T_b) + 0.37$$

$$\eta = 0.238$$

$$\rho_{iw} := \eta \cdot \rho_w + (1 - \eta) \cdot \rho_i$$

$$\rho_{iw} = 926.132$$

$$\rho_{ia} := \eta_s \cdot \rho_a + (1 - \eta_s) \cdot \rho_i$$

$$\rho_{ia} = 738.234$$

$$A_w := \left(h_k - \frac{\rho_i \cdot h_i}{\rho_w} \right) \cdot B$$

$$A_w = 142.851$$

$$A_{a1} := \left[h_s - \frac{(\rho_w - \rho_i) \cdot h_i}{\rho_w} \right] \cdot B$$

$$A_{a1} = 38.149$$

$$A_{a2} := w_k \cdot B$$

$$A_{a2} = 617.78$$

$$Q := h_s - \frac{(\rho_w - \rho_i) \cdot h}{\rho_w}$$

$$Q = 1.924$$

Forces calculation

$$F_{da} := 0.5 \cdot \rho_a \cdot C_{da} \cdot A_{a1} \cdot u_a^2 + C_{sa} \cdot \rho_a \cdot A_{a2} \cdot u_a^2$$

$$F_{da} = 1.219 \times 10^4$$

$$F_{dw} := 0.5 \cdot C_{dw} \cdot \rho_w \cdot A_w \cdot u_c^2$$

$$F_{dw} = 3.232 \times 10^4$$

$$W := \rho_{iw} \cdot B \cdot g \left[\frac{\rho_{ia}}{\rho_{iw}} Q^2 \cdot \frac{1}{\tan(\alpha_s)} + h \cdot w_k \cdot \frac{\rho_i}{\rho_{iw}} + 0.5 \cdot (w_k + w_b) \cdot \left(h_k - h \frac{\rho_i}{\rho_w} \right) \right]$$

$$W = 2.518 \times 10^7$$

$$F_b := \rho_w \cdot g \cdot B \left[0.5 \cdot (w_k + w_b) \cdot \left(h_k - h \frac{\rho_i}{\rho_w} \right) + h \cdot w_k \cdot \frac{\rho_i}{\rho_w} \right]$$

$$F_b = 2.596 \times 10^7$$

$$F_i := 0.43 \cdot 4.059 \cdot B^{0.622} \cdot h_i^{0.628}$$

$$F_i = 10.158$$

$$K_p := \frac{\cos(\phi)^2}{\cos(\phi_w) \cdot \left(1 - \sqrt{\frac{\sin(\phi + \phi_w) \cdot \sin(\phi + \beta)}{\cos(\phi_w) \cdot \cos(\beta)}} \right)^2}$$

$$K_p = 12.055$$

$$P_f(d) := 0.5 \cdot K_p \cdot \rho_s \cdot g \cdot (d + 0.635 \cdot d)^2 \cdot B$$

$$P_s(d) := \frac{1}{6} \cdot K_p \cdot \rho_s \cdot g \cdot d^2 \cdot w_b \cdot \left(w_b + \frac{d}{2 \cdot \tan(\alpha_k)} \right)$$

$$F_{cx}(d) := \mu \cdot P_f(d) \cdot \cos(\phi_w) \cdot \cos(\alpha_k) + \mu \cdot P_s(d) \cdot \cos(\phi_w)$$

$$F_{cy}(d) := \mu \cdot P_f(d) \cdot \cos(\phi_w) \cdot \sin(\alpha_k)$$

$$N(d) := F_{cy}(d)$$

$$F_a(d) := \mu \cdot N(d)$$

$$F_{da} + F_{dw} + F_i \cdot 1000000 - F_a(d) - F_{cx}(d) = 0 \text{ solve } \rightarrow \begin{pmatrix} 2.0250656953152774937 \\ -2.0961376079332254252 \\ -59.725652597870959081 \end{pmatrix}$$